Cationic Complexes of the Group 13-15 Elements Supported by N-, P-, and O-based Ligands

by

Paul A. Gray
B.ScH, Acadia University, 2012

A Dissertation Submitted in Partial Fulfillment
of the Requirements for the Degree of

DOCTOR OF PHILOSOPHY

in the Department of Chemistry

Supervisory Committee

Cationic Complexes of the Group 13-15 Elements Supported by N-, P-, and O-based Ligands

by

Paul A. Gray

B.ScH, Acadia University, 2012

Dr. Neil Burford, (Department of Chemistry)
Supervisor

Dr. Robin G. Hicks, (Department of Chemistry)
Departmental Member

Dr. David J. Berg, (Department of Chemistry)
Departmental Member

Dr. Jay T. Cullen, (Department of Earth and Ocean Sciences)
Outside Member

Abstract

Supervisory Committee

Dr. Neil Burford, (Department of Chemistry)
Supervisor

Dr. Robin G. Hicks, (Department of Chemistry)
Departmental Member

Dr. David J. Berg, (Department of Chemistry)
Departmental Member

Dr. Jay T. Cullen, (Department of Earth and Ocean Sciences)
Outside Member

This dissertation presents the synthesis and characterization of a variety of neutral and cationic complexes featuring Group 13-15 element centres stabilized by N-, P-, and O-based donors. Unique aluminum and gallium cationic complexes are obtained from equimolar reactions of the metal halide with the chelating alkyl phosphine dmpe. However, using the analogous amine donor tmeda, neutral adducts are preferred for aluminum as well as for $GaCl_3$, while cations are obtained for $GaBr_3$ and GaI_3. New cations of Ge(II) and Sn(II) were also discovered, featuring the coordination of either bipyridine ligands or dmpe. Utilizing bipyridine led to the expected mono and dicationic chelate complexes, however, using dmpe led to the formation of unprecedented tetracationic molecules. The reactivities of the bipyridine complexes were investigated with a variety of substrates which showcased their Lewis acidity as well as their ability to be oxidized. Finally, a new series of high oxidation-state main group cations have been synthesized using a variety of ligands. The ligand choice was found to be an important role

in compound isolation as ligand degradation occurred for some of the compounds due to their high electrophilicity. Additionally, the Lewis acidity of some of the complexes leads to interesting reaction chemistry including sp^3 C-H activation. Overall, the results presented herein represent new coordination chemistry for the main group elements and opens the door towards new reactivity pathways including small molecule activation and catalysis.

Table of Contents

List of Figures

List of Schemes

List of Tables

Acknowledgments

I was incredibly fortunate to have the opportunity to work with Prof. Neil Burford during the course of my graduate studies. The freedom and independence that he has given me has allowed me to really take ownership of the results that I obtained. He has been an outstanding mentor, both with in-lab and out-of-lab matters and not only do I value his guidance, but also his friendship and kindness. I certainly would not be where I am today without it.

I have had the pleasure to meet and work with many fantastic people at UVic. My labmates were the family that made going to work every day exciting and a never-ending source of support and entertainment. In particular, Dr. Alasdair Robertson, Dr. Saurabh Chitnis, Dr. Riccardo Suter, Stewart Lucas, Chris Frazee, Hannah Sinclair, and Max Poller were excellent colleagues, but more importantly, great friends. The "Burf-Herd" will always hold a special place in my heart moving on from UVic. To those friends outside of my research group, you all have made everyday a more rewarding experience, whether it is coffee breaks or burger and beers at the Grad House. I am incredibly fortunate to have forged strong friendships and that I know will continue long after our degrees are finished.

I am deeply grateful for the collaborations that I have enjoyed over the past several years. Dr. Robert McDonald and Dr. Michael J. Ferguson at the University of Alberta, as well as Dr. Brian O. Patrick at UBC, are responsible for essentially all of the diffraction experiments discussed in this dissertation. Their understanding of the sensitivity of the crystals that were sent to them and their motivation to at least try and collect data, even when I had no idea what they really were, was greatly appreciated. Additionally, Chris Barr has been instrumental in the NMR characterization of these complexes and his knowledge and insight was always a welcome contribution.

I would like to thank Prof. Robin Hicks, Prof. David J. Berg, and Prof. Jay T. Cullen for being my committee members and overseeing this process from start to finish. Your input along the way has helped shape my degree into something I am proud of. I would also like to thank Prof. Kim Baines for agreeing to be the external examiner for my defence. I am also grateful for the financial support from various awards and fellowships, especially the Natural Sciences and Engineering Research Council, and the University of Victoria Department of Chemistry.

Last, but certainly not least, I have to thank my family. To my mom who is always so proud to see what I achieve, I am grateful for your loving words of encouragement over the years. To my in-laws, knowing your door was always open for a place to work or for a customary hot beverage was always comforting during the writing of this thesis, and on my many coast-to-coast trips home. Finally, to my loving wife Kristen, you have been the rock to which I have been anchored throughout the past 12 years. This thesis could never seek to make up for how many missed FaceTime dates there were, or how many airport goodbyes we have endured. But I would never have completed it without your love and compassion throughout the entire journey and I can never thank you enough for being “my person”. I love you.

List of Abbreviations and Symbols

° : degree

Å : angstrom

Ar : generic aromatic substituent

avg : average

$BIMEt_3$: tris(1-ethyl-benzoimidazol-2-ylmethyl)amine

$BIMEt_2Pyr$: 2,6-bis(1-ethylbenzimidazol-2-yl)pyridine

bipy : 2,2'-bipyridine

Bu : butyl

Cy : cyclohexyl

DFT : density functional theory

dmap : 4-dimethylaminopyridine

dmpe : 1,2-bis(dimethylphosphino)ethane

e.g. : for example

Et : ethyl

Et_2O : diethyl ether

FT-IR : Fourier transform Infrared Spectroscopy

g : grams

HOMO : highest occupied molecular orbital

% : percent

iPr : isopropyl

K : Kelvin

LUMO : lowest unoccupied molecular orbital

m : medium intensity (*FT-IR*)

m : multiplet (*in NMR)*

Me : methyl

MeCN : acetonitrile

Mes : mesityl (2,4,6-trimethylphenyl)

Mes* : super-mesityl (2,4,6-tri-tBu-phenyl)

NHC : N-heterocyclic carbene

J : coupling constant

NMR : nuclear magnetic resonance

NPA : natural population analysis

OTf : triflate (trifluoromethanesulfonate)

PCM : polarization continuum model

Ph : phenyl

PIm_3 : tris(N-methylimidazole)phosphine

Hz : hertz

i.e. : that is

R : generic organic substituent

Σ_{CR} : sum of covalent radii

Σ_{vdW} : sum of van der Waals radii

s : singlet (*in NMR*)

s : strong intensity (*in FT-IR*)

tBubipy : 4,4’-di-tert-butyl-2,2’-bipyridine

TMS : Me_3Si

t : triplet (*in NMR*)

tBu : tert-butyl

ppm : parts per million

q : quartet (*in NMR*)

terpy: 2,2’:6’,2’’-terpyridine

tBu_3terpy : 4,4’,4’’-tri-tert-butyl-2,2’:6’,2’’-terpyridine

vs. : versus

VSEPR : valence shell electron pair repulsion

w : weak intensity (*in FT-IR*)

Δ : difference

ΔG : change in free energy

ΔH : change in enthalpy

ΔS : change in entropy

δ : chemical shift

Chapter 1 - Introduction

1.1 Renaissance of Main Group Chemistry

The study and observation of main group compounds has led to the development of many of the fundamental theories that today form the basis of general chemistry. Concepts such as VSEPR theory, acid-base chemistry, and molecular orbital (MO) theory originated from the study of the bonding trends of main group elements. Despite this, the transition metals, generally located from groups 3-12 on the periodic table, are regarded as the work horses of molecular transformations and catalysis. The term catalysis was first defined in 1836 by Berzelius,[1] but in fact, patents dating back to the earlier 1800s describe the use of platinum wire as participating in these types of reactions.[2] As such, the development of catalysts to target specific chemical transformations continues to be one of the most active and lucrative areas of molecular chemistry. However, while compounds featuring main group elements had been prepared, including what is believed to be the first organometallic compound (which turned out to be the dimeric arsenic compound of the type $(H_3C)_2As\text{-}As(CH_3)_2$, and its oxygenated equivalent$(H_3C)_2As\text{-}O\text{-}As(CH_3)_2$),[3,4] the development of molecules which parallel the characteristics and reactivity of the transition metals has only recently garnered renewed interest. The general evolution of main group chemistry during the last 35 years is colloquially referred to as the "Renaissance of Main Group Chemistry".[5]

The paradigm shift is often attributed to three almost simultaneous discoveries in the early 1980s, related to the first examples of main group multiple bonds supported by bulky substituents. The preparation of the first disilene, $Mes_2Si{=}SiMes_2$,[6] a heavier analogue of

ethylene, was the first example of two heavier elements (*i.e.* principle quantum number n>2) forming a double bond (Figure 1.1.1a). Prior to this report, it was postulated that only the first-row elements could form stable element-element double bonds, supported by the theoretical work of Pitzer and Mulliken.[7,8] due to the insufficient overlap of more diffuse *p*-orbitals compared to those on carbon. In addition to the disilene, the first diphosphene, Mes*P=PMes*,[9] was prepared (Figure 1.1.1b), and the first example of a phospha-alkyne ^{t}BuC≡P,[10] featuring phosphorus-carbon triple bond was also synthesized in this year (Figure 1.1.1c).

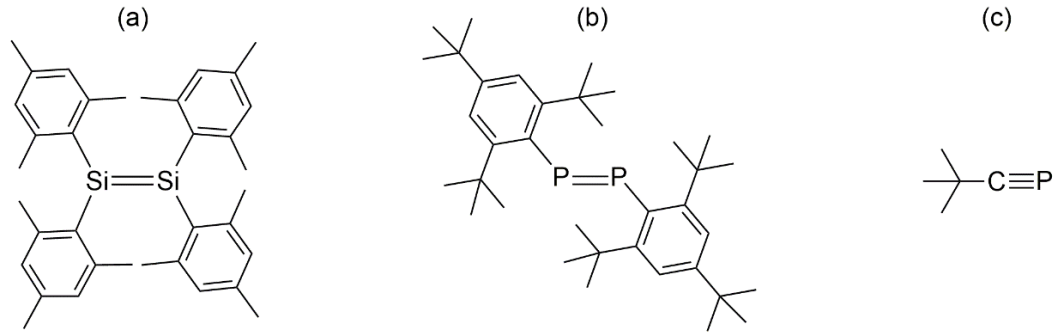

Figure 1.1.1: A (a) disilene, (b) diphosphene, and (c) phosphalkene as heavier analogues of alkenes and alkynes.

1.2 Approaches to Stabilizing Reactive Main Group Centres

The development of new complexes which exhibit reactivity with small molecules depends on stabilizing these complexes to an extent to facilitate their isolation and study their reaction chemistry. Upon surveying the literature, the two general approaches to stabilizing reactive molecular species most often employed involve either steric protection with large, highly substituted organic substituents to kinetically shield the reactive centre, or through coordination of a strong donor ligand to electronically stabilize the molecule. In some cases, both of these methodologies are employed in one ligand framework and work in tandem with each other.

1.2.1 Effects of Sterically Demanding Substituents

In all three cases presented above in Figure 1.1.1, the stability of the complexes is attributed to the sterically-demanding organic substituents at each of the element centres. Arguably, the most well known bulky substituents are those based off of aromatic frameworks, such as the 2,4,6-trimethylphenyl (mesityl or Mes),[11] 2,6-di-*iso*-propylphenyl (Dipp),[12] and 2,4,6-tri-*tert*-butylphenyl (Mes*)[13] substituents. The ability to easily modify the substitution at the aromatic moiety is a major advantage as it allows for the evaluation of a broad array of substituents. Through simple Friedel-Crafts alkylation of the aromatic ring and the vast scope of halide-containing substrates with which to employ as the alkylating agent, modification possibilities are essentially endless. However, for some highly reactive molecules, even larger substituents are required. These bulky substituents, often containing polycyclic or multiply-substituted aromatic groups,[14–18] as well as highly substituted amides[19–21] which provide a shield for the reactive centres or bonds and offer both kinetic and thermodynamic stability. The bulky ligands hinder the access of the reactive centres to substrates (kinetic stability), and can also increase the strain energy that would result from oligomerization (thermodynamic stability).[22] Some examples of these groups are illustrated in Figure 1.2.1. The advent of these ligands has allowed for the isolation of many main group compounds featuring unusual and peculiar bonding environments and has facilitated the design of these compounds to have transition metal-like reactivity.

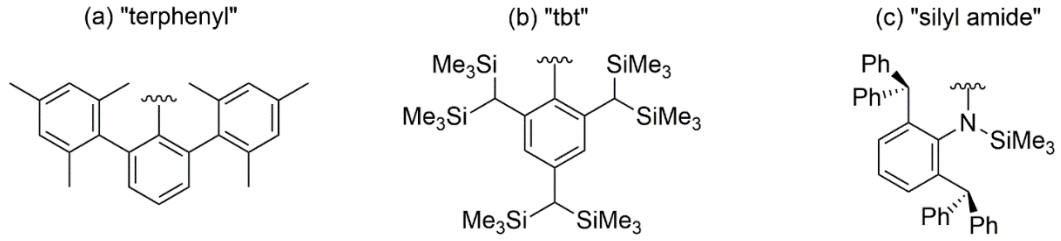

Figure 1.2.1: Selected bulky ligands for the stabilization of reactive main group centres.

One of the main applications of these ligands in main group chemistry is the stabilization of low-valent alkene and alkyne analogues. Unlike their carbon congeners, these heavier unsaturated systems are unstable and the employment of mechanisms of stabilization are required for their isolation. This is mainly due to the ineffective overlap of the larger and more diffuse *p*-orbitals, which do not participate in efficient π-bonding like carbon and are prone to oligomerization and reduction. As such, the use of bulky ligands prevents these reaction pathways. In particular, the heavier group 14 analogues of alkenes and alkynes have been realized due to the kinetic and thermodynamic stabilization imposed by large *m*-terphenyl ligands and other highly substituted aryl and alkyl substituents.[23–26]

While these bulky substituents are typically used to impede or prevent reactivity at a given element centre, they can also influence the outcomes of reactions when they do take place. In the case of low-valent main group chemistry, one recent example involves the reactivity of *m*-terphenyl-substituted primary aluminium hydrides with olefins and unsaturated compounds (Scheme 1.2.1).[27] When compounds of the type $(ArAlH_2)_2$ are allowed to react with various unsaturated organic molecules, their reaction rates were found to be directly proportional to the size of the *m*-terphenyl substituent at the aluminium centre (Table 1.2.1). Upon first inspection, this correlation appears counterintuitive since the bulkiest alane, which should have the most restricted access to the reactive aluminium centres, reacts more quickly with olefins than the alanes with less-bulky substituents.

However, it is generally accepted that the first step in the hydroalumination of olefins[28,29] is coordination of an olefin to a *p*-type orbital of a monomeric aluminium hydride, followed by Al-H addition across the C=C unsaturation. As such, the solution equilibria of the alanes between their monomeric and dimeric forms has a significant influence on the reaction rates. Thus, it stands that the compound which has the largest concentration of the monomeric form in solution will exhibit the fastest rate and rationalizes the observed trend of inverse proportionality between ligand size and reaction rates, as the larger substituents shift the monomer-dimer equilibrium towards favouring the monomer, promoting reactivity.

Scheme 1.2.1: Reaction $(Ar^*AlH_2)_2$ with various substituted alkynes.

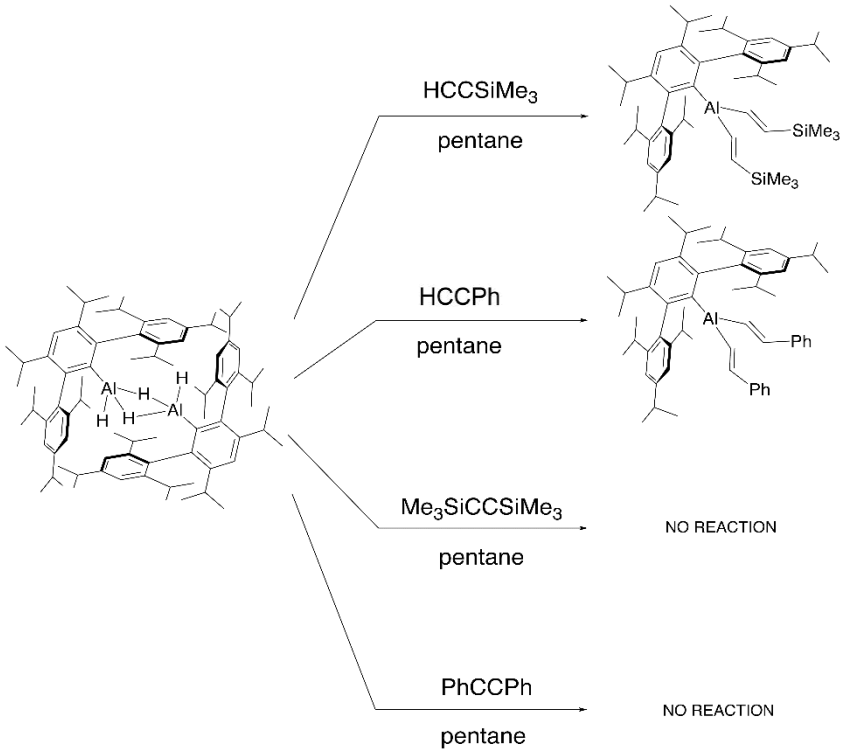

Table 1.2.1: Examining the influence of ligand steric bulk on reaction rate in the hydroalumination of alkenes.[27]

$Ar^{X}AlH_2$	Olefin	Temperature (°C)	Reaction Time (h)
$(Ar^{Me_6}AlH_2)_2$		20	<12
		20	>48
		50	48
		50	no reaction
$(Ar^{iPr_4}AlH_2)_2$		20	8
		20	24
		50	24
		50	no reaction
$(Ar^{iPr_8}AlH_2)_2$		20	3
		20	0.5
		50	16
		50	no reaction

1.2.2 Coordinative Stabilization from Strong Donor Molecules

In addition to the use of bulky ligands to kinetically stabilize the reactive centres, strong donor ligands such as pyridines, phosphines, and carbenes are also sufficient to stabilize a variety of reactive centres. This approach is classically associated with transition metal coordination complexes, which often employ these donor moieties to occupy coordination sites at the metal centre and have led to a variety of transition metal-based catalysts which are used in a wide variety of synthetically useful processes (Figure 1.2.2).[30–35]

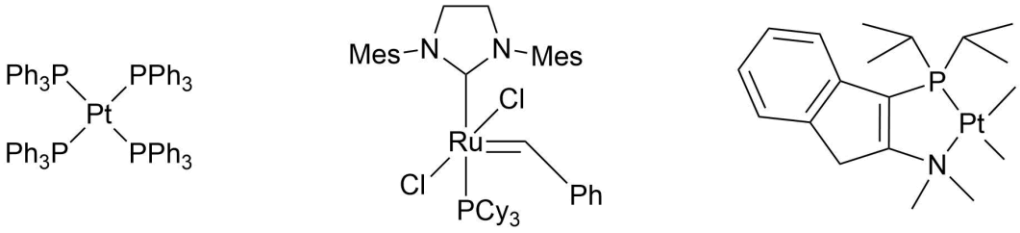

Figure 1.2.2: Examples of transition metal catalysts featuring strong donor ligands.

Overall, amines, pyridines, and phosphines represent prototypical ligands in the broad array of established coordination chemistry of *d*- and *f*-block metals and many *p*-block elements. Moreover, any group 15 element (the pnictogens, Pn = N, P, As, Sb, Bi) in a neutral framework (*e.g.* PnX_3, PnR_3, R-Pn=R, etc.) has the potential to act as a $2e^-$ donor (Lewis bases), although the donor strength is generally greater for elements with smaller atomic radii. Consequently, complexes involving heavier pnictines (Sb, Bi) as ligands are rare compared to those involving amines or phosphines, and to our knowledge, no structurally characterized examples of bismuth acting as a $2e^-$ donors exist.[36–38] In fact, bismuth is prone to act as an acceptor when coordinated to a metal rather than as a donor.[39]

Compared to pnictogen-based donors, carbenes are a relatively new addition to the field of coordination chemistry. Carbenes feature a divalent carbon centre which possesses both a lone pair of electrons, as well as a formally unoccupied *p*-orbital perpendicular to the lone pair-containing orbital, contributing to a valence electron configuration containing only six electrons.[40] The first report of a stable crystalline carbene appeared in 1991 by Arduengo, detailing the preparation of the prototypical *N*-Heterocyclic carbene (NHC) (Figure 1.2.3a) featuring two nitrogen atoms outfitted with bulky adamantyl substituents flanking the divalent carbene centre.[41] Since then, the library of isolated carbenes, both NHCs and other types, has been expanded to include compounds featuring almost every heteroatom (O, P,

S, etc.) with endless examples of substituents, and many structural motifs including cyclic and acyclic variants (Figure 1.2.3b).[42–45] NHCs offer an advantage in their use as ligands over typical phosphines as tuning their steric and electronic properties through modification of the precursor imidazolium salts is straightforward. Additionally, the formally vacant *p*-orbital at the carbon centre allows for a degree of metal-to-ligand back-donation from the metal to the carbene, a phenomenon which does not occur to a great extent in phosphines. Because of these characteristics, their use in transition metal complexes, and by extension metal-based catalysis, has endured significant advances as of late.[46–48]

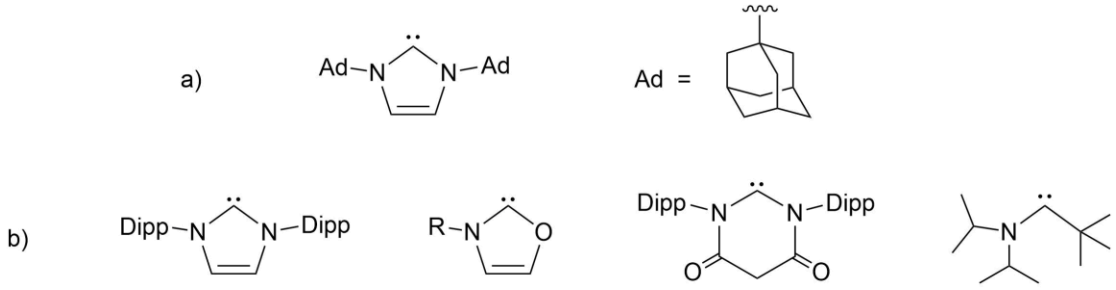

Figure 1.2.3: (a) The first stable crystalline carbene and (b) other examples of carbenes with a variety of structural features.

In terms of main group chemistry, carbenes have shown great utility in the stabilization of low coordinate complexes which are otherwise too reactive to isolate and characterize on a laboratory scale. In particular, a series of homoatomic main group molecules of the *p*-block elements have been studied due in part to the employment of carbenes (mainly NHCs) to stabilize these fragments (Figure 1.2.4).[49–53] With the exception of the diphosphorus and diarsenic examples, these chemical curiosities represent a growing library of low-valent main group compounds that feature formal multiple bonding. In all cases, the compounds feature a *trans*-bent geometry, enforced by the presence of either a lone pair at the element centre, or in the case of the formal diborene, the B-H bonding environment.

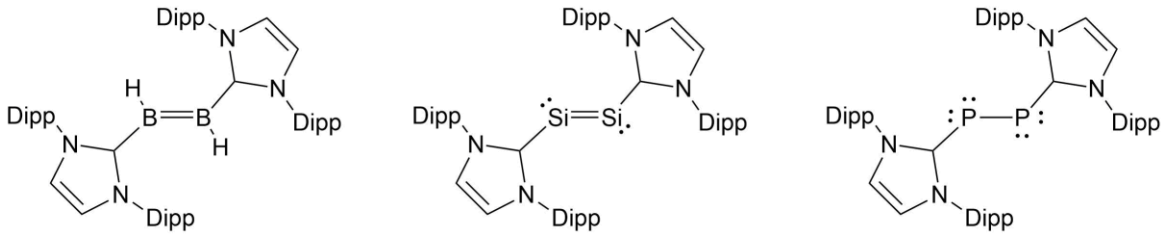

Figure 1.2.4: Examples of carbene-stabilized homoatomic E(0) complexes.

Employing a similar methodology, carbenes have also shown utility in stabilizing low-coordinate group 14 hydrides. The EH_2 units (E = Si, Ge, Sn) have a formally vacant *p*-orbital into which the carbene can donate into.[54–56] Additionally, the lone pair at each of the metal centres, upon coordination of the carbene, behave as Lewis bases themselves and can be used to donate to other electrophiles. This "push-pull" stabilization is key to the isolation of these reactive moieties.[57] In the case of the SiH_2 or GeH_2 unit, the serendipitous transfer of a BH_3 unit as the acceptor of the Si- or Ge-based lone pair is accomplished during the reduction with $LiBH_4$ and is a sufficient Lewis acid to effect the isolation of the complex. In the case of SnH_2, the use of $W(CO)_5$ as the acceptor is needed (Figure 1.2.4).

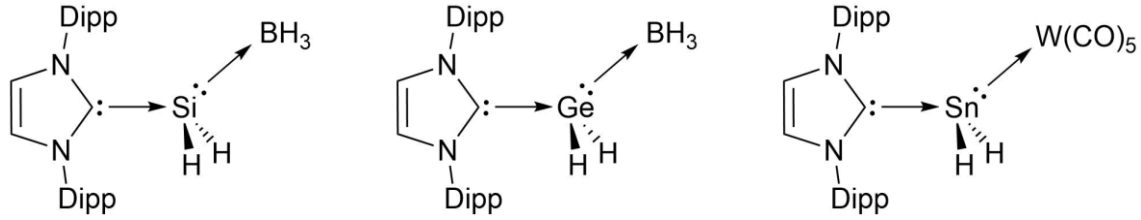

Figure 1.2.5: Examples of carbene-stabilized element hydrides complexes. Note that the arrows are not intended to indicate "dative bonding" but to illustrate the direction of the "push-pull" stabilization.

1.3 Reactivity of Unsaturated Heavy C=C and C≡C Analogues

One of the quintessential examples of a heavier main group alkene- or alkyne-analogue undergoing facile reactivity with small molecules, mimicking processes which transition

metals are known for, was reported by Power and co-workers,[58] in which a digermyne (Ar'Ge≡GeAr') activated H_2 at remarkably mild conditions to give a mixture of hydrogenation products (Scheme 1.3.1). The mechanism for this involves the interaction of the H-H σ-bonding electrons with a formally empty orbital at the germanium centre, which occurs with the concomitant donation of the electrons of the π-type HOMO into the σ*-orbital of H_2 (Figure 1.3.1a) and is analogous to the frontier orbital mechanism invoked for transition metal H_2 activation Figure 1.3.1b).[59]

Scheme 1.3.1: Reaction of a digermyne with H_2 at ambient temperature.

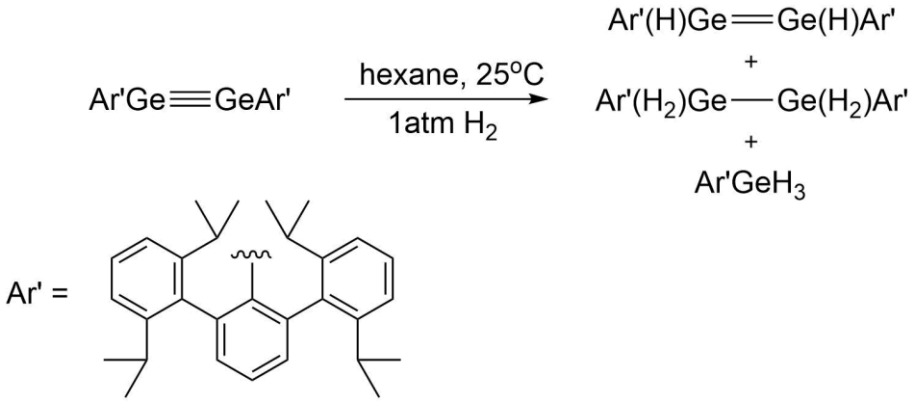

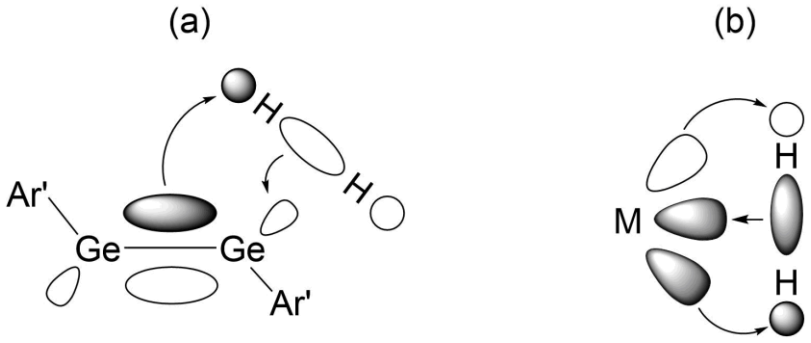

Figure 1.3.1: (a) Orbitals involved in the activation of H_2 by a digermyne and (b) the frontier orbitals of transition metal H_2 activation

These types of complexes are extremely reactive, due in part to their low-valent states and the large terphenyl substituents enable their isolation and characterization. Since this

seminal observation, the reactivity of the series of group 14 analogues of ethylene and acetylene has been examined.[60–64] One notable example is the triply bonded tin analogue, known as a distannyne (Ar'Sn≡SnAr' or Ar*Sn≡SnAr*), which not only complexes two equivalents of ethylene to give the addition product, but undergoes retro-cycloaddition to spontaneously release free ethylene and regenerate the distannyne under reduced pressure (Scheme 1.3.2),[62] mirroring traditional reversible oxidative addition and reductive elimination processes seen with metals like platinum and palladium.

Scheme 1.3.2: Reversible activation of ethylene by a distannyne

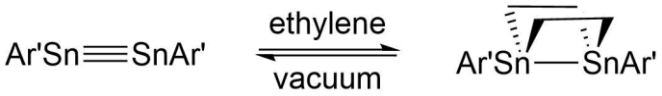

This type of reactivity is not limited to the group 14 elements. Analogous compounds of the group 13 elements have also been prepared and characterized,[65–69] and in the case of the aluminum and gallium derivative, show reactivity with a variety of molecules.[70,71] In these cases, the proposed reactivity differs from those observed in the group 14 cases. While germanium and tin alkene and alkyne analogues undergo reactions with H_2 and ethylene to give cycloaddition products in which some E-E bond character (E = Ge, Sn) is retained, the equivalent reactions of alkenes and alkynes, along with $B(C_6F_5)_3$ (BCF), with gallium, indium, and thallium do not retain any M-M bonding character (M = Ga, In, Tl). Instead, the resulting products appear to originate from the monomeric M(I) compounds ArM**:** (Ar = *m*-terphenyl) (Scheme 1.3.3).[72] The rationale for this observation is similar to the case for the rates of reactions in the aluminium hydrides presented above. The large *m*-terphenyl substituents facilitate the dissociation of the M=M bond in the dimer into their constituent M(I) monomers, and Power and co-workers have shown that the degree of M=M bonding is dependent on the size of the substituents.[72] In this case, the two largest terphenyl

substituents used do not lead to a difference in colour between the solutions of the ArM=MAr vs the crystals in the solid state, while the smaller of the terphenyl substituents exhibits different photometric properties in solution vs the solid state. In line with this, the reaction chemistry with unsaturated molecules, as well as Lewis acids, supports this assertion. Upon reaction with BCF and transition metal carbonyls, the ArGa=GaAr compounds give rise to the coordination complex $ArGa–B(C_6F_5)_3$ and $ArGa–M(CO)_n–GaAr$ (M = Cr, W, Mo), implying a monocoordinated metal centre in solution (Scheme 1.3.3). This is inline with the theoretical investigations into the bonding of the group 13 dimetallenes.[73,74]

Scheme 1.3.3: Reactivity of a digallane with boranes and transition metal carbonyls.

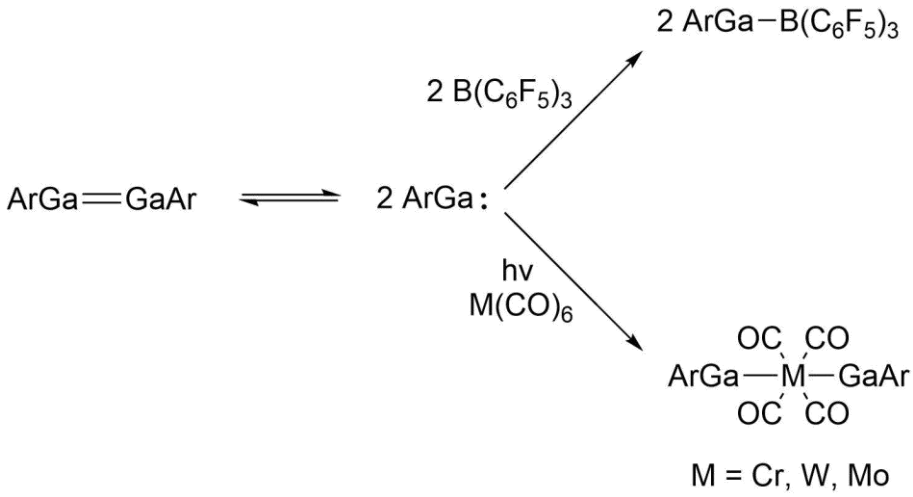

While not as prevalent as the alkene and alkyne analogues stabilized with bulky ligands, the carbene-stabilized homoatomic analogues still enjoy a rich reaction chemistry, which exhibits several instances of different reactivity comparatively. For example, addition of four equivalents of BH_3·THF to the carbene-stabilized disilicon results in the isolation of a complex which features several interesting characteristics including a ligand stabilized Si(II) hydride, and a cyclic B_3H_7 moiety stabilized from the coordination of a NHC→Si(H) unit

(Scheme 1.3.4a).[75] Additionally, when one equivalent of $Fe(CO)_5$ is added to the disilicon compound, the isolated compound features the coordination of one of the Si(0) units to the iron centre, with the elimination of a CO unit (Scheme 1.3.4b).[76] Interestingly, when an additional equivalent of $Fe(CO)_5$ is added and the mixture heated, the resulting compound features formal insertion of CO into the Si=Si double bond, along with the two silicon centers bound to each iron atom of a $(CO)_3Fe\text{-}Fe(CO)_3$ dimer. This coordination complex can also be accessed by heating the disilicon compound with an excess of $Fe(CO)_5$.

Scheme 1.3.4: Reactions of carbene-stabilized disilicon with (a) $BH_3{\cdot}THF$ and (b) $Fe(CO)_5$.

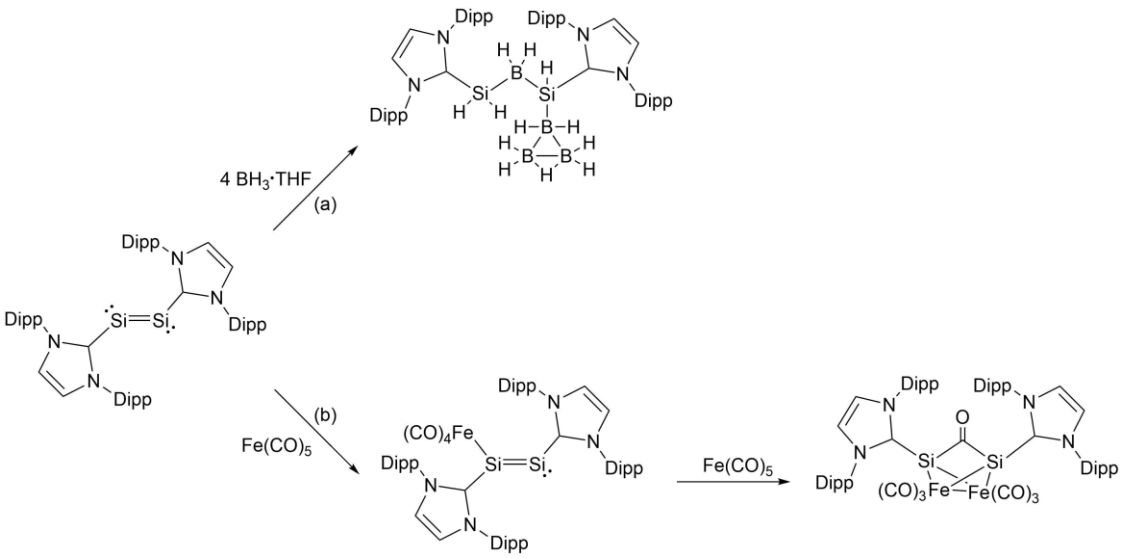

In contrast to this, reaction of the diphosphorus analogue with three equivalents of $BH_3{\cdot}THF$ results in the formation of a *bis*-chelated BH_2^+ unit which is bound to both phosphorus atoms, and the compound retains the P-P bonding interaction forming a three-membered ring (Scheme 1.3.5a). This compound is similar in structure to the recently reported hydride-bridged distannane resulting from the hydrostannylation of *tert*-butylethylene by the terphenyl-substituted distannene.[77] Additionally, the carbene-stabilized diphosphene undergoes reaction with the protonated pyridine salt $[C_5H_5N\text{-}H][Cl]$ to give the carbene-stabilized HP_2^+ cation (Scheme 1.3.5b). with retention of the P-P. Interestingly, the

diphosphorus precursor can be regenerated via addition of a free carbene. These complexes nicely show the general applicability of a donor stabilization at a reactive centre and represent non-classical examples of Lewis acids-base chemistry.

Scheme 1.3.5: Reactions of carbene-stabilized diphosphorus with (a) BH_3·THF and (b) [Pyr-H][Cl]

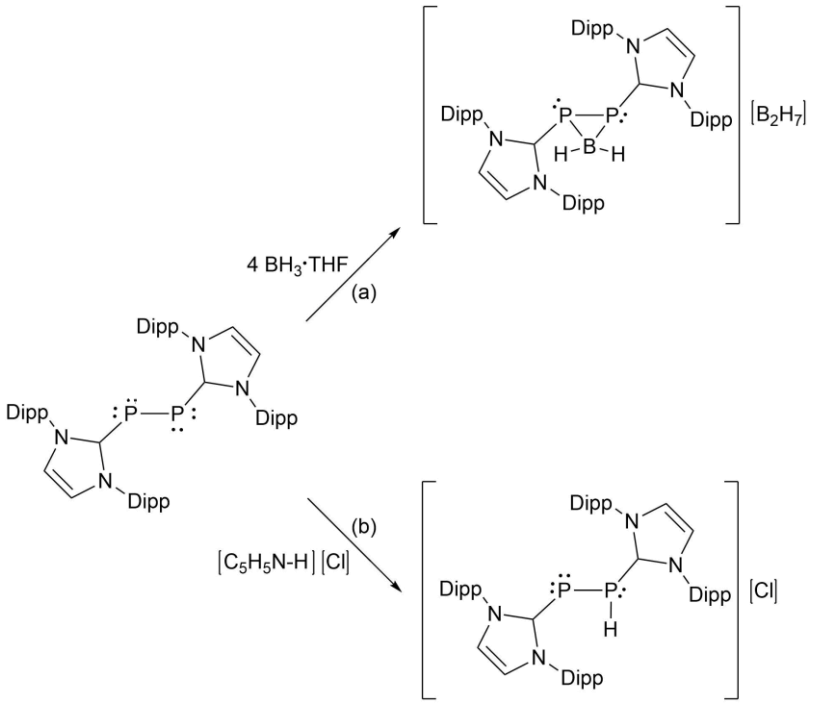

1.4 Lewis Acid-Base Chemistry

1.4.1 Classical Lewis Acid-Base Adducts

The notion of Lewis acid-base chemistry was first described over 100 years ago by Gilbert Lewis in his work entitled "The Atom and the Molecule".[78] Within the text, and his subsequent publications, he explains that the reactivity of most molecules is attributed to the idea that one molecule can donate a pair of electrons (Lewis base) and the other which can accept a pair of electrons (Lewis acid).[78,79] The product of the interaction of these two types of molecules are often referred to as a Lewis acid-base adduct. Typically, a Lewis base with

a non-bonding electron interacts with a Lewis acid with a vacant orbital, forming an adduct (Scheme 1.4.1).

Scheme 1.4.1: Combination of a Lewis acid and Lewis base to form an adduct. Modified from Stephan.[82]

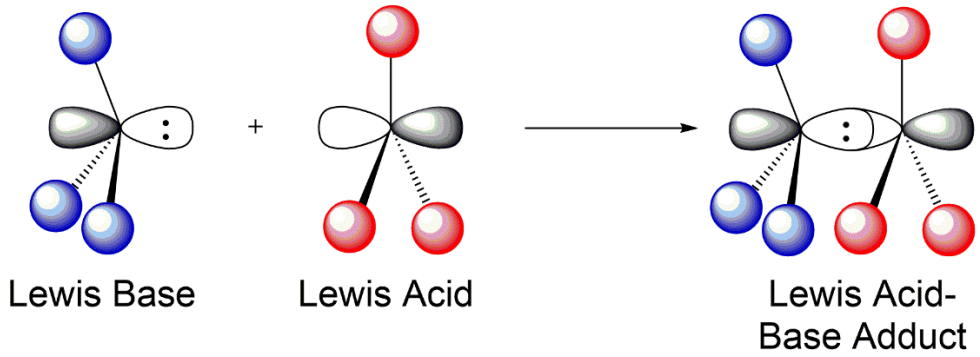

Lewis acids and bases have each found their respective uses in chemical transformations, particularly in organic chemistry. For example, Friedel-Crafts alkylation and acylation are both mediated by Lewis acids such as $AlCl_3$ or AgOTf, during which the Lewis acid abstracts an X^- (X = Cl, Br, I) from an alkyl or aryl halide, which is then sequestered by a nucleophile.[80] Lewis bases, such as phosphines and amines, are archetypal ligands on transition metal catalysts.[81]

1.5 Frustrated Lewis Pairs

While the basis of most chemical reactions is a result of the interaction of both an electrophilic and nucleophilic species, there are systems which deviate from this general motif, as first observed in 1942.[82] Typically, this type of behaviour is due to a significant amount of steric hindrance at one or both element centres (Scheme 1.5.1). The repulsion of the substituents can preclude a close approach of the electrophilic and nucleophilic centres, resulting in no adduct formation, or a “frustration” of the two moieties.

Scheme 1.5.1: A frustrated Lewis pair (FLP) due to steric interference of bulky substituents. Image modified from Stephan.[82]

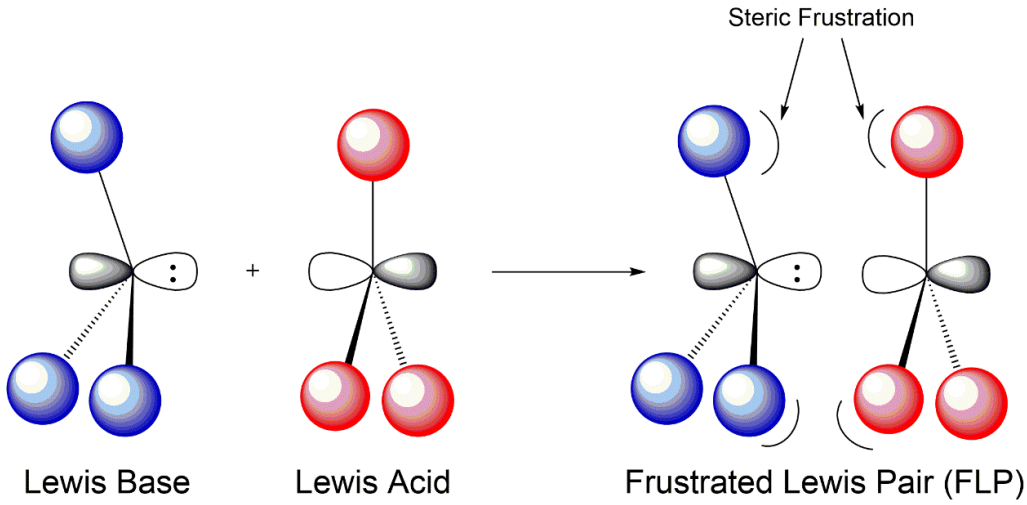

The groups of Stephan and Erker have pioneered a highly successful area of research stemming from this concept of frustrated Lewis pairs, or FLPs.[83–86] While the reactivity of the Lewis acid and base are quenched with respect to each other, their existence as separate fragments allows them to participate in cooperative chemistry. The first reported small molecule activation by an FLP was made by Stephan and co-workers on the cleavage of H_2, using a tethered phosphino-borane, generated from the thermal elimination (>100°C) of H_2 from the phosphonium-borate salt.[87] Remarkably, it was found that at 25°, the compound reacted with H_2 to reform the phosphonium-borate, indicating its ability to cleanly and reversibly activate small molecules (Scheme 1.5.2). The only molecular main group system prior to this to activate H_2 was the digermyne reported by Power and co-workers and discussed previously.[58]

Scheme 1.5.2: Activation of H_2 by a phosphino-borane FLP

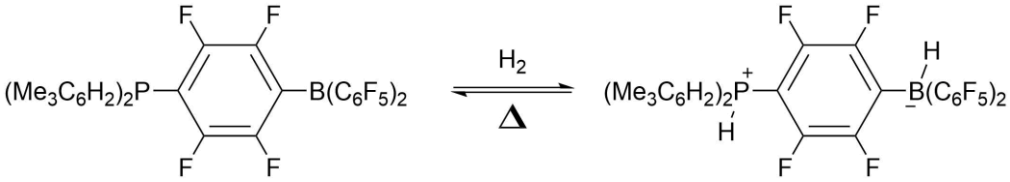

While the reactivity with small molecules on their own is novel, the utility of these compounds in catalytic transformations, as a substitute for traditional transition metal catalysts, is of great interest. The ability of FLPs to reversibly cleave H_2 lends itself well to the idea that these could be used to perform hydrogenations of substrates. In theory, the activation of H_2 by a phosphino-borane or similar compound results in the formation of both a protic and hydridic moiety. As such, these can be envisaged to react with polar substrates through H^+/H^- transfer, regenerating the FLP to carry out the process in a catalytic fashion. Indeed, this is the case with a variety of substrates, and was first reported by Stephan with the catalytic hydrogenation of imines by the phosphonium-borate discussed previously.[88] These types of systems have now been utilized in a variety of hydrogenation reactions including enamines, silylenol ethers, and olefins.[89–91] The discovery of these remarkable complexes is arguably the most feasible opportunity to replace the toxic and costly metals which have been employed in this capacity for decades and as the field continues to develop, the possibility of transitioning from typical metal catalysts towards industrially-viable metal-free alternatives becomes increasingly accessible.

Nonetheless, to continue to push the envelope of application-based main group chemistry, constant evolution and experimentation is required to advance towards the utility that transition metals enjoy. In this vein, interestingly, through all of the research presented above on FLPs, there remains a constant motif of using mostly the same strong donor ligands

such as amines, phosphines, and carbenes as the relevant Lewis base in FLP chemistry. Because of their commercial availability, wide range of structural variety, and relative ease of modification through synthesis, the ubiquity established by these donors is obvious. However, the development of novel Lewis acids to employ in this capacity has not been as well established. In the majority of FLP chemistry, BCF has been the Lewis acid of choice. While it's advantages of NMR nuclei and commercial nature are attractive, it suffers from instability when in contact with air and moisture. As such, the development of new Lewis acids are desirable to further advance this field. One methodology to do this would be to invoke highly electrophilic substituents at the acceptor centre. However, from a synthetic point-of-view, electrophilic substituents such as $-C_6F_5$ are difficult to handle safely and require significant time investment during their preparation. A more straightforward methodology would be to augment the Lewis acidity at the element centre through introduction of a cationic charge and this approach to generating Lewis acids has shown great promise in the application towards FLP chemistry from preliminary reports.[92–95] A greater library of these cationic complexes is needed to examine their viability as Lewis acids, however their electrophilicity is likely to result in their instability. To this end, at least at the onset, stabilizing these cations through a donor-acceptor methodology is an appropriate approach to initially studying these types of complexes.

1.6 Bonding Considerations in Donor-Acceptor Main Group Complexes

Donor-stabilized complexes of main group acceptors can be described using two valid bonding notations. For example, the archetypal cations of cationic group 15 acceptors, known as phosphino-phosphonium cations of the form $[R_3P\text{-}PR'_2]^+$ can be described as featuring either a "coordinate" interaction, or a classical "Lewis"-type bonding environment.

The coordinate notation invokes a phosphine (e.g. trimethylphosphine) ligand on a phosphenium-type (R'_2P^+) acceptor, reminiscent of transition metal phosphine complexes. One can envisage the P-P bond in this model being represented by an arrow (donor→acceptor; Figure 1.6.1a). Alternatively, the Lewis model would dictate a phosphino-substituent bound to a tetravalent phosphonium fragment with a classical Lewis-type bond between the two phosphorus atoms (Figure 1.6.1c). This duality of bonding models has led to the division of the main group community into either supporting or opposing the use of dative-type descriptors for main group compounds.[96–98] As such, the compounds presented in this thesis will generally avoid treating one model as more or less valid than another, and will use a general hybrid description (Figure 1.6.1b). However, relevant computational data describing the distribution of charge and nature of the bonding will be discussed in context of the electronic structure to rationalize observed geometries and reactivities of the resulting complexes.

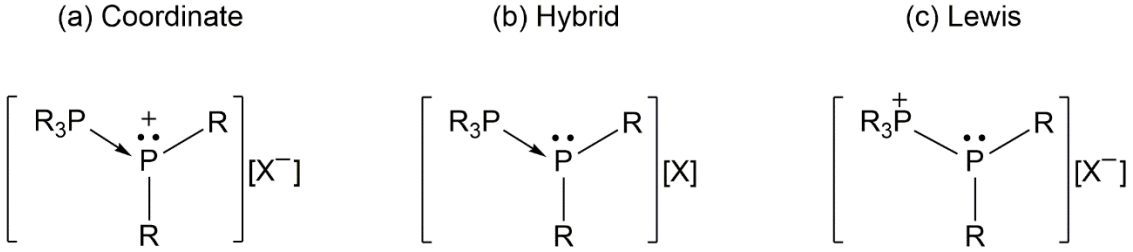

Figure 1.6.1: Coordinate, Hybrid and Lewis notations for the bonding in prototypical phosphino-phosphonium salts.

For derivatives of these compounds featuring the pnictogen elements (R_3Pn-PnR'_2; Pn = N, P, As, Sb, Bi), computational studies of the charge distribution have examined the electronic considerations of bonding,[99–102] and within these studies, complexes calculated to have high positive charge at the 'donor' sites are presented using the Lewis notation.[96]

Ligand exchange reactions are experimentally observed for some of these interpnictogen salts implicating heterolytic bond cleavage/formation, and suggesting coordinate character in these Pn-Pn bonds. A computational study of prototypical pnictenium (R'_2Pn^+) acceptors with amine and phosphine ligands concludes that the character of the Pn-Pn bond in derivatives of $[R_3Pn\text{-}PnR'_2][X]$ is influenced by the substitution at the pnictenium center.[103] We perceive that the character of the Pn-Pn bond varies significantly depending on the elements involved, with the coordinate character greater for the heavier, more metallic elements. It is generally understood that coordinate bonds are significantly longer than Σ_{CR}, and weaker than covalent bonds for which homolytic cleavage is of lower energy than heterolytic cleavage.[104] However, definitive conclusions based on bond length data alone are precluded by other contributing factors including coordination number and oxidation state.

1.7 Synthetic Methodologies

The synthesis of most main group cations has been achieved through the exploitation of a small number of fundamental methods that invoke bond formation through coordinate interactions, and are summarized in Schemes 1.4, 1.5 and 1.6 for the archetypal phosphino-phosphonium complexes. However, these methodologies have been exploited for a variety of main group element centres.

The displacement (or exchange) of a halide substituent by a neutral donor represents a versatile approach to element-element bond formation. Recently likened to the Menschutkin S_N2 reaction of amines with alkyl halides to yield ammonium salts,[105] the example reaction of a chlorophosphine with a trialkylphosphine, for example, yields a P-P bonded cationic

complex $[R_3P\text{-}PR_2]^+$ with a chloride anion,[106] as illustrated generically for Pn-E bond formation in Scheme 1.7.1.

Scheme 1.7.1: Halide displacement from a pnictogen halide by a pnictogen donor to form $[R_3Pn\text{-}PnR_2][Cl]$ salts.

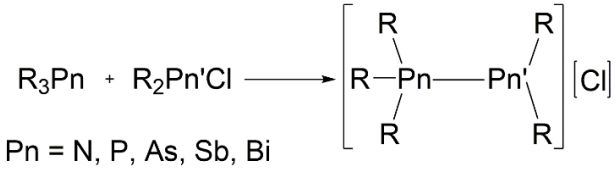

In cases where the neutral halopnictine has insufficient Lewis acidity to engage a ligand, abstraction of the halide with either group 13 halides (EX_3, E = Al or Ga, X = Cl, Br or I) (Scheme 1..6.2a) or *via* a metathesis reaction with a salt of a weakly coordinating anion [OTf, PF_6^-, BF_4^-, ClO_4^-, *etc*.] or ROTf (R = Me or Me_3Si) (Scheme 1.6.2b),[107,108] produces a *pseudo*-phosphenium cation with consequential enhanced Lewis acidity. The reactions are enthalpically driven by the formation of strong element halide bonds, gas evolution, or the lattice enthalpies of resulting ionic products. In cases where residual P-X (X = halide) bonds remain, coincident or subsequent redox coupling of pnictogen centers can also lead to the formation of polycationic species.[109–111]

Scheme 1.7.2: Generic reactions to form $[R_3Pn'\text{-}PnR_2][X]$ salts via halide abstraction by (a) group 13 compounds and (b) salt metathesis.

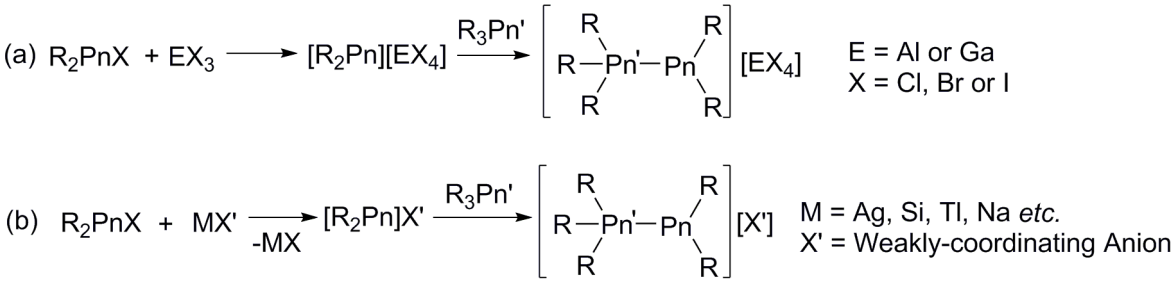

1.8 Scope of Thesis

This dissertation primarily examines the synthesis of cationic complexes of elements of group 13-15 in both their lower and higher oxidation states. In some cases, subsequent investigations into their reactivity were undertaken to examine how the invocation of cationic charges affects their reaction pathways. While parts of the previous sections deal with the stabilization of reactive species with large bulky substituents, it is desired to employ smaller ligands which do not impose steric strain on the molecules to get a better idea of their fundamental structure and bonding. Additionally, while mono- and dications of the *p*-block elements are known, the investigation into the preparation of more highly charged cationic species ($\leq$ +3 charge) is superficial at best. Targeting complexes with higher cationic charge likely means a greater reactivity towards a variety of substrates and potential applications towards Lewis acid catalysis and FLP chemistry.

Chapter 2 describes the synthesis and characterization of a series of group 13 complexes with chelating amine and phosphine ligands. The complexes are examined from a structural standpoint by examining the solid-state structures. In the cases of the cationic complexes obtained, computational data is used to rationalize the formation of the ionic salts, as well as examines the energetics of possible neutral adduct outcomes. Chapter 3 reports the systematic study of Ge(II) and Sn(II) with the prototypical chelating donors 2,2'-bipyridine (bipy) and 1,2-*bis*(dimethylphosphino)ethane (dmpe) to afford cationic triflate salts. These complexes are described in terms of their bonding and computational data is used to examine the charge distribution at the element centre, as well as look at the nature of the donor-acceptor bonding environment. Chapter 4 examines the reactivity of the cationic bipy complexes towards a variety of substrates. Reaction products are assessed spectroscopically

and structurally where available. Computational data is used to examine the nature of the reactions and assess the thermochemistry of the reactions where appropriate. The reactions look to examine both the opportunity of the complexes to act as a Lewis acid and a Lewis base through the presence of both a cationic charge along with a lone pair of electrons. Finally, Chapter 5 details the exploration of polycationic high oxidation-state complexes and a variety of complexes are isolated which exhibit further reactivity due to the increased Lewis acidity. Structural trends of the resulting cations, as well as computational insights into their structure, bonding, and redox chemistry will be discussed.

Chapter 2 - Amine and Phosphine Complexes of Aluminum and Gallium Halides

2.1 Introduction

Aluminum and gallium are prototypical Lewis acids of the *p*-block elements. AlX_3 and GaX_3 are useful in many facets of synthetic chemistry as halide abstractors and homogenous catalysts. Most notable is their employment in Friedel-Crafts reactions for alkyl- or acylations from their strong ion affinity for halides, most notably chlorides, to form $[AlX_4]^-$ or $[GaX_4]^-$ anions. From the perspective of coordination chemistry, they are well known to engage neutral monodentate donors through interaction with the formally vacant *p*-type orbital at the metal centre and are often seen adopting tetrahedral or octahedral geometries. Typically, Al(III) and Ga(III) behave as hard Lewis acids, and are often stabilized with hard Lewis bases such as N- or O-based donors. As such, Al(III) and Ga(III) are often referred to as oxophilic. Most notably, aluminum and gallium species featuring the salen-based ligand framework have seen multiple applications in catalysis for ring-opening processes of lactides and other cyclic esters (Figure 2.1.1).[112]

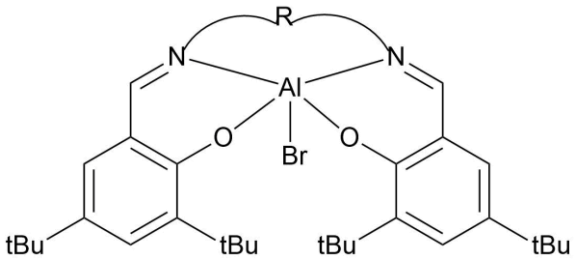

Figure 2.1.1: Aluminum salen complex, similar to those used in ring-opening catalysis.

Interestingly, their chemistry typically differs greatly from that of the other group 13 elements. Boron, being a second-row element, has a much higher electronegativity and as

such, it does not suffer from the same electron deficiency as aluminum and gallium do. Additionally, boron's small size does not typically allow for the same ligation potential as aluminum and gallium, allowing only reasonably small nuclei (F^-, Cl^-, etc.) or molecules (monodentate donors) to engage the boron centre, preferring only a tetrahedral coordination environment. On the contrary, indium has a lesser electronegativity compared to aluminum and gallium. However, due to it's atomic size, it typically adopts much larger coordination numbers than the smaller group 13 elements. Finally, with thallium, Tl(III) complexes are notoriously unstable with regards to redox due to their high reduction potentials. A common example of this is the supposed compound TlI_3, which is actually formulated as $[Tl(I)^+][I_3^-]$ featuring the tri-iodide anion.[113]

As of late, cations of aluminum and gallium continue to receive considerable attention. The first postulated discrete cationic species of gallium was isolated in 1968,[114] while the first aluminum cations, along with their x-ray structure, were isolated in 1984.[115] Since then, a number of aluminum- and gallium-based cations have been prepared, and this area has been recently reviewed.[116,117] However, the vast majority of the complexes characterized to date involve the ligation of Al(III) or Ga(III) by N- or O-based donors. As such, the analogous chemistry with simple, non-sterically imposing alkylphosphines has been superficially developed. In this vein, we set out to investigate the outcomes of reactions of aluminum and gallium halides with monodentate and bidentate phosphine donors, and compare their complexes to those obtained from harder nitrogen-based donors. It should be noted that during the preparation of a manuscript on the cationic aluminum phosphine complexes described in the following section, Levason and co-workers reported the synthesis and characterization of identical compounds.[118]

2.2 Cationic Phosphine Complexes of Aluminum

Cationic complexes of aluminum are known for a variety of different ligands.[116,117] While these seminal reports show the abundance of hard Lewis bases stabilizing cationic aluminum centres, they also reveal the few examples of phosphine-stabilized complexes. This can be rationalized due to the hard Lewis acidic aluminum centre, made more so by invoking a positive charge at the metal centre, preferentially favouring hard nitrogen and oxygen donors over the softer phosphines. Until our study, and the concurrently reported examples,[118] no study of the interaction of bidentate phosphine complexes had been reported.

Treatment of a CH_2Cl_2 solution of AlX_3 (X = Cl, Br, and I) with 1,2-bis(dimethyl-phosphino)ethane led to the quantitative formation of colourless solids of the formula $[AlX_2(dmpe)_2][AlX_4]$ (Scheme 3.1.1). The solids were characterized primarily by ^{31}P and ^{27}Al NMR spectroscopy. In the ^{31}P NMR spectrum, one signal arising from the four equivalent phosphorus atoms was apparent for each of the compounds. For $[AlCl_2(dmpe)_2][AlCl_4]$, the signal was split into a sextet with $^1J_{Al\text{-}P}$ = 156 Hz due to the coupling to the spin 5/2 ^{27}Al nucleus. For both $[AlBr_2(dmpe)_2][AlBr_4]$ and $[AlI_2(dmpe)_2][AlI_4]$, the signal in the ^{31}P NMR spectrum was significantly broadened and the coupling constants could not be obtained (Table 2.2.1). In the ^{27}Al NMR spectrum, a pentet was observed for $[AlCl_2(dmpe)_2][AlCl_4]$ at 1.1 ppm for the coupling to four ^{31}P nuclei. A sharp singlet also appeared at 100.3 ppm for the $AlCl_4^-$ anion. The solid-state structures are presented in Figure 2.2.1. These observations are consistent with the aforementioned report of Levason and co-workers.

Table 2.2.1: $^{31}P\{^{1}H\}$ and $^{27}Al\{^{1}H\}$ NMR chemical shifts for $[AlX_2(dmpe)_2][AlX_4]$

	$^{31}P\{^{1}H\}[^{1}J_{P\text{-}Al}]$ (ppm/Hz)	**$^{27}Al\{^{1}H\}$ $[^{1}J_{Al\text{-}P}]$ (ppm/Hz)**
X = Cl	-40.1 [162]	102.1 ($AlCl_4$) - 0.9 [162]
X = Br	-38.2 [NA]	82.3 ($AlBr_4$) -11.8 [NA]
X = I	-38.7 [NA]	-27.4 (AlI_4) -34.1 [NA]

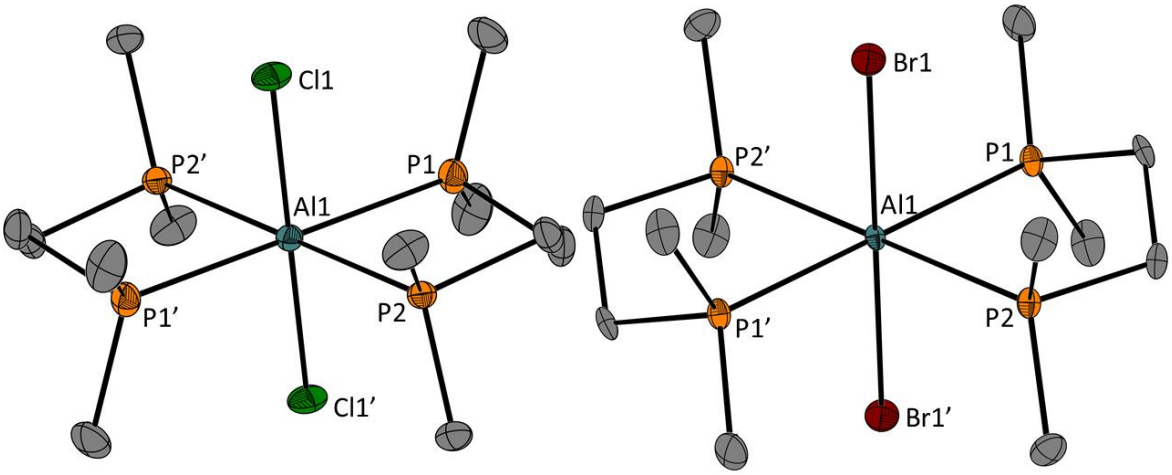

Figure 2.2.1: Solid-state structures of the cations of $[AlX_2(dmpe)_2][AlX_4]$ (X = Cl, Br). Hydrogen atoms and anions are omitted for clarity. Thermal ellipsoids are presented at 50% probability.

Within the unit cell, the asymmetric unit of $[(dmpe)_2AlCl_2][AlCl_4]$ contains two separate cations. The Al-P distances range from 2.4760(5)-2.5170(6)Å, which are shorter than the Al-P interactions in the prototypical neutral molecules $Ph_3P\text{-}AlCl_3$ and are outside of the sum of the covalent radii (Σ_{CR} =2.28 Å).[11] Additionally, the Al-Cl bonds are lengthened, presumably due to the increase in steric crowding at the aluminum centre with the incorporation of two chelating ligands. This could also be rationalized by the donation

of electron density from the phosphorus centres onto the aluminum centre. The closest contact to the $AlCl_4$ anion is an H---Cl contact at 2.769Å, which remains within the sum of the van der Waals radii.[12] The phosphine ligands reside in the equatorial plane of the distorted octahedron, with the chlorides occupying the axial positions. This is in contrast to the structure of a cationic complex featuring a chelating 2,2-bipyridine donor,[13] which features one axial and one equatorial chloride, and the two chelating ligands in a *cis*-configuration. However, this is consistent with results seen previously with gallium and indium featuring chelating phosphine donors.[8] and is likely due to the lower basicity of phosphines compared to pyridine donors, resulting in a *trans* arrangement of phosphorus atoms being more favourable than with pyridine donors. Analogous reactions of other aluminum halides resulted in formation of the corresponding $[(dmpe)_2AlX_2][AlX_4]$ (X = Br, I) ion pairs. Selected structural features of the chloride and bromide derivative are presented in Table 2.2.2

The gas-phase structures were computed at the PBEPBE/6-311+g(d) level of theory and show good agreement with the solid-state structures. The calculated Al-P interactions for the chloride derivative are 2.544 Å and 2.547 Å, and the bromide derivative are 2.553 Å and 2.544 Å. The Al-X bond lengths are found to be 2.320 Å and 2.510 Å for the chloride and bromide derivatives respectively (Table 2.2.2).

Table 2.2.2: Selected experimental solid-state and calculated gas-phase structural parameters for the cations in $[AlCl_2(dmpe)_2][AlCl_4]$ and $[AlBr_2(dmpe)_2][AlBr_4]$

	$[AlCl_2(dmpe)_2][AlCl_4]$	**$[AlBr_2(dmpe)_2][AlBr_4]$**
Al-P1 (Å)	2.5103(5) [2.547]	2.511(2) [2.553]
Al-P2 (Å)	2.4878(5) [2.544]	2.484(2) [2.544]
Al-X in cation (Å)	2.2824 [2.320]	2.4474(9) [2.510]
***cis*-P1-Al-P2 (°)**	82.84(4) [82.7]	82.80(7) [82.7]
***cis*-P1-Al-P2' (°)**	97.16(1) [97.3]	97.20(7) [97.3]
***trans*-P-Al-P (°)**	180 [180.0]	176.66(3) [177.2]
X1-Al-P1 (°)	90.36(1) [90.6]	90.55(5) [90.6]
X1'-Al-P1 (°)	89.65(1) [89.4]	89.45(5) [89.4]
X1-Al-P2 (°)	88.31(1) [88.0]	88.30(6) [88.0]
X1'-Al-P2 (°)	91.69(1) [92.0]	91.70(6) [92.0]
X-Al-X' in cation (°)	179.61(4) [180.0]	177.57(2) [180.0]
Cation-Anion Contact (Å)	3.054 H---Cl	3.036 H---Br

The electronic structure of the cations were also explored computationally (Figure 2.2.2). The HOMO for each of the aluminum complexes are similar with the majority of the electron density on the phosphorus donors in the lone pair-containing orbital. The LUMOs of each of the aluminum complexes shows a slightly more complicated electronic structure with the MO more spread out over the complex. This is rationalized based on the smaller energy difference between the orbitals on aluminum, which results in a higher degree of orbital mixing. Phosphine coordination to the aluminum centre is through the interaction of the phosphorus lone pairs with two of the perpendicular *p*-type orbitals on the aluminum centre (HOMO-2, HOMO-3) which, consequently, also features antibonding Cl-Al-Cl π-type interactions. However, this antibonding interaction is counteracted by the lower energy bonding Cl-Al-Cl π-type interaction (HOMO-6, HOMO-7), which is

consistent with an increased covalency of the Al-Cl bonds due to the augmented electrophilicity of the aluminum centre due to the increase in charge. This is in addition to the Al-Cl σ-bonding MO (HOMO-8). The orbitals on the bromide derivative are very similar in shape and, as such, are not depicted. The only energetic difference is that the Br-Al-Br π-type interactions are the HOMO-6 and HOMO-8, where as the Al-Br σ-bonding MO is the HOMO-7.

Additionally, Natural Bond Order (NBO) calculations were carried out on the cations to examine the degree of charge present on the heteroatoms, as well as the degree of bonding, within the complex (Table 2.2.3). The partial positive charge located on aluminum in the cation are small compared to that on the phosphorus centre, indicating significant delocalization of charge into the dmpe ligands. The chloride derivative has slightly more positive charge on aluminum, rationalized by the higher negative charge located on the chlorine atoms in $[GaCl_2(dmpe)_2]^+$ compared to the bromides in $[GaBr_2(dmpe)_2]^+$. In both cases, the Wiberg Bond Indices (WBIs) show that the Al-P bonding is essentially the same, and is significantly less than unity, implying some ionic character for the Al-P bonds.

Table 2.2.3: NBO partial charges and Wiberg Bond Indices for $[GaX_2(dmpe)_2]^+$, X = Cl and Br.

	Charge (Al)	**Charge (P)**	**Charge (X)**	**WBI (P-Al)**
$[AlCl_2(dmpe)_2]^+$	0.47	0.94	-0.53	0.55
$[AlBr_2(dmpe)_2]^+$	0.37	0.93	-0.47	0.55

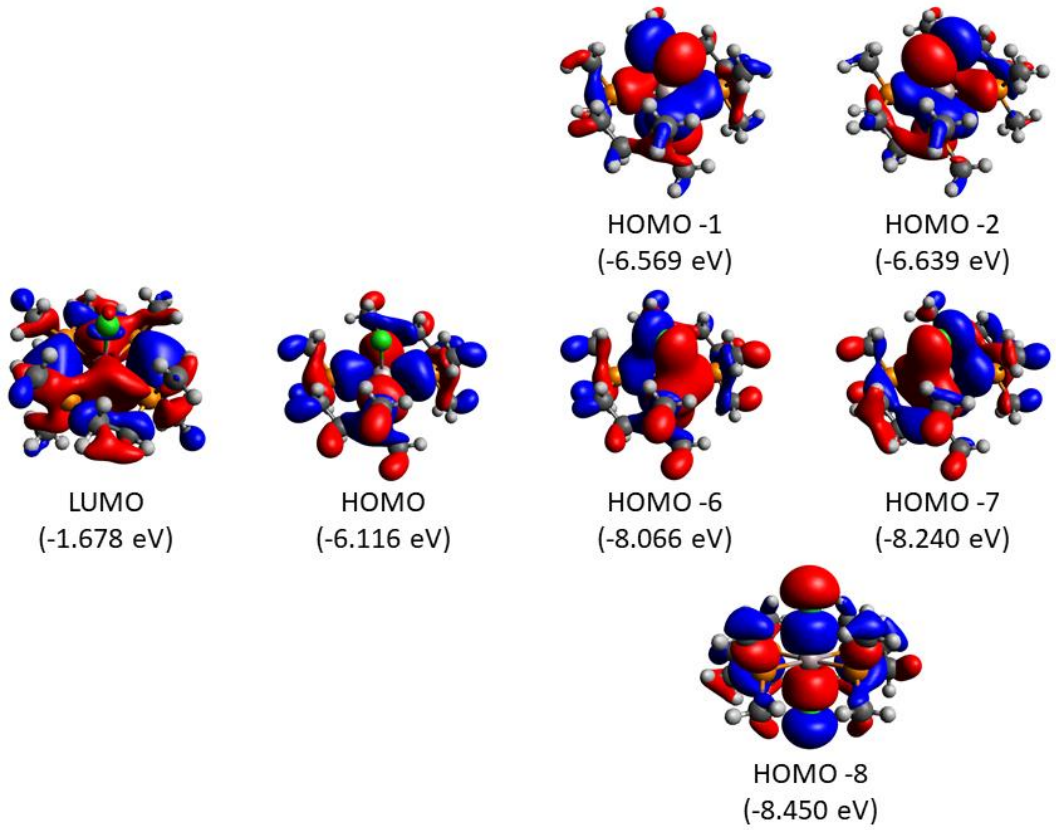

Figure 2.2.2: Calculated (PBEPBE/6-311g+(d,p)) molecular orbitals relevant to the bonding interactions in the $[(dmpe)_2AlCl_2]^+$ cation.

While the preparation and characterization of the cations are reported, there still remains the question of what governs the formation of these complexes. For this, DFT calculations were performed at the B3LYP/6-311g+(d,p) level of theory to examine the thermodynamics of the reaction (Figure 2.2.3). A Born-Haber-Fajans cycle was constructed for $[AlCl_2(dmpe)_2][AlCl_4]$ and $[AlBr_2(dmpe)_2][AlBr_4]$ using experimentally measured enthalpies of vaporization[119] (ΔH_{vap}), and sublimation[120] (ΔH_{sub}), calculated ion affinities for $AlCl_3$ and $AlBr_3$, calculated Al-P bond strengths in the cations, and lattice energies obtained through Volume-Based Thermodynamics.[121] The formation of the cationic complex is thermodynamically driven by the strong halide ion affinity of AlX_3 (to form the tetrahedral AlX_4), the strong Al-P bond strength, and the significant lattice energy. This

leads to an overall reaction enthalpy of -518 kJ mol^{-1} and -442 kJ mol^{-1} respectively for the chloride and bromide derivatives, as presented in Table 2.2.4. As the lattice energy is inversely proportional to the size of the ions, if larger phosphine ligands are employed, a less favourable lattice energy may result, precluding formation of these complexes.

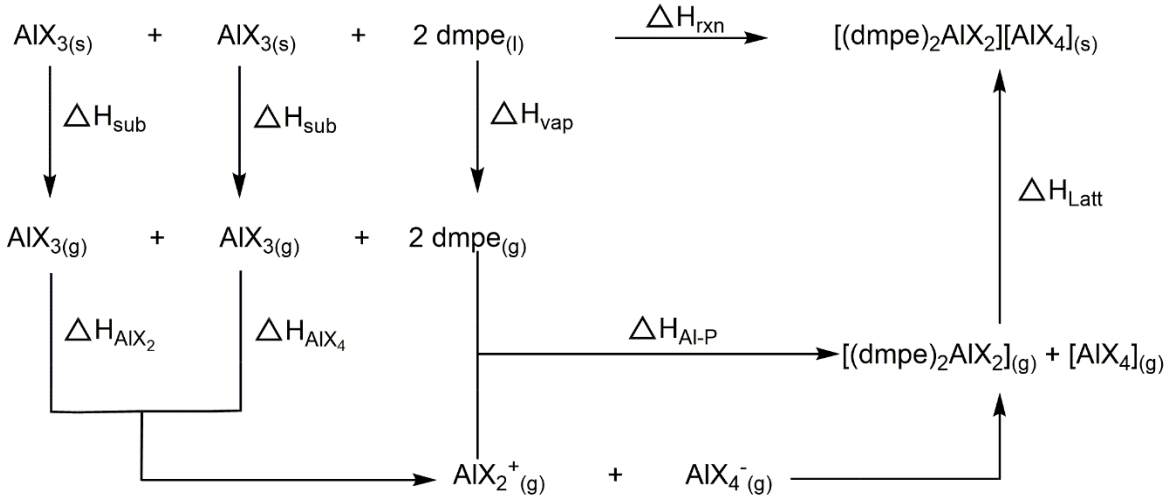

Figure 2.2.3: Born-Haber-Fajans thermodynamic cycles for the formation of the complex $[AlCl_2(dmpe)_2][AlCl_4]$ from an equimolar combination of $AlCl_3$ and dmpe.

Table 2.2.4: Thermodynamic values for Born-Haber-Fajans cycle in Figure 2.2.3, corrected using dichloromethane as solvent. All values are in kJ mol^{-1}.

	ΔH_{sub}	ΔH_{vap}	ΔH_{AlX_2}	ΔH_{AlX_4}	$\Delta H_{Al\text{-}P}$	ΔH_{Latt}	ΔH_{Rxn}
X = Cl	121.0	53.1	387	-321	-570	-363	-518
X = Br	89.9	53.1	350	-173	-545	-360	-442

2.3 Cationic Phosphine Complexes of Gallium

While reports of solid state structures for phosphine complexes of gallium are relatively rare,[122] Levason *et al.* have previously revealed structural diversity for diphosphine complexes of gallium,[123] including a neutral complex of a diphosphine ligand bound to two $GaCl_3$ acceptors (Figure 2.3.1a), an *o*-benzodiphosphine ligand chelating a $GaCl_2^+$ acceptor (Figure 2.3.1b), and two *o*-benzodiphosphine ligands chelating a GaX_2^+

acceptor (Figure 2.3.1c), to give a distorted octahedral environment for gallium. The observed structures have been rationalised on the basis of the electronic and steric features of the diphosphine ligand, and with the expectation that a four-coordinate tetrahedral environment is favoured for gallium. However, as presented in the proceeding section, reactions of gallium(III) halides with the prototypical ligand dmpe preferentially form derivatives of $[GaX_2(dmpe)_2][GaX_4]$ (X = Cl, Br, I) which feature a *pseudo*-octahedral motif. The solid-state structures of the $[GaX_2(dmpe)_2]^+$ cations (Figure 2.3.1d), are analogous to derivatives of (Figure 2.3.1e), despite the absence of a preorganized structure for chelation that is present in an *o*-benzodiphosphine ligand. Moreover, the $[GaX_2(dmpe)_2]^+$ cations are analogous to the structures observed for the cation in $[AlCl_2(dmpe)_2]$ $[AlCl_4]$ presented in the previous section.[118]

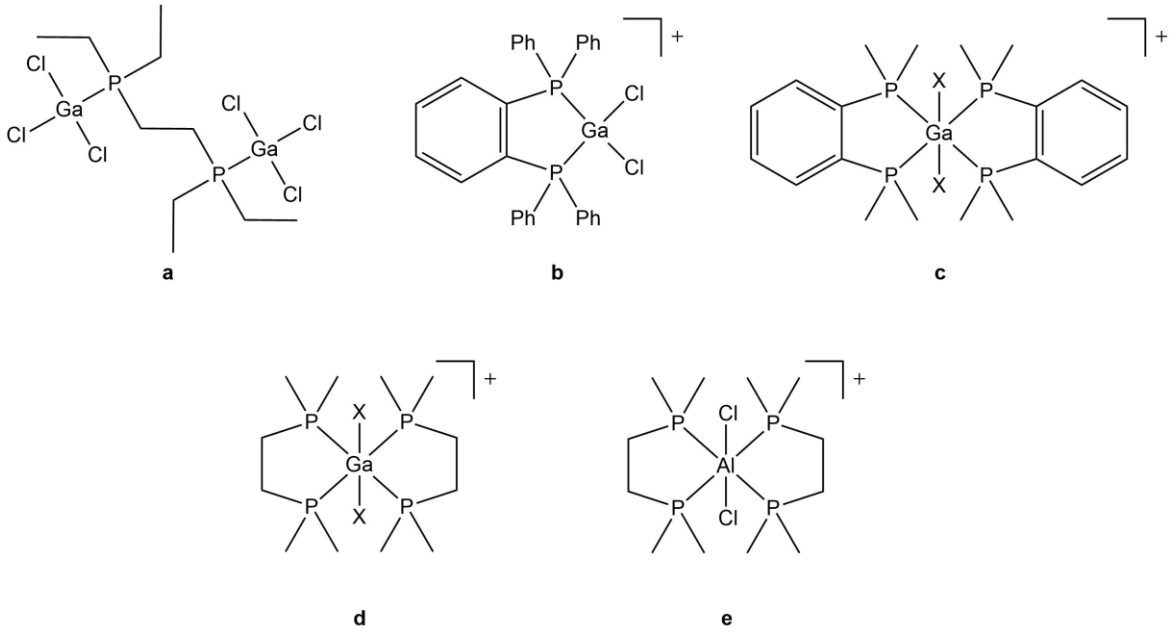

Figure 2.3.1: Examples of phosphine complexes of gallium acceptors

Treatment of $GaCl_3$, $GaBr_3$ or GaI_3 with 1 equiv. of 1,2-*bis*(dimethylphosphino)ethane (dmpe) in CH_2Cl_2 at ambient temperature over 1 h led to the formation of colourless

precipitates in high yields (Scheme 2.3.1). The solids have been characterized as the salts $[GaX_2(dmpe)_2][GaX_4]$. The ^{31}P NMR signal for each complex (X = Cl, -36.2 ppm; X = Br, -39.4 ppm; X = I, -41.0 ppm) appears as a sharp, well resolved singlet as the only signal, shifted downfield relative to the free ligand (-49 ppm). The chloride derivative is the most downfield-shifted, and the iodide derivative is least shifted, consistent with the relative electronegativities of the halogens. Similar to the aluminum complexes, the ^1H NMR spectra exhibit only slight downfield shifts (1.78 ppm and 3.23 ppm), for the methyl and methylene protons respectively, relative to the free ligand (1.43 and 3.02 ppm).

Scheme 2.3.1: Synthesis of $[GaX_2(dmpe)_2][GaX_4]$ ionic salts.

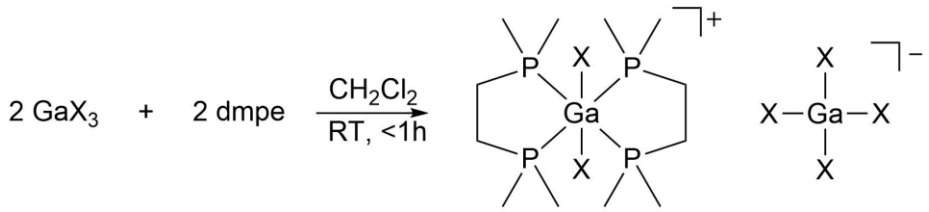

The chloride and bromide derivatives crystallize in the Pbca and P-1 space groups, respectively. In the solid state, the cations $[GaCl_2(dmpe)_2]^+$ and $[GaBr_2(dmpe)_2]^+$ (Figure 2.3.2) show the gallium centre adopting a distorted octahedral geometry with the halogen atoms adopting a *trans*-configuration. The cations are structurally analogous to the previously reported cations shown in Figure 2.3.1c[5] and those presented in the previous section. For $[GaCl_2(dmpe)_2][GaCl_4]$, the Ga1-Cl bond lengths are 2.3691(9) Å and 2.3928(9) Å, which are greater than the sum of the covalent radii for Ga and Cl (Σ_{CR} = 2.23 Å). In the cation of $[GaBr_2(dmpe)_2][GaBr_4]$, Ga1-Br1 [2.6249(4) Å] and Ga1-Br2 [2.4896(5) Å] are much longer than the sum of the covalent radii (Ga-Br Σ_{CR} = 2.38 Å), likely due to the lower electrophilicity at gallium compared to that in the chloride derivative. The Ga1-P bonds range from 2.4684(1) Å to 2.5158(11) Å for $[GaCl_2(dmpe)_2][GaCl_4]$ for

the two molecules in the unit cell, and range from 2.4872(8) Å to 2.5206(9) Å for $[GaBr_2(dmpe)_2][GaBr_4]$, all of which are longer than the sum of the covalent radii (Ga-P Σ_{CR} = 2.35 Å), and is rationalized by the *trans*-influence of the phosphine ligands.[124] The shortest cation-anion contact in either complex is an H---X interaction of 2.989 Å and 3.345 Å, indicating the complex is best described as a tetraphosphine complex of a GaX_2^+ cation with a GaX_4^- counter-anion. Similar structural features are present in $[GaI_2(dmpe)_2][GaI_4]$, although the data was insufficient to provide for reliable bond length analysis.

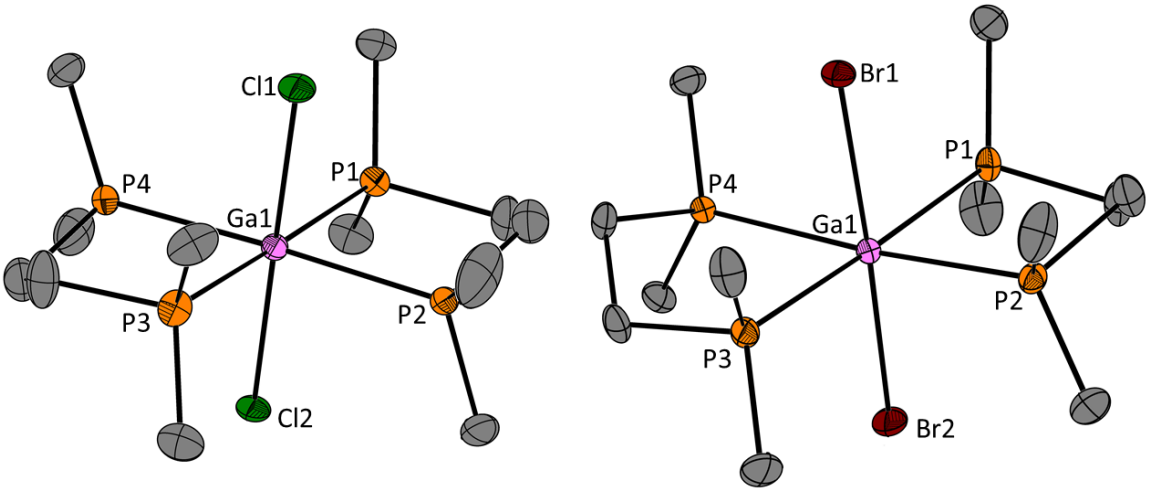

Figure 2.3.2: Structural views of the cations in $[GaX_2(dmpe)_2][GaX_4]$ (X = Cl, Br) in the solid state.

DFT calculations at the PBEPBE/6-311g+(d,p) level of theory provide optimized geometrical parameters for the cations in the gas phase that are in good agreement with those observed in the solid-state structures of $[GaCl_2(dmpe)_2][GaCl_4]$ and $[GaBr_2(dmpe)_2][GaBr_4]$ (Table 1). The calculated Ga-P bond lengths are, on average, 0.069 Å longer in the gas-phase structures. This may be partially due to the long interion H---X contacts with the aliphatic backbone of dmpe in the sold state, which is not modelled in the gas phase. Images

of the HOMO and LUMO of $[GaBr_2(dmpe)_2]^+$ are presented in Figure 3.2.2. The HOMO, similar to that seen in the aluminum complexes, is primarily based on the phosphorus centre, with major contribution from the now bonding orbital containing what were previously the σ-type lone pairs on the phosphorus atoms. In contrast to the aluminum complexes, the LUMO features much more localization on the gallium, due to the greater separation in orbital energies between the phosphorus-based ligand orbitals and the corresponding gallium-based orbitals. The primary interaction in the LUMO is evidently the Ga-X antibonding orbital. In terms of other MOs relevant to bonding within the gallium-centred cations, the shapes of the MOs have the same shape and relative ordering as for $[AlCl_2(dmpe)_2]$ and $[AlBr_2(dmpe)_2]$ in Figure 2.2.2.

Table 2.3.1: Selected experimental solid-state and [calculated gas-phase] structural parameters for the cations in $[GaCl_2(dmpe)_2][GaCl_4]$ and $[GaBr_2(dmpe)_2][GaBr_4]$

	$[GaCl_2(dmpe)_2][GaCl_4]$	**$[GaBr_2(dmpe)_2][GaBr_4]$**
Ga-P1 (Å)	2.5071(11) [2.537]	2.4961(8) [2.555]
Ga-P2 (Å)	2.4684(10) [2.517]	2.4872(8) [2.550]
Ga-P3 (Å)	2.5158(11) [2.537]	2.5003(8) [2.550]
Ga-P4 (Å)	2.4792(10) [2.517]	2.5206(9) [2.559]
Ga-X1 in cation (Å)	2.3928(9) [2.421]	2.6248(4) [2.604]
Ga-X2 in cation (Å)	2.3691(9) [2.421]	2.4897(4) [2.598]
P1-Ga-P2 (°)	83.48(3) [82.9]	83.23(3) [82.9]
P1-Ga-P3 (°)	178.62(4) [180]	175.37(3) [178.2]
P1-Ga-P4 (°)	96.95(4) [97.1]	97.28(3) [97.5]
P2-Ga-P3 (°)	96.46(3) [97.1]	96.48(3) [96.7]
P2-Ga-P4 (°)	177.55(3) [180]	177.96(3) [177.3]
P3-Ga-P4 (°)	83.18(4) [82.9]	82.86(3) [83.0]
Avg. X1-Ga-P (°)	89.73(3) [90.6]	88.35(2) [89.8]
Avg. X2-Ga-P (°)	90.26(3) [89.4]	91.65(3) [90.2]
X1-Ga-X2 in cation (°)	179.31(4) [180.0]	177.57(1) [180.0]
Cation-Anion Contact (Å)	2.989 H---Cl	3.345 H---Br

As for the aluminum derivatives, the NBO partial charges and WBIs were computed for $[GaCl_2(dmpe)_2]^+$ and $[GaBr_2(dmpe)_2]^+$ and are listed in Table 2.3.2. The partial positive charge located on gallium in the cation are small compared to that on the phosphorus centre, indicating significant delocalization of charge into the dmpe ligands. The chloride derivative has slightly more positive charge on gallium, rationalized by the higher negative charge located on the chlorine atoms in $[GaCl_2(dmpe)_2]^+$. In both cases, the WBIs show that the Ga-P bonding is essentially the same, and is significantly less than unity, implying some ionic character for the Ga-P bonds.

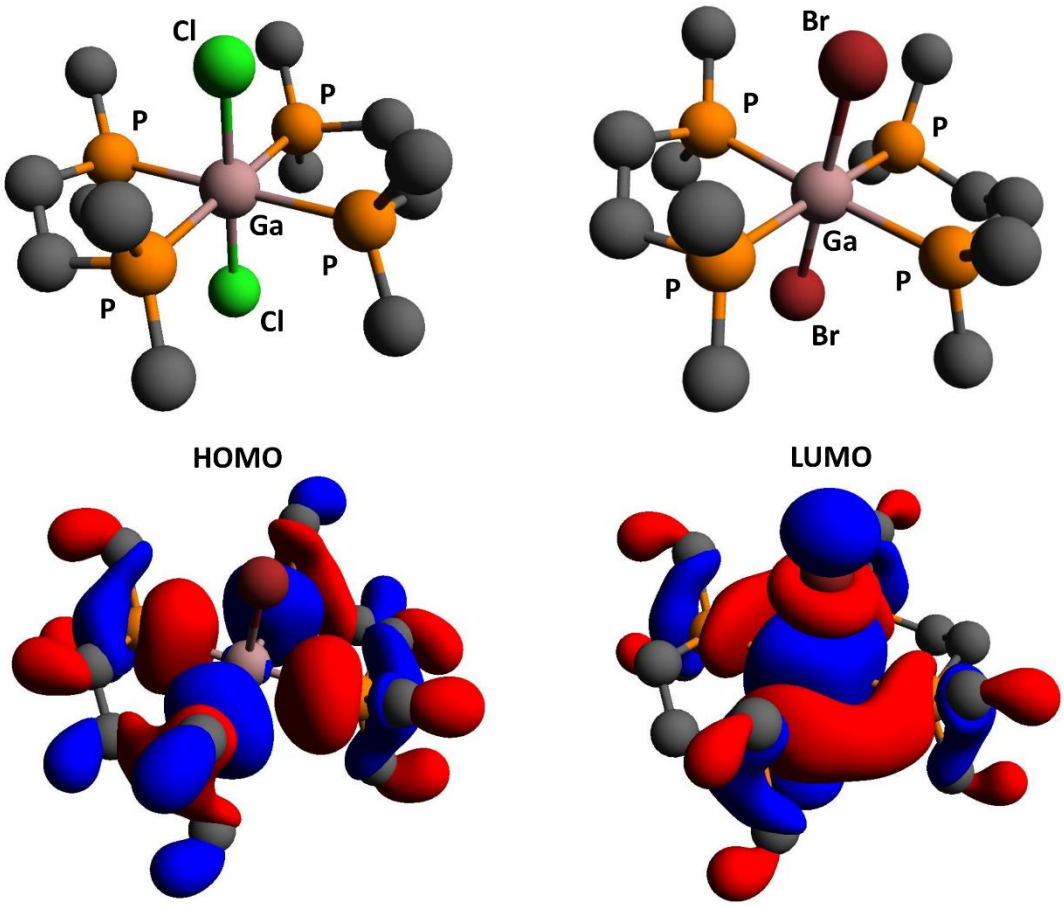

Figure 2.3.3: Gas-phase structures of the cations in $[GaCl_2(dmpe)_2][GaCl_4]$ and $[GaBr_2(dmpe)_2][GaBr_4]$, along with the HOMO (left) and LUMO (right) of $[GaBr_2(dmpe)_2]^+$

Table 2.3.2: NBO partial charges and Wiberg Bond Indices for $[GaX_2(dmpe)_2]^+$, X = Cl and Br.

	Charge (Ga)	**Charge (P)**	**Charge (X)**	**WBI (P-Ga)**
$[GaCl_2(dmpe)_2]^+$	0.30	0.98	-0.53	0.56
$[GaBr_2(dmpe)_2]^+$	0.19	0.98	-0.47	0.56

To assess the thermodynamic factors responsible for formation of $[GaX_2(dmpe)_2][GaX_4]$ in the equimolar reactions of GaX_3 with dmpe, Born-Haber-Fajans cycles were constructed for both $[GaCl_2(dmpe)_2][GaCl_4]$ and $[GaBr_2(dmpe)_2][GaBr_4]$ using

literature values as in the cycles for $[AlX_2(dmpe)_2][AlX_4]$.[119,121,125,126] The energy values labeled in Figure 5.2.3 are listed in Table 2.3.3. Overall, the reactions are exothermic with ΔH_{Rxn} = -431 kJ mol^{-1} and -376 kJ mol^{-1} for $[GaCl_2(dmpe)_2][GaCl_4]$ and $[GaBr_2(dmpe)_2][GaBr_4]$, respectively, and are less than those seen for the aluminum derivatives. These values rely heavily on the two largest exothermic components of the reactions, $\Delta H_{Ga\text{-}P}$ and ΔH_{Lat}. If phosphines with less σ-donor character are used, a smaller stabilization results from Ga-P bond formation. Additionally, ligands which feature larger organic groups are expected to result in lower ΔH_{Lat} due to the inverse proportionality of ΔH_{Lat} mentioned previously, and may favor adduct formation. The large lattice energies are needed to overcome the substantial energy required for the ionization of GaX_3 to GaX_2^+ in the Born-Haber-Fajans cycle. This offers insight into the 1:2 reaction of GaX_3 with an *o*-benzodiphosphine in which significant heating was required to effect formation of salts.[123,127]

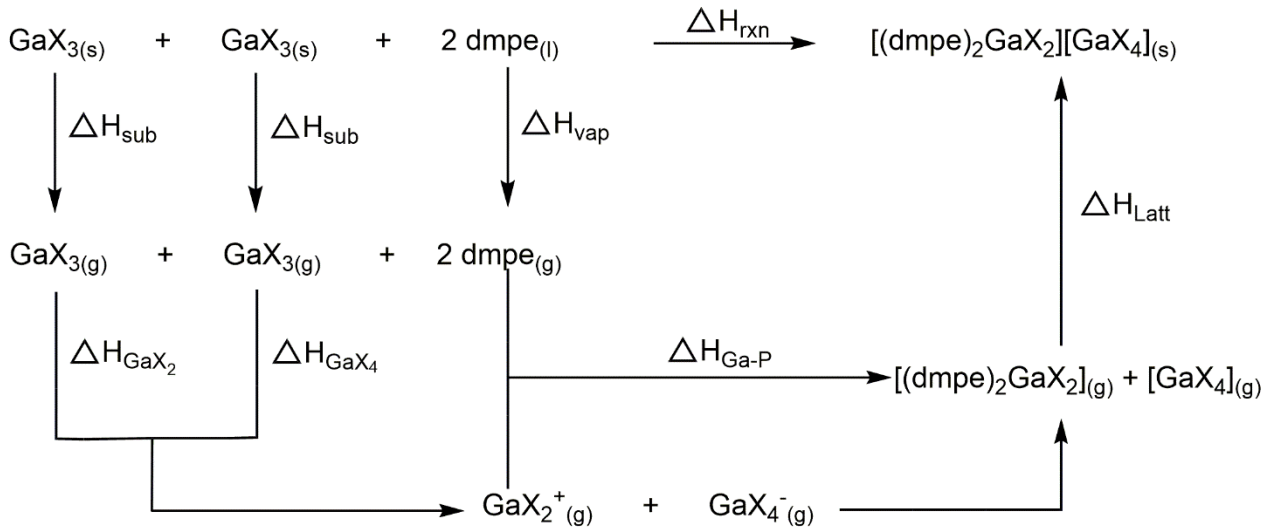

Figure 2.3.4: Born-Haber-Fajans thermodynamic cycles for the formation of $[GaCl_2(dmpe)_2][GaCl_4]$ and $[GaBr_2(dmpe)_2][GaBr_4]$ from an equimolar combination of GaX_3 and dmpe.

Table 2.3.3: Thermodynamic values for Born-Haber-Fajans cycle in Figure 2.3.4, corrected using dichloromethane as solvent. All values are in kJ mol^{-1}.

	ΔH_{sub}	ΔH_{vap}	ΔH_{GaX_2}	ΔH_{GaX_4}	$\Delta H_{Ga\text{-}P}$	ΔH_{Latt}	ΔH_{Rxn}
X = Cl	87.1	53.1	351	-179	-514	-369	-431
X = Br	92.5	53.1	314	-152	-464	-366	-376

2.4 Structural Alternatives to Cationic Molecules

To provide further insight into the formation of structural alternatives, we have used DFT methods to calculate the reaction enthalpies for the gas phase formation of potential neutral outcomes from the equimolar combination of dmpe and MX_3 (M = Al, Ga; X = Cl, Br) listed in Scheme 2.4.1. Scheme 2.4.1a illustrates the coordination of one MX_3 unit to one phosphorus centre of the dmpe ligand, Scheme 2.4.1b illustrates the coordination of MX_3 units to each of the phosphorus centre of one dmpe ligand and a free dmpe ligand,

Scheme 2.4.1c illustrates the bidentate coordination of one dmpe to one MX_3 unit, and Scheme 2.4.1d represents the title reaction to form the separated ion pair in the gas phase.

Scheme 2.4.1: Neutral outcomes for the equimolar reaction of GaX_3 with dmpe

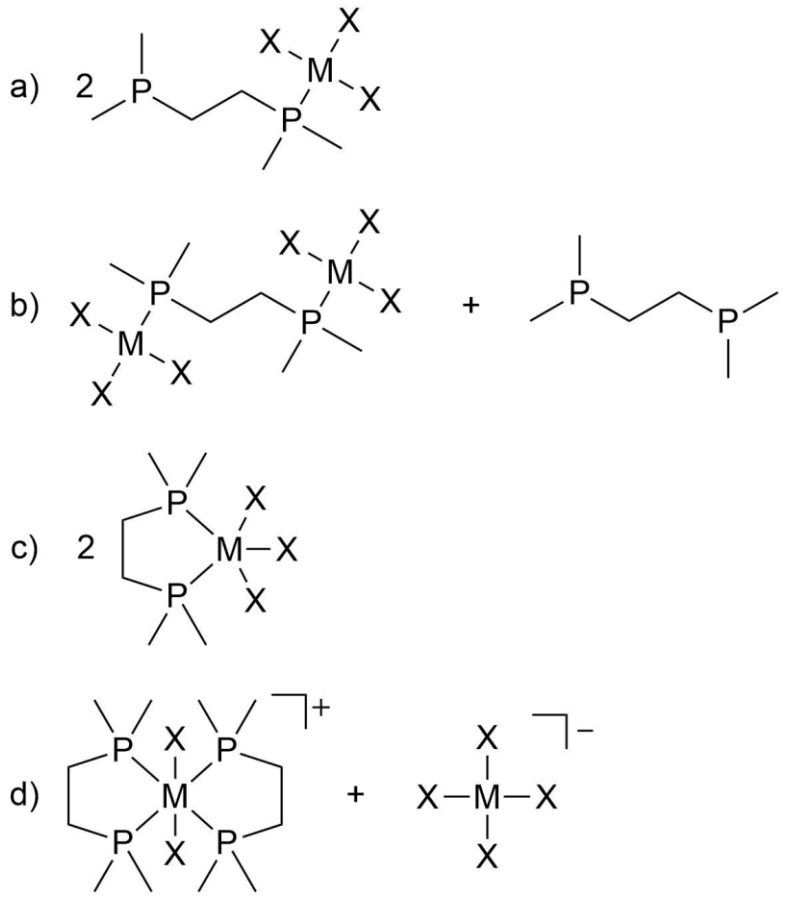

Table 2.4.1: Calculated (solvent-uncorrected) enthalpies for the gas phase equimolar reaction of GaX_3 with dmpe to give the products presented in Scheme 2.4.1.

ΔH_{rxn}	Scheme 2a	Scheme 2b	Scheme 2c	Scheme 2d
M = Al, X = Cl	-295	-287	-260	-91
M = Al, X = Br	-281	-273	-245	-79
M = Ga, X = Cl	-285	-277	-256	-65
M = Ga, X = Br	-260	-253	-229	-35

Table 2.4.2: Calculated (solvent-corrected for CH_2Cl_2) enthalpies for the gas phase equimolar reaction of GaX_3 with dmpe to give the products presented in Scheme 2.4.1

ΔH_{rxn}	**Scheme 2a**	**Scheme 2b**	**Scheme 2c**	**Scheme 2d**
M = Al, X = Cl	-312	-304	-323	-350
M = Al, X = Br	-299	-286	-305	-332
M = Ga, X = Cl	-317	-306	-314	-342
M = Ga, X = Br	-291	-276	-273	-301

Gas-phase calculations were carried out on both uncorrected gas-phase structures, as well as using the Polarizable Continuum Model (PCM) to account for the influence of dichloromethane solvent. To remain consistent and allow comparison between these methods, all energy values are reported as ΔH_{rxn} of equimolar combinations of the phosphine and gallium halide. In the uncorrected calculations, the formation of all neutral compounds is significantly more exothermic than the formation of the separated cation-anion pair in the gas phase for both. However, when correction to account for solvent influence is applied, the formation of the separated cation-anion pair is more exothermic than both the solvent-uncorrected values, as well as all of the neutral adducts. Presumably, this is due to the ability of the polar CH_2Cl_2 to stabilize the separated cation-anion pair, and help to dissipate charge density from the cations. In all cases, the exothermicities for the formation of each of the neutral outcomes are similar and, unsurprisingly, do not vary to the same extent when solvent correction is introduced as there is a lessened need of charge dissipation. It is interesting that, as the formation of the neutral compounds are energetically similar to those of the ion pairs, there may be a fluxional nature to these compounds in solution. This is

supported for the complexes by the sharp singlets observed in the ^{31}P NMR, as opposed to the observation of $^{27}Al/^{31}P$ or $^{69/71}Ga$ -^{31}P spin-spin coupling, indicating the system may be kinetically labile and may undergo exchange processes and/or isomerization. As such, we postulate that the formation of the ionic salts in solution is viable due to the charge dissipation offered by the polar CH_2Cl_2 solvent and their isolation in the condensed phase is made possible by the significantly exothermic lattice energy.

2.5 Amine Complexes of Aluminum and Gallium Halides

Compared to phosphorus donors, the analogous nitrogen donors are considered to be harder donors due to the small atomic radius and less diffuse orbitals on the nitrogen atoms. As such, it is expected that they lead to the formation of different complexes than those obtained from the reactions of AlX_3 or GaX_3 with the softer phosphine donors. In this regard, we set out to examine how the electronic difference between nitrogen and phosphorus affect the product formed from their equimolar reactions, while maintaining an identical steric environment. As such, N,N,N',N'-tetramethylethylene diamine (tmeda) was employed as the ligand of choice, and is analogous to dmpe in terms of chemical structure.

Previously, it has been shown that subjecting AlX_3 and GaX_3 to 2:1 mixtures of MX_3:en and MX_3:tmeda (M = Al, Ga; X = Cl, Br, I; en = ethylenediamine) to form ionic structures of the type $[LMX_2][MX_4]$, where L = en or tmeda, in the solid state from a melt-approach synthesis.[128] However, in all cases, the melts were subject to temperatures above 170°C, and in come cases, reaching upwards of 300°C, with the absence of solvent. We set out to examine whether, at milder reaction conditions, the same preference for ionic structures applies with a 1:1 stoichiometry as is the case with the dmpe complexes

previously discussed as the lack of significant heating should affect the overall complex type obtained from the reaction.

Treatment of CH_2Cl_2 solutions of the aluminum or gallium halide with tmeda afforded colourless solids which were readily soluble. The ^{27}Al NMR spectra of the tmeda:AlX_3 complexes show sharp singlets as the only quantitative signals, which are centred between 40-100 ppm. In solution, this is indicative of neutral adduct formation, compared to the ionic nature of the dmpe complexes which show two signals for the cation and anion pair. For both the aluminum and gallium complexes, the ^{1}H and ^{13}C NMR spectra show a single set of resonances for the tmeda framework.

In the solid state, it was found that the complexes of aluminum adopt neutral structures of the form (tmeda)AlX_3 (Figure 3.3.1). The aluminum centre adopts a *pseudo*-trigonal bipyramidal geometry with one of the nitrogen atoms and a halide in the axial position, and the remaining nitrogen atom and two chlorides adopting the equatorial positions. The bond distances for N1-Al are all very similar, ranging between 2.0802(10) Å and 2.097(3) Å. There is greater variation, however, in the axial N2-Al bond distances. The general trend shows a shortening of the N2-Al bond distance as the Al-X3 bond distance elongates. As the bond elongates, there is likely less efficient Al-I bonding, weakening the bond, and allowing a more effective N-Al bonding interaction. Presumably, this is due to a *trans*-influence phenomenon as having a strong electron-donating nitrogen in the axial position forces the elongation. Additionally, it is likely more favourable to have one nitrogen in the equatorial position and one in the axial position than both nitrogen atoms occupying the equatorial plane as the halides are typically good leaving groups during an S_N2-type process. One can envisage the elongation of the Al-X bond as an intermediary between fully bound

and fully dissociated on the S_N2-type reaction coordinate. This type of phenomenon has been observed previously in prototypical phosphine complexes of antimony halides.[124]

For the complexes of gallium halides, the progression from bound to unbound halide is even more pronounced. For $GaCl_3$, the neutral complex (tmeda)$GaCl_3$ is obtained, and is analogous in structure to the aluminum complexes (Figure 2.5.1). The Ga-Cl bond lengths range from 2.2141(3) Å to 2.2964(3) Å, with the longest Ga-Cl bond being *trans* to the axial nitrogen. However, with $GaBr_3$ and GaI_3, ionic salts of the form [(tmeda)GaX_2][GaX_4] are formed, leaving a half-equivalent of unreacted tmeda, as confirmed by ^{1}H NMR of the reaction mixture when the reaction was carried out in CD_2Cl_2, with a second set of tmeda resonances. The dissociation of the halide can be considered the culmination of the S_N2-type process discussed with the aluminum complexes. Indeed, in both cases, the Ga---X3 contact is outside of the van der Waals radii for the respective atoms (Σ_{vdW} Ga-Br: 3.70 Å; Σ_{vdW} Ga-I: 3.85 Å).[129] However, other factors could also influence the formation of molecular vs ionic complexes, including differing bond dissociation energies between Ga-Cl vs Ga-Br/I, as well as the lattice energies of the resulting salts.

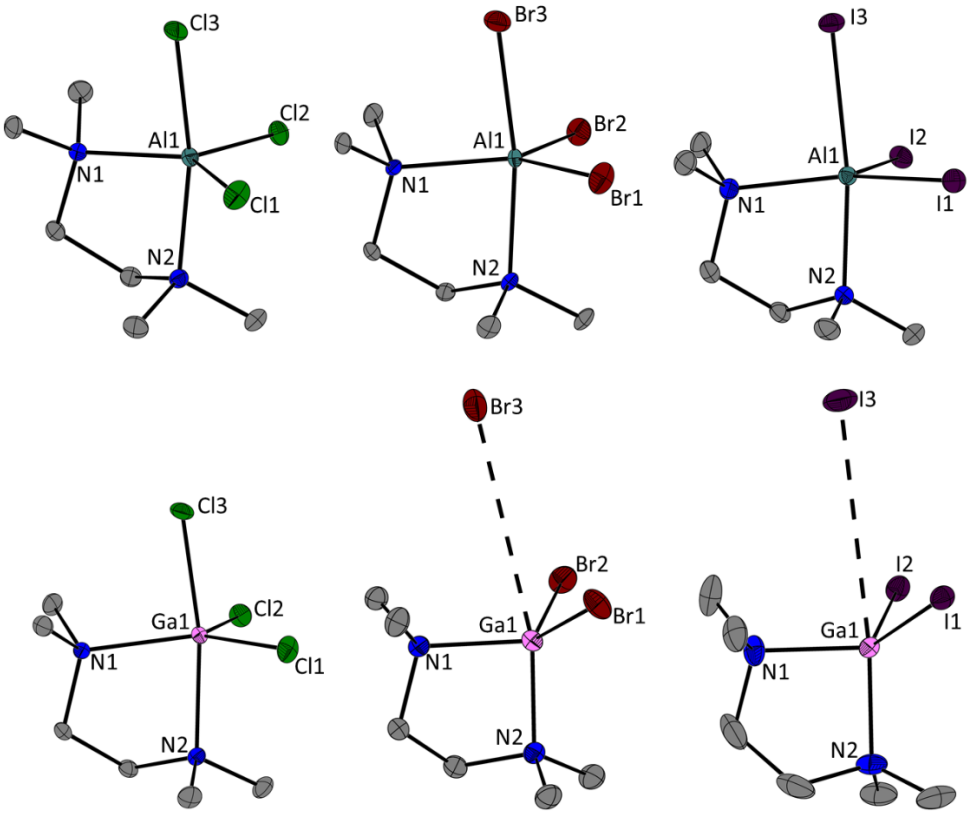

Figure 2.5.1: Solid-state structures of the complexes formed from the reaction of aluminum and gallium halides with tmeda. Ellipsoids presented at the 50% probability level.

Table 2.5.1: Selected structural parameters for (tmeda)AlX_3 complexes

	(tmeda)$AlCl_3$	**(tmeda)$AlBr_3$**	**(tmeda)AlI_3**
Al1-N1 (Å)	2.0802(10)	2.084(3)	2.097(3)
Al1-N2 (Å)	2.1161(10)	2.105(3)	2.095(2)
Al1-X1 (Å)	2.1883(5)	2.3367(11)	2.6152(8)
Al1-X2 (Å)	2.1753(4)	2.3220(11)	2.5778(8)
Al1-X3 (Å)	2.2481(5)	2.4096(12)	2.7373(8)
N1-Al1-N2 (°)	81.55(4)	81.74(12)	81.96(9)
N1-Al1-X1 (°)	135.49(3)	137.40(9)	140.77(7)
N1-Al1-X2(°)	108.11(3)	108.35(9)	105.93(7)
N1-Al1-X3 (°)	89.86(3)	89.93(9)	91.41(7)
N2-Al1-X1(°)	88.65(3)	89.65(9)	89.80(7)
N2-Al1-X2(°)	93.50(3)	94.84(9)	97.26(7)
N2-Al1-X3 (°)	168.23(3)	167.91(10)	168.03(7)
X1-Al1-X2 (°)	115.78(2)	113.93(4)	113.16(3)
X1-Al1-X3 (°)	91.919(18)	90.60(4)	89.08(2)
X2-Al1-X3 (°)	96.830(18)	96.11(4)	94.13(2)
Σ_{eq} Angles (°)	359.38(3)	359.67(9)	359.85(7)

Table 2.5.2: Selected structural parameters for (tmeda)$GaCl_3$ and [(tmeda)GaX_2] [GaX_4] complexes

	(tmeda)$GaCl_3$	**[(tmeda)$GaBr_2$] [$GaBr_4$]**	**((tmeda)GaI_2] [GaI_4]**
Ga1-N1 (Å)	2.1188(9)	2.018(2)	2.030(5)
Ga1-N2 (Å)	2.1776(10)	1.996(2)	2.030(5)
Ga1-X1 (Å)	2.2233(3)	2.2674(5)	2.4957(5)
Ga1-X2 (Å)	2.2141(3)	2.2763(4)	2.4957(5)
Ga1-X3 (Å)	2.2964(3)	4.2602(5) (to anion)	4.3626(4) (to anion)
N1-Ga1-N2 (°)	80.94(4)	89.46(10)	89.9(3)
N1-Ga1-X1 (°)	135.39(3)	113.34(7)	111.84(17)
N1-Ga1-X2(°)	108.85(3)	112.39(7)	111.31(18)
N1-Ga1-X3 (°)	90.03(3)	79.03(7) (to anion)	83.6(3) (to anion)
N2-Ga1-X1(°)	88.75(3)	113.12(7)	111.31(18)
N2-Ga1-X2(°)	91.61(3)	109.47(7)	111.84(17)
N2-Ga1-X3 (°)	167.97(3)	165.65(7) (to anion)	171.49(3) (to anion)
X1-Ga1-X2 (°)	115.884(13)	116.05(2)	117.40(3)
X1-Ga1-X3 (°)	92.194(13)	79.64(1)	66.54(3)
X2-Ga1-X3 (°)	96.748(13)	67.99(1)	75.78(3)
Σ_{eq} Angles (°)	360.12(3)	--	--

2.6 Summary

Several series of phosphine and amine complexes of aluminum and gallium halides have been synthesized and structurally characterized. It is evident that the nature of the ligand and metal halide are both important factors in determining the outcome of the reaction. Through equimolar reactions with the less nucleophilic chelating phosphine dmpe, *pseudo*-octahedral complexes of the type [(dmpe)MX_2][MX_4] are formed exclusively. It is evident from the Born-Haber-Fajans cycle that the driving force behind the reaction is the

strong M-P bond energies, as well as the large lattice energies present in the ionic salts. However, based on gas-phase reactions, it was suggested that neutral 1:1 complexes are stable, and energetically accessible based on DFT calculations. Additionally, computational data shows that employing a polar solvent plays a crucial role in the formation of the complexes by dissipating charge within the complex. Additionally, there is a large degree of charge delocalization from the metal centre on to the ligands within the cations, and there is a degree of iconicity to the M-P bonds.

Access to neutral and cationic complexes from the equimolar reactions of tmeda with aluminum or gallium halides were shown to give either neutral or cationic products depending on the metal halide used. For aluminum halides, the resulting products were neutral chelate complexes which featured a *pseudo*-trigonal bipyramidal geometry at the aluminum centre, with two halides and a nitrogen atom in the equatorial plane and a halide and the other nitrogen atom in the axial positions. The axial halide exhibited a much longer Al-X bond distance, due to the *trans*-labilizing effect of the axial nitrogen atom. These complexes can be regarded as "snapshot" intermediaries on an S_N2-type reaction pathway between completely bound to completely unbound halide substituents. The analogous reactions of gallium halides show an even more marked S_N2-type reaction pattern, as the bromide and iodide complexes are, in fact, ionic with the axial halide completely dissociated to form a tetrahalogallate anion with a contact outside of the van der Waals radii.

Chapter 3 - Donor-Acceptor Complexes of Ge(II) and Sn(II) Cations

3.1 Introduction

The chemistry of the heavier tetrel elements (Group 14 – Si, Ge, Sn, Pb) are often compared to the chemistry of carbon due to their isolobal relationship. However, the chemical properties of the heavier carbon-like elements differ greatly even in their atomic form. Spanning a range of atomic sizes, and existing as non-metals, metalloids, and metals, the chemistry of group 14 compounds is as diverse as the elements themselves. Carbon, the smallest of the elements, typically exists as either amorphous carbon, graphite, or diamond, each with their own distinct structure and properties. Carbon also likes to form neutral catenated structures, known as hydrocarbons, which are kinetically stable with respect to reactivity with other compounds.[130] In contrast to this, the rest of the group 14 elements are usually found in binary ores (oxides and sulfides) in the earth's crusts and the "atomic" forms of these elements are a rare find in a natural setting.[131,132] Additionally, analogous neutral catenated compounds of Si, Ge, Sn, and Pb are very uncommon due to the low strength of E-E single bonds.[133] Instead, tetrels will often form Zintl clusters (anionic homo- and heteroatomic clusters) upon reduction, similar to boranes and carboranes, and do follow a modified Wade's rules motif (Scheme 3.1.1).[134,135]

Scheme 3.1.1: Classical synthesis of the prototypical Zintl phase of K_4Sn_9.[136,137]

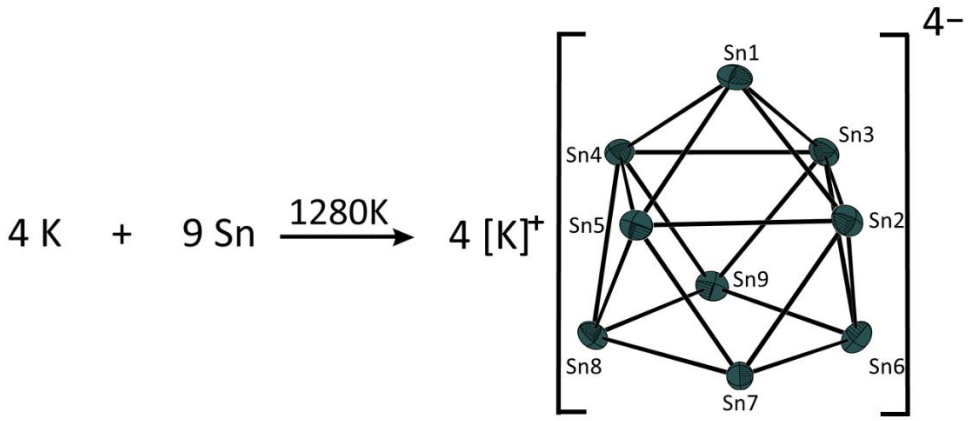

One consideration for group 14 is the possibility of two different oxidation states. Unlike the group 13 elements, stable complexes can be envisaged for both E(II) and E(IV) centres (E = group 14 element). For complexes of E(II) acceptors, which will be the focus of the following chapter, the presence of a stereochemically-active lone pair can potentially result in different structural conformations. In these cases, it is likely that the obtained complexes will conform to an AX_nE geometry, according to VSEPR theory. As there are fewer sites available for ligand bonding, the resulting complexes of E(II) centres will have lower coordination numbers. However, depending on the types of ligands employed (monodentate, bidentate chelates, bidentate bridging, etc.), a diverse range of structural outcomes is still possible despite the lower coordination numbers invoked at the element centre due to the presence of the lone pair.[138,139] Additionally, the presence of a lone pair often precludes ligand coordination due to the increased electron density. To augment the Lewis acidity and diminish the electronic role of the lone pair, the introduction of a cationic charge (up to +2

for E(II) centres) is desirable to allow access to a greater structural diversity of ligand-stabilized E(II) centres.

3.2 Cationic 2,2'-Bipyridine Complexes of Ge(II) and Sn(II)

Coordination complexes of the group 14 elements have been developed with a variety of donors, including crown ether,[140,141] cryptand,[142] azamacrocycle,[141] and carbene[143] ligands. These complexes involve the encapsulation of the metal centre by the frame of the ligand and/or the steric presence of the substituent on the ligand and can preclude further reactivity. In contrast, smaller chelating ligands, such as those based on 2,2'-bipyridine (bipy), offer strong donor centres within a planar framework that does not impose steric shielding of the acceptor centre.

Recently, a series of complexes with the generic formula $[(bipy)_2Pn]^{3+}$ (Pn = P, As, Sb, Bi) have been synthesized and show how the cationic charge enhances the Lewis acidity of the p-block centre.[101,144] In contrast to phosphine complexes of highly charged pnictogen acceptor centres that are susceptible to ligand oxidation with concomitant reduction of the pnictogen centre,[145–147] complexes involving the bipy ligand are more resistant to redox chemistry. Consequently, these complexes can be used to study redox chemistry at the pnictogen centre without affecting the ligand.[144] Contrary to the complexes of the pnictogen elements, a systematic study of these prototypical bidentate ligands has not been undertaken with cationic Ge(II) or Sn(II) centres, although bipy complexes of Pb^{2+} have been structurally authenticated.[148] As such, it was our goal to expand the coordination chemistry of the tetrel elements using the classical bipy ligand which engage cationic Ge(II) and Sn(II) centres hemispherically, leading to the complexes presented in this chapter. The triflate salts are isoelectronic with the pnictogen complexes $[(bipy)_2As]^{3+}$ and $[(bipy)_2Sb]^{3+}$ described

above, and a comparison of their structural parameters, as well as gas-phase structures, is presented.

Reactions of $GeCl_2$·dioxane or $SnCl_2$ with bipy in the presence of trimethylsilyl trifluoromethanesulfonate (TMSOTf) occur rapidly at room temperature, as observed by NMR spectra of the reaction mixtures. The stoichiometry of the reaction mixtures determines the formation of [(bipy)ECl][OTf], and $[(bipy)_2E][OTf]_2$ (E = Ge and Sn), which have been isolated and comprehensively characterized, including ^{119}Sn NMR spectroscopy for E = Sn. Equimolar mixtures of TMSOTf, bipy, and the ECl_2 reagent results in [(bipy)ECl][OTf] exclusively. Likewise, combination of one equivalent of ECl_2 with two equivalents each of bipy and TMSOTf results in $[(bipy)_2E][OTf]_2$. In the absence of the halide abstractor, equimolar combination of bipy with either $GeCl_2$·dioxane or $SnCl_2$ were found to be consistent with the previously reported[149,150] neutral adducts $(bipy)GeCl_2$ and $(bipy)SnCl_2$. These complexes are only sparingly soluble and can be isolated as bright yellow powders in excellent yield. These complexes can be used as starting materials to access either [(bipy)ECl][OTf] or $[(bipy)_2E][OTf]_2$, through the combination of the adducts with either one equivalent of TMSOTf, or with two equivalents of TMSOTf with one equivalent of bipy respectively. This synthetic route is advantageous as the conversion of the bright yellow neutral complexes to colourless monocations, and subsequently the yellow dicationic complexes, can be easily distinguished visually. The various synthetic routes are summarized below in Scheme 3.2.1.

Scheme 3.2.1: Synthetic routes to (bipy)ECl_2, [(bipy)ECl][OTf] and [$(bipy)_2$E][$OTf]_2$ (E = Ge and Sn)

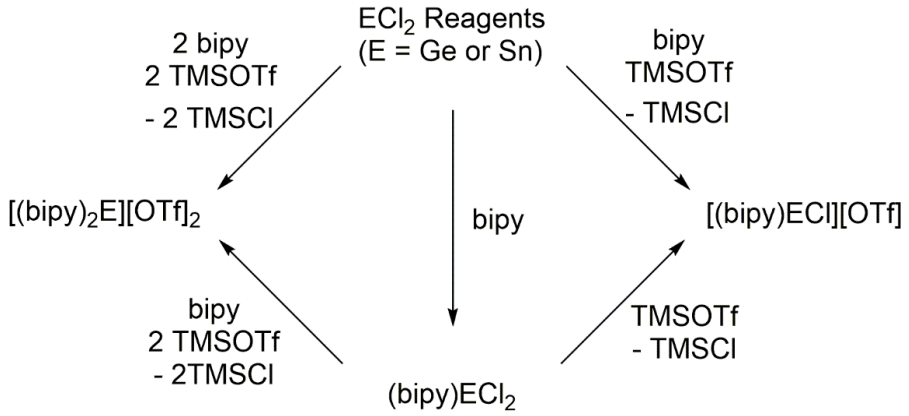

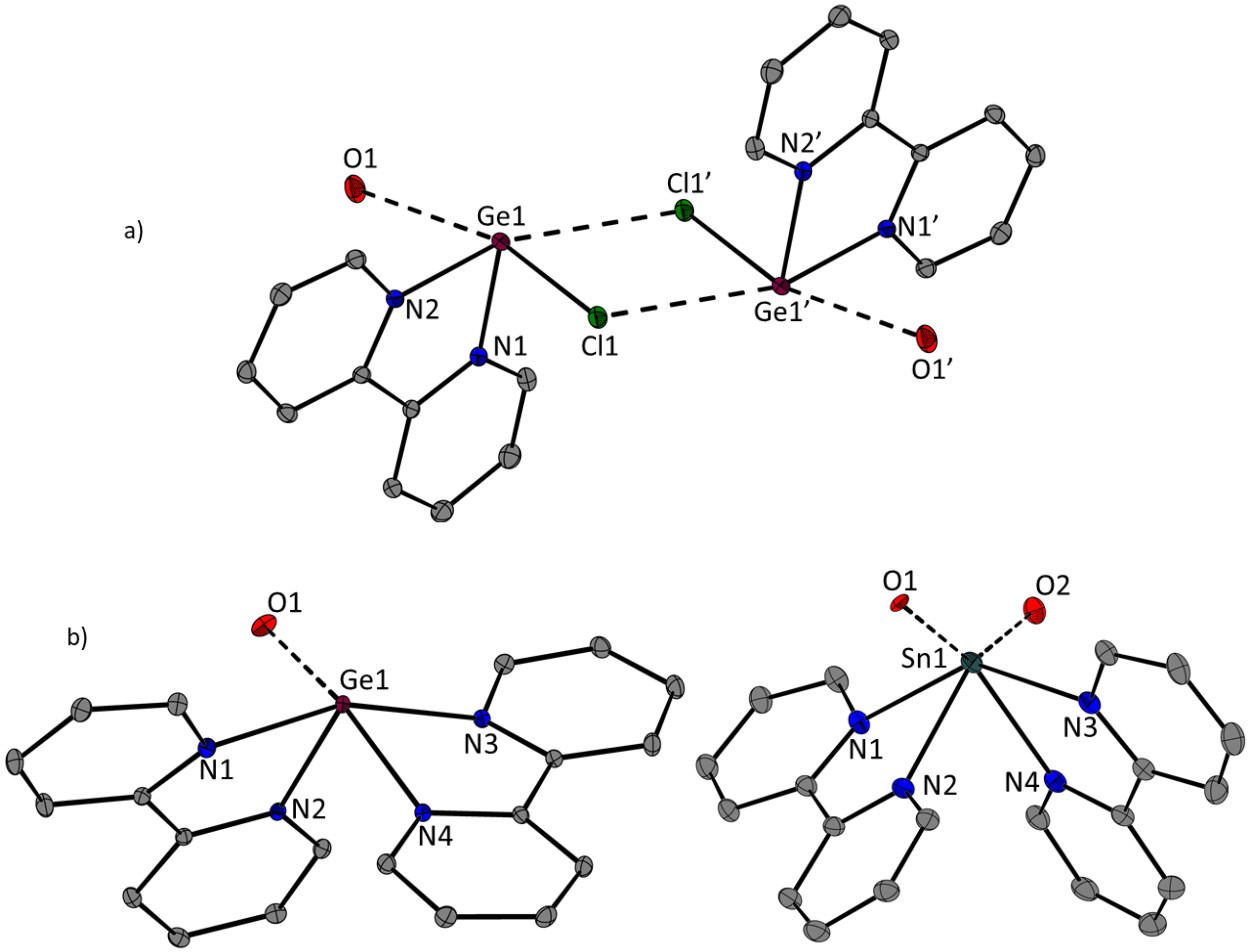

Figure 3.2.1: a) Coordination dimer formed in the solid-state structure of the [(bipy)GeCl][OTf] and b) Solid-state structures of dications $[(bipy)_2Ge][OTf]_2$ and $[(bipy)_2Sn][OTf]_2$ showing oxygen atoms of the closest contacting triflate anions. Thermal ellipsoids are shown at the 50% probability level. Hydrogen atoms are omitted for clarity.

In the solid state (Figure 3.2.1), the Ge centre of $[(bipy)GeCl]^+$ adopts a trigonal pyramidal molecular geometry and the Ge and Sn centres of $[(bipy)_2E]^{2+}$ adopt a distorted see-saw molecular geometry. The Ge-N distances of 2.063(2) Å and 2.092(2) Å in $[(bipy)GeCl]^+$ (Table 1) are slightly longer than the sum of the Ge-N covalent radii (Ge-N Σ_{CR} = 1.92 Å), and are consistent with those in the previously reported $[(bipy)GeBr][GeBr_3]$.[149] A cation-anion contact in [(bipy)GeCl][OTf] at a distance of 2.827(2) Å imposes a see-saw geometry at germanium. This is consistent with the structure reported for $(bipy)GeCl_2$, which also adopts the see-saw geometry, although the observed

structure was found to be an artifact of the solid-state packing from contacts with nearby molecules, and not an energetic global minimum, which was found to be a cis-chloride structure, for the isolated gas-phase molecule.[149] Cation-anion contacts in the solid-state structures of $[(bipy)_2Ge][OTf]_2$ (2.9276(9) Å and 3.348(1) Å) and $[(bipy)_2Sn][OTf]_2$ (2.786(6) Å and 3.190(6) Å) impose a distorted octahedral molecular structure for the tetrel centre with the bipy ligands in a *cis* configuration, due to the stereochemically-active lone pair. In all cases, the Ge---O contacts are outside of the sum of the covalent radii (Σ_{CR} = 1.84 Å),[151] but within the sum of the van der Waals radii (Σ_{vdW} = 3.63 Å).[152] The *trans*-configured (axial) Ge-N bonds in $[(bipy)_2Ge][OTf]_2$ (2.228(1) Å and 2.237(1) Å) are significantly longer (Table 3.2.1) than those in *cis*-configured equatorial positions (2.091(1) Å and 2.097(1) Å) consistent with the *trans*-effect. Distinction between the Sn-N bond lengths in $[(bipy)_2Sn][OTf]_2$ is less obvious (axial: 2.389(5) Å and 2.387(5) Å: equatorial: 2.373(6) Å and 2.357(6) Å) due to a greater distortion from a see-saw geometry, as evidenced by the smaller inter-ligand angle within $[(bipy)_2Sn]^{2+}$ (Table 3.2.1). For [(bipy)GeCl][OTf], the plane of the bipy ligand is orthogonal to the Cl substituent, with an average Cl-Ge-N angle of 90.3°. Additionally, a short inter-cation Ge--- Cl' contact of 3.2569(7) Å (Σ_{vdW} = 3.86 Å)[152] imposes a dimer structure in the lattice. This is similar to that observed for $(bipy)GeCl_2$, which was found to form a polymeric coordination network in the solid state.[149] Presumably, [(bipy)GeCl][OTf] is dimeric due to absence of a second donor molecule. The ability of the Ge centre to engage another donor indicates it does remain Lewis acidic despite bipy coordination, and has the potential for interactions with other small molecules, with possibility for their activation. Also, the lack of sterically-protecting groups, which are often used to stabilize reactive main group centres, leaves the metal centre

more accessible to coordination. Most cationic complexes of Ge(II) and Sn(II) that have been structurally characterized are supported by bulky substituents[153] that sterically shield the acceptor from reactivity.

Table 3.2.1: Selected bond lengths (Å) and angles (deg) for [(bipy)GeCl][OTf], $[(bipy)_2Ge][OTf]_2$, $[(bipy)_2Sn][OTf]_2$, $[(bipy)_2As][OTf]_3$ and $[(bipy)_2Sb][OTf]_3$. Values in square brackets denote calculated parameters for gas-phase structures at the PBE0/Def2-TZVPP level.

	[(bipy)GeCl][OTf]	**$[(bipy)_2Ge][OTf]_2$**	**$[(bipy)_2Sn][OTf]_2$**	**$[(bipy)_2As][OTf]_3$**	**$[(bipy)_2Sb][OTf]_3$**
E-N1	2.063(2) [2.113]	2.228(1) [2.266]	2.389(5) [2.430]	2.124(2)	2.284(2)
E-N2	2.092(2) [2.113]	2.091(1) [2.122]	2.373(6) [2.336]	1.997(2)	2.233(2)
E-N3	--	2.237(1) [2.266]	2.387(5) [2.430]	2.125(2)	2.332(2)
E-N4	--	2.097(1) [2.122]	2.357(6) [2.336]	1.999(2)	2.243(2)
E-Cl1	2.2997(6)				
E---O1	2.827(2)	2.9276(9)	2.786(6)	2.705(2)	2.598(2)
E---O2	--	3.348(1)	3.190(6)	2.742(2)	2.650(2)
N1-E-N2	77.11(7) [76.1]	74.31(4) [74.4]	68.5(2) [69.3]	77.67(8)	72.09(4)
N1-E-N3		159.26(4) [161.2]	143.1(2) [150.1]	162.75(8)	156.02(4)
N1-E-N4		90.30(4) [92.5]	83.2(2) [89.4]	89.96(8)	87.87(4)
N2-E-N3		91.11(4) [92.5]	82.4(2) [89.4]	90.45(8)	91.42(4)
N2-E-N4		89.55(5) [92.4]	77.1(2) [90.4]	91.54(8)	78.66(4)
N3-E-N4		74.63(4) [74.4]	68.2(2) [69.3]	77.76(8)	71.53(4)
N1-E-Cl	90.60(5) [93.9]	--	--		
N2-E-Cl	90.07(5) [93.9]	--	--		
Cl-E-O	165.03(4)	--	--		

The DFT optimized geometries for cations $[(bipy)GeCl]^+$, $[(bipy)_2Ge]^{2+}$ and $[(bipy)_2Sn]^{2+}$ in the gas phase, listed in Table 3.2.1, are in good agreement with the experimental solid-state structures. The solid-state and calculated N1-Ge and N2-Ge bond lengths in $[(bipy)GeCl]^+$ are significantly shorter than those in $[(bipy)_2Ge]^{2+}$, likely due to the additional steric pressure on the Ge atom in $[(bipy)_2Ge]^{2+}$ due to the second bipy coordination, which forces a longer donor-Ge interaction due the presence of the lone pair. The computed axial E-N bonds for both $[(bipy)_2Ge]^{2+}$ and $[(bipy)_2Sn]^{2+}$ are longer than the equatorial E-N bond lengths, consistent with the solid-state structures. The equatorial interligand N-E-N angle in the solid state for $[(bipy)_2Sn]^{2+}$ is significantly smaller than that of the dication in the gas-phase, showing that the presence of a cation---anion contact, which are not modelled in the gas phase, enforces a more acute angle between the two bipy ligands. The smaller coordination sphere of germanium inhibits more than one cation---anion interaction, and results in a longer contact (Ge---O: 2.926 Å vs 2.788 Å for the Sn-O interaction). The trications in the previously reported $[(bipy)_2As][OTf]_3$ and $[(bipy)_2Sb][OTf]_3$) are isoelectronic with the dications in $[(bipy)_2Ge][OTf]_2$ and $[(bipy)_2Sn][OTf]_2$, respectively and exhibit shorter bond lengths due to the higher cationic charge. The interligand angles between the two bipyridine ligands are significantly more acute in the heavier analogues of Sn and Sb, likely due to their larger atomic radii compared to the lighter Ge and As congeners.

In all of the E(II) bipy complexes, the HOMO is primarily a non-bonding orbital located on germanium or tin, indicating the possibility of nucleophilic reactivity (Figure 3.2.2a and 3.2.2b). For $[(bipy)GeCl]^+$, the LUMO is mainly based on the bipyridine ligand. However, for $[(bipy)_2Ge]^{2+}$ and $[(bipy)_2Sn]^{2+}$, the LUMO is interpreted to be primarily a π-type orbital

based on the bipyridine ligand, however, some *p*-type orbital character is present at the Ge or Sn centre, which may facilitate the engagement of another donor molecule. However, this has not been realized experimentally, as even with a large excess of bipy, no reaction was observed by ^{1}H or ^{119}Sn NMR spectroscopy. Despite *tris*-bipy complexes of transition metals being common, the formation of *tris*-bipy complexes of Ge(II) and Sn(II) is likely kinetically disfavored by the stereochemically active lone pair seen in the HOMO of both molecules, as well as the triflate contacts. In terms of other orbitals relevant to the bonding at the Ge or Sn centre, in the monocation, the HOMO-6 and HOMO-7 are the primary N-Ge σ-type bonding orbitals. For the Ge-Cl moiety, the relevant bonding orbitals are spread out between five orbitals between HOMO-3 and HOMO-11. There is some π-type bonding character in the HOMO-6 and HOMO-8, with the primary σ-type interaction being the HOMO-11. It also appears that the HOMO-3 and HOMO-7 shows hyperconjugation of a *p*-type orbital at the Ge centre to the lone pair-containing *p*-type orbital at the chlorine centre. For the dications, the primary N-Ge bonding orbitals are the HOMO-8, HOMO-9, HOMO-10, and HOMO-11. It is evident that the HOMO-10 and the HOMO-11 are primarily the nitrogen donors interacting with two perpendicular *p*-type orbitals at the germanium.

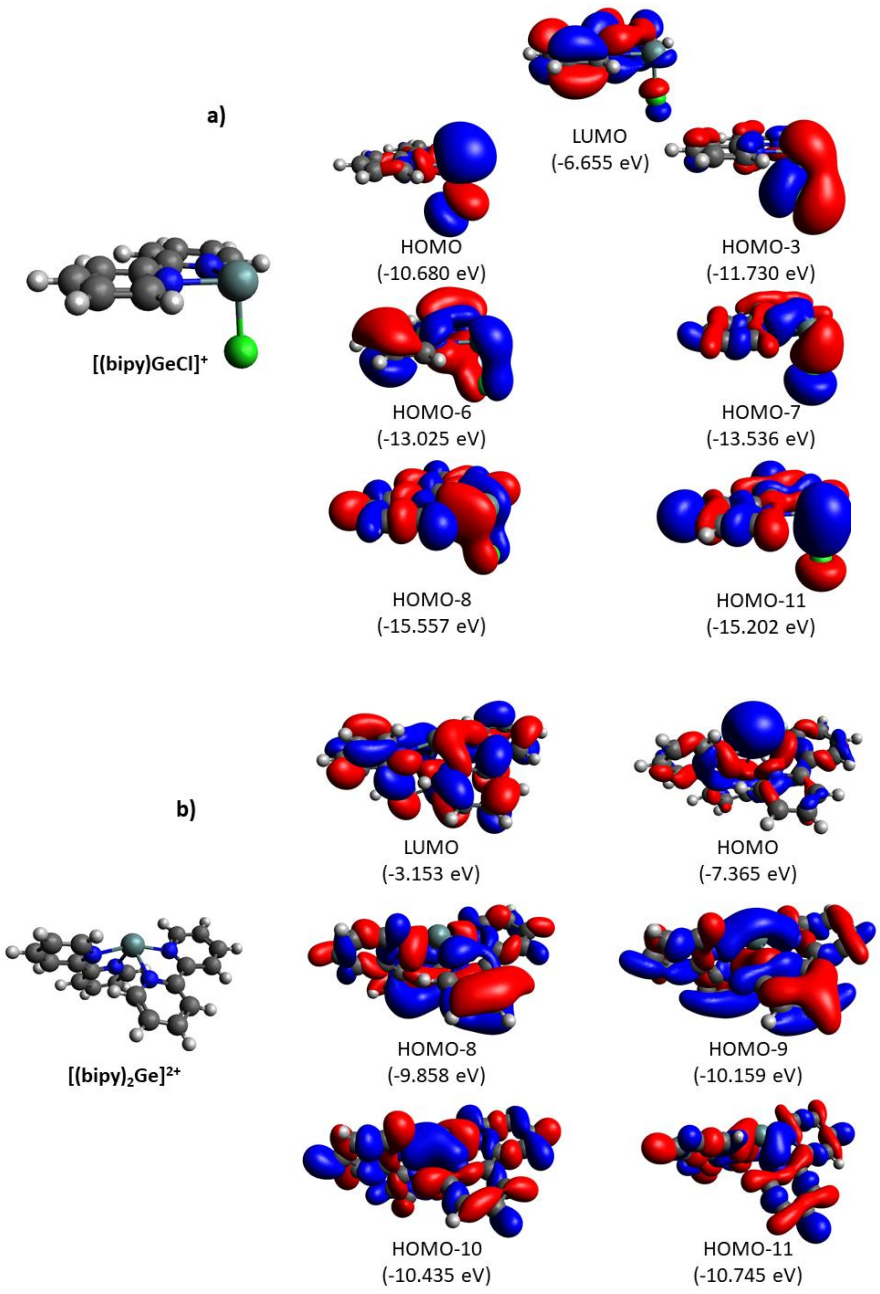

Figure 3.2.2: Relevant bonding orbitals for the cations) $[(bipy)GeCl]^{+}$ and b) $[(bipy)_2Ge]^{2+}$ calculated at the PBE0/def2-TZVPP level of theory (isovalue = 0.02).

Calculations of the Natural Bond Order (NBO) and Wiberg Bond Indices (WBI) for $[(bipy)GeCl]^{+}$, $[(bipy)_2Ge]^{2+}$ and $[(bipy)_2Sn]^{2+}$ listed in Table 3.2.2 indicate a positive

charge of +1.09*e*,+1.25*e* and +1.34*e*, respectively. This indicates that the monocation, which still has one chloride remaining, distributes a larger proportion of the cationic charge onto the germanium, while the dications distribute more charge into the ligands once that second chloride is removed. The N-Ge WBI for $[(bipy)GeCl]^+$ is slightly less than that for the equivalent equatorial N-Ge bonds in $[(bipy)_2Ge]^{2+}$, likely due to the higher charge and greater electrostatic attraction in $[(bipy)_2Ge]^{2+}$. However, the bond indices for the equatorial Sn-N bonds in $[(bipy)_2Sn]^{2+}$ are smaller than the equivalent Ge-N bonds in $[(bipy)_2Ge]^{2+}$, which implies more ionic character in the bond, which is consistent with the relative orbital sizes of Ge vs Sn and the effective overlap with nitrogen. For both dicationic derivatives, the axial N-E-N interactions are more ionic than the corresponding equatorial interactions, likely due to the *trans*-effect.

Table 3.2.2: NBO charges and Wiberg Bond Indices for [(bipy)GeCl][OTf], $[(bipy)_2Ge][OTf]_2$, and $[(bipy)_2Sn][OTf]_2$

	Charge (E)	**Charge (N_{ax})**	**Charge (N_{eq})**	**WBI (N_{ax}-E)**	**WBI (N_{eq}-E)**
$[(bipy)GeCl]^+$	+1.09*e*	--	-0.53*e*	--	0.35
$[(bipy)_2Ge]^{2+}$	+1.25*e*	-0.54*e*	-0.52*e*	0.27	0.38
$[(bipy)_2Sn]^{2+}$	+1.34*e*	-0.53*e*	-0.53*e*	0.24	0.32

3.3 Cationic Phosphine complexes of Ge(II) and Sn(II)

Employing bidentate alkyl phosphines which do not feature a rigid framework predisposed for chelation allow for several different possible structural outcomes. The lack of rigidity in the conformationally-labile phosphine results in the possibility of several possible bonding modes, including chelating, bridging, or a single monodentate coordination. Additionally, the inclusion of a phosphine is synthetically useful for more efficient reaction monitoring through ^{31}P NMR spectroscopy.

Equimolar mixtures of $GeCl_2$·dioxane or $SnCl_2$, 1,2-bis(dimethylphosphinoethane) (dmpe) leads to the formation of colourless solids, identified as [dmpeGeCl][OTf] and [dmpeSnCl][OTf], that precipitates from CH_2Cl_2. Formation of [dmpeGeCl][OTf] and [dmpeSnCl][OTf] exhibit sharp signals in the ^{31}P NMR spectrum [Ge: δ = 18.7 ppm; Sn: δ = 7.6 ppm] of the respective reaction mixture, and of the isolated solids upon redissolution in CD_3CN. The significant downfield shift of the phosphorus resonance of the complexes compared to that of free dmpe [δ = -48.1 ppm], is indicative of the coordination to an electrophilic centre. Additionally, for [dmpeSnCl][OTf], the ^{31}P NMR spectrum shows resolved coupling to the ^{117}Sn and ^{119}Sn nuclei [$^1J^{117}_{SnP}$ = 1766 Hz, $^1J^{119}_{SnP}$ = 1847 Hz], indicating both phosphorus atoms are bound in an identical manner to the tin centre, suggesting a chelating interaction with minimal dynamics in solution.

Dissolving the solids in CH_3CN and cooling to -35°C overnight led to colourless prismatic crystals suitable for X-ray analysis. The solid-state structures of [dmpeGeCl][OTf] and [dmpeSnCl][OTf] are displayed in Figure 3.3.1 and selected structural parameters are presented in Table 3.3.1. The germanium complex adopts a distorted disphenoidal geometry due to the E---O interaction of the triflate counterion. There is also a much longer Ge---O (3.494(2) Å) contact, which is just inside of the sum of the Ge-O van der Waals radii (Σ_{vdW} = 3.63 Å). For the tin complex, there are two triflate contacts at each tin centre, as well as a Sn-Cl contact, forming a coordination dimer in the solid state. For [(dmpe)GeCl][OTf], the complex crystallizes with two molecules in the asymmetric unit (orthorhombic $Pna2_1$) whereas [(dmpe)SnCl][OTf] crystallizes with a single molecule in the asymmetric unit (monoclinic $P2_1/n$) as the centrosymmetric dimer.

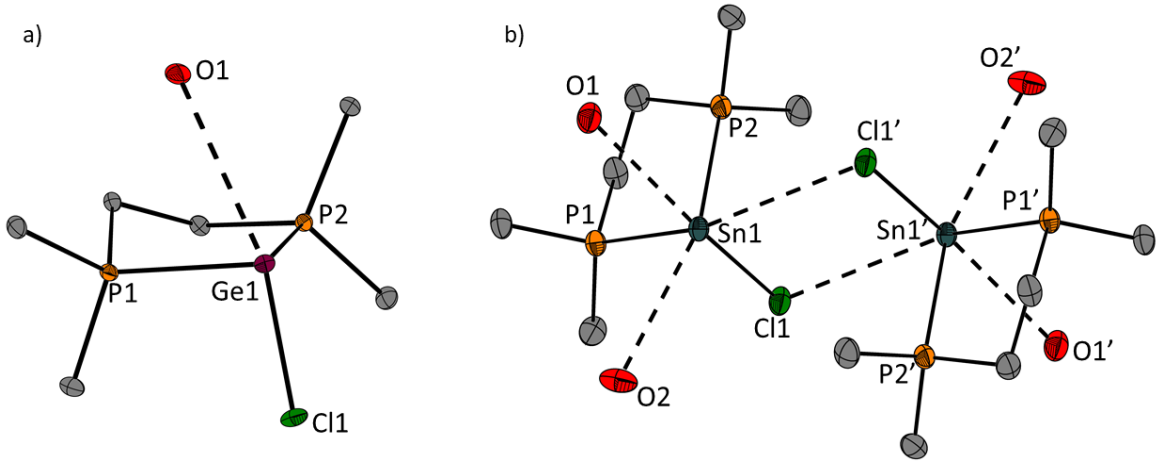

Figure 3.3.1: Solid-state structures of a) [(dmpe)GeCl][OTf] b) coordination dimer formed in the solid-state structure of the [(dmpe)SnCl][OTf] showing oxygen atoms of the closest contacting triflate anions. Thermal ellipsoids are shown at the 50% probability level. Hydrogen atoms are omitted for clarity.

The average Ge-P bond lengths in the cation of $[dmpeGeCl]^+$ are 2.4529(7) Å and are essentially the same across the two molecules in the asymmetric unit, which is outside of the sum of the Ge-P covalent radii [Σ_{CR} = 2.32 Å], and are similar to other coordination complexes featuring Ge-P bonds.[154,155] The average cation-anion Ge---O interaction [3.004(5) Å] is significantly outside the sum of the covalent radii [Σ_{CR} = 1.84 Å] but shorter than the sum of van der Waals radii [Σ_{vdW} = 3.63 Å]. The Ge-Cl bond exhibits a significant shortening [2.2885(7) Å] compared to 2.5803(5) Å in the analogous neutral derivative (depe)$GeCl_2$ [depe = 1,2-bis(diethylphosphinoethane)],[154] due to the introduction of a cationic charge at the Ge centre. The Sn-P bonds in [dmpeSnCl] [average 2.687(1) Å] are similar, and are in excess of the sum of the covalent radii Sn-P covalent radii [Σ_{CR} = 2.51 Å] and are similar to the previously reported neutral analogue.[156] The average cation-anion Sn---O interaction [2.870(3) Å] is significantly outside the sum of the covalent radii [Σ_{CR} = 2.03 Å] but is much shorter than the sum of van der Waals radii [Σ_{vdW} = 3.69 Å]. The shorter Sn-

--O interaction (2.870(3) Å) compared to the Ge---O interaction (2.996(2) Å) is likely due to the larger radius of the heavier tin atom accommodating more donors. Akin to the germanium analogue, the Sn-Cl bond [2.5189(8) Å] is much shorter than the corresponding neutral analogue,[156] unsurprising due to the increased cationic charge at the tin centre. The centrosymmetric dimer also features short Sn---Cl inter-ion contacts of 3.3185(8) Å, which are significantly less than the sum of van der Waals radii [Σ_{vdW} = 3.92 Å].

Based on the success of these experiments, we attempted to prepare dicationic derivatives of the type $[(dmpe)_2Ge][OTf]_2$ and $[(dmpe)_2Sn][OTf]_2$, analogous to the bipyridine complexes presented in the previous section. Upon combination of a 1:2 mixture of dmpe to the corresponding EX_2 reagent, in the presence of two equivalents of TMSOTf, again led to the formation of colourless solids that precipitate from CH_2Cl_2. When carrying out the reaction in CD_2Cl_2, the products are so insoluble that only signals attributed to unreacted dmpe could be resolved in the ^{31}P NMR and ^{1}H spectra. The CH_2Cl_2 was removed under reduced pressure, giving colourless powders. The solids are only sparingly soluble in CD_3CN, and both Ge and Sn reaction mixtures give broad signals in both the ^{1}H and ^{31}P NMR spectra [^{31}P: Ge: -2.5ppm; Sn: -8.1ppm] which is indicative of an exchange process of the phosphine ligands at the germanium or tin centre. Upon layering a saturated CD_3CN solution of the germanium reaction mixture with Et_2O, colourless crystals precipitated suitable for X-ray analysis, elucidating the structures as $[(dmpe)_3Ge_2)][OTf]_4$ which features two dicationic germanium centres, each with one chelating diphosphine, bridged by another equivalent of dmpe (Figure 3.3.2), giving an overall tetracationic salt with four triflate anions. Unfortunately, attempts to crystallize the tin analogue were unsuccessful, giving only microcrystalline powders.

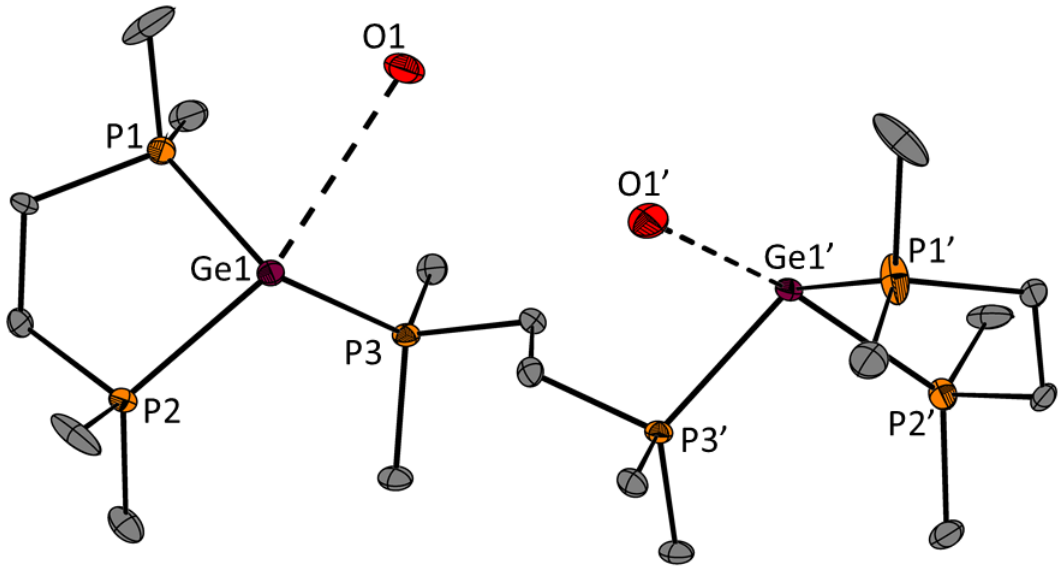

Figure 3.3.2: Solid-state structure of tetracation $[(dmpe)_3Ge_2][OTf]_4$ showing oxygen atoms of the closest contacting triflate anions. Thermal ellipsoids are shown at the 50% probability level. Hydrogen atoms are omitted for clarity.

The complex $[(dmpe)_3Ge_2][OTf]_4$ crystallized in the $C_{2/c}$ space group. The chelating diphosphine Ge-P bond lengths are 2.388(2) Å and 2.428(2) Å, indicating a slightly asymmetric binding mode for the two phosphines, and the identical bridging diphosphine Ge-P distances are 2.4114(7) Å. Both interatomic distances are outside of the sum of the Ge-P covalent radii [Σ_{CR} = 2.32 Å], and are shorter than those found in $[dmpeGeCl]^+$, suggesting a higher cationic charge at each germanium centre. The two distinct Ge---O anion contacts are 3.237(2) Å and 3.776(2) Å, with the latter being outside the sum of the Ge-O van der Waals radii, indicating true iconicity within the compound.

Table 3.3.1: Selected bond lengths (Å) and angles (deg) for [(dmpe)GeCl][OTf], [(dmpe)SnCl][OTf], and $[(dmpe)_3Ge_2][OTf]_4$. Values in square brackets denote calculated parameters for gas-phase structures at the PBE0/def2-TZVPP level.

	[(dmpe)GeCl] [OTf]	**[(dmpe)SnCl] [OTf]**	**$[(dmpe)_3Ge_2]$ $[OTf]_4$**
E-P1	2.4421(6) [2.444]	2.6941(9) [2.692]	2.388(2) [2.431]
E-P2	2.4634(6) [2.467]	2.6800(8) [2.676]	2.428(2) [2.430]
E-P3	--	--	2.4154(18) [2.422]
E-Cl1	2.2885(6) [2.278]	2.5189(8) [2.461]	--
E---O1	2.996(2)	2.870(3)	3.179(6)
P1-E-P2	81.04(2) [80.9]	76.57(2) [76.4]	83.77(7) [83.5]
P1-E-P3			103.54(7) [101.7]
P2-E-P3			101.47(7) [99.9]
P1-E---O			67.3(1)
P2-E---O	--	--	146.6(1)
P3-E---O	--	--	71.1(1)
P3 to P3' Torsion	--	--	145.1(3)
P1-E-Cl	92.60(2) [92.2]	87.91(3) [89.2]	--
P2-E-Cl	90.77(2) [89.9]	83.56(2) [86.6]	--
Cl-E-O	168.53(4)	154.00(6)	--

The DFT optimized geometries for the mono- and dications in the gas phase, calculated at the PBE1PBE/def2-TZVPP level of theory using a solvent-field of acetonitrile, are listed in Table 3.3.1, and are in-line with the experimental solid-state structures for those which data is available. For the isolated monocations, the average computed Ge-P and Sn-P bond distances are 2.476 Å and 2.709 Å respectively, and the computed Ge-Cl and Sn-Cl bond distances are 2.248 Å and 2.416 Å respectively. The noticeable deviation of the E-Cl bond distances from those in the solid-state structure are likely due to the Ge---O and Sn---O

cation-anion contacts, and for the tin analogue, the long Sn---Cl contacts present in the solid-state coordination dimer.

Figure 3.3.3a presents the MOs relevant to the bonding within the cation of [(dmpe)GeCl], and are analogous to those in the tin derivative. In the monocations, similar to the bipyridine derivatives, the HOMO is best described as the lone pair on the germanium and tin atoms. The LUMO is primarily a formally unoccupied *p*-type orbital at the tetrel centre, which results from the abstraction of chloride from the EX_2 moiety, and is presumably where the triflate Ge---O contact is based. We can also see that the Ge-P bonding interactions are present in the HOMO-1, HOMO-3 and HOMO-4. The HOMO-2 appears to be primarily Ge-based with some hyperconjugation to the chloride. Additionally, there is evident π-type and σ-type Ge-Cl bonding in the HOMO-3 and HOMO-4 respectively. In the bridging dications (Figure 3.3.3b), the HOMO and HOMO-1 are essentially degenerate and are also the lone pair at each of the Ge or Sn atoms. This implies that the lone pairs are spread out over two orbitals and are of equal energy. This could potentially mean both are equally available for further reactivity. Additionally, the LUMO is a *p*-type orbital at the Ge or Sn centre, indicating that each of the tetrel elements may be able to engage another donor. It is apparent that the primary Ge-$P_{chelate}$ bonding interactions occur in the HOMO-2 and HOMO-3 as an almost-degenerate pair, and the Ge-P_{bridge} interactions are the HOMO-4 and HOMO-5.

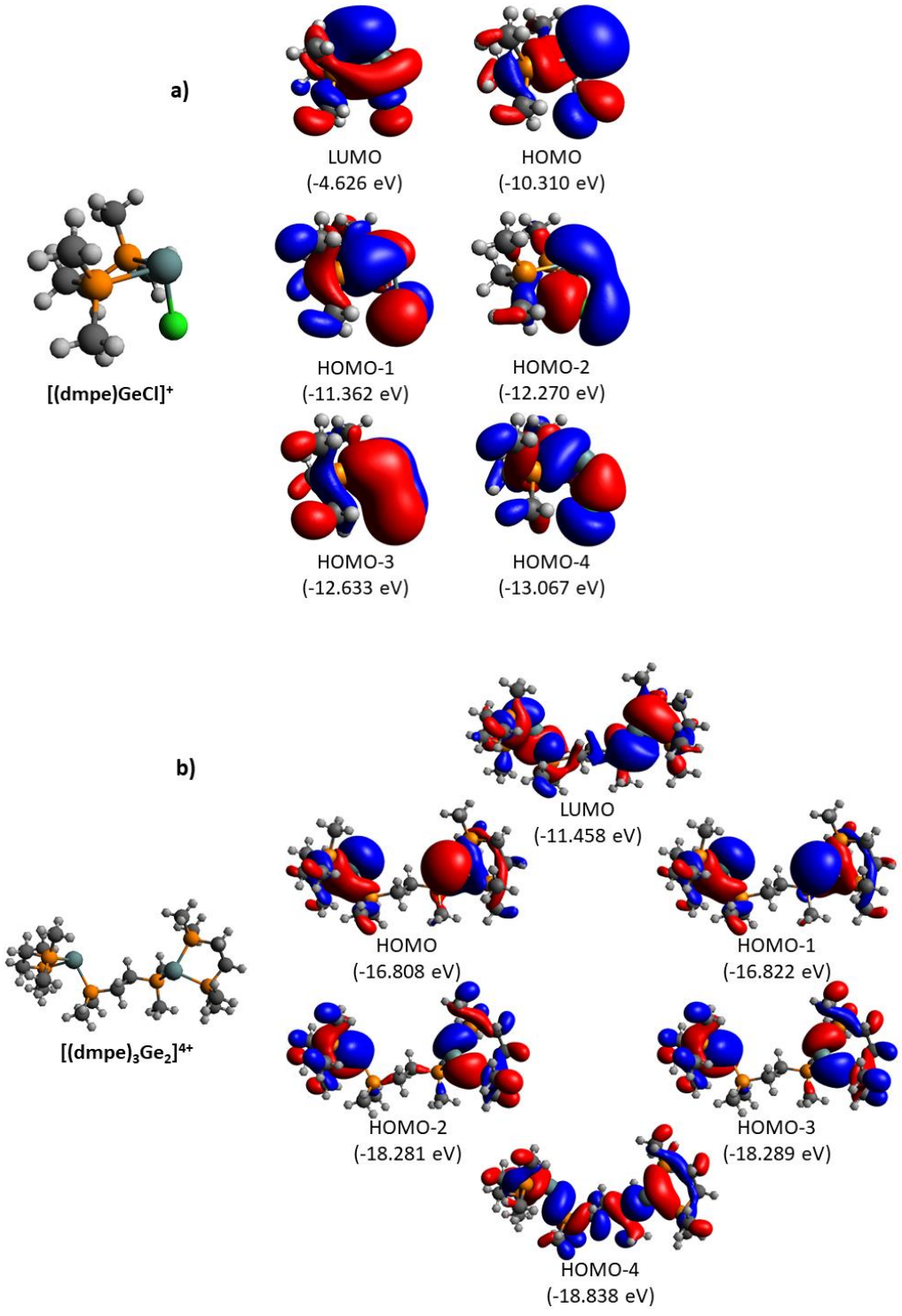

Figure 3.3.3: Calculated (PBE1PBE/def2-TZVPP) molecular orbitals relevant to the bonding interactions in a) [(dmpe)GeCl]+ and b) $[(dmpe)_3Ge_2]^{4+}$.

Once can envisage that the first step of the reaction is to generate the chelate complexes $[(dmpe)Ge]^{2+}$ or $[(dmpe)Sn]^{2+}$ from the corresponding chloride precursors. However, several possible structural arrangements are possible on addition of the second equivalent of dmpe (Scheme 3.2.1). To gain further insight into the formation of these complexes, the energetics of some of these gas phase reactions were examined. The reaction of two equivalents of $[(dmpe)Ge]^{2+}$ with one equivalent of dmpe to give $[(dmpe)_3Ge_2]^{4+}$, leaving one unreacted equivalent of the phosphine to stay consistent with reaction stoichiometry (Scheme 3.3.1a), was shown to be both endothermic and endergonic when no solvent-based dielectric constants were used. Interestingly, when dichloromethane was used as a solvent, it was impossible to find a structure that converged, always resulting in one negative frequency and indicating a transition-state in the gas phase. Within an acetonitrile solvent field, which was the crystallization solvent, the reaction is exothermic with a ΔH_{rxn} = -91 kJ mol^{-1}. Comparatively, the reaction of two equivalents each of dmpe and $[(dmpe)Ge]^{2+}$ to yield two equivalents of $[(dmpe)_2Ge]^{2+}$ (Scheme 3.3.1b) also results in an exothermic process with ΔH_{rxn} = -76 kJ mol^{-1}. These two values are quite close together, implying both may be present in the reaction equilibrium. Likewise, the equivalent values for the tin derivatives were ΔH_{rxn} = -26 kJ mol^{-1} (Scheme 3.2.1a) and ΔH_{rxn} = -14 kJ mol^{-1} (Scheme 3.3.1b), which are also only slightly different. Experimentally, as the ^{31}P NMR spectra of the reactions show broad signals, it is likely that there is an interconversion between multiple complexes where the equilibrium is on the timescale of the NMR spectrometer experiment. Along these lines, it was hoped that low-temperature NMR would resolve the signals of the interconversion into their constituent compounds. However, as the compounds were only

soluble in CD_3CN, which has a low temperature threshold around -40°C, no temperature was reached where the spectrum was fully resolved. Additionally, even on addition of an excess of the diphosphine, in hope of forcing the reaction towards the *bis*-chelate complex, the broad signals remained in the ^{31}P NMR spectra after isolation and redissolution in CD_3CN.

Scheme 3.3.1: Possible outcomes of equimolar reactions of dmpe with *in situ*-generated "$[(dmpe)E]^{2+}$, investigated at the PBE1PBE/def2-TZVPP level of theory.

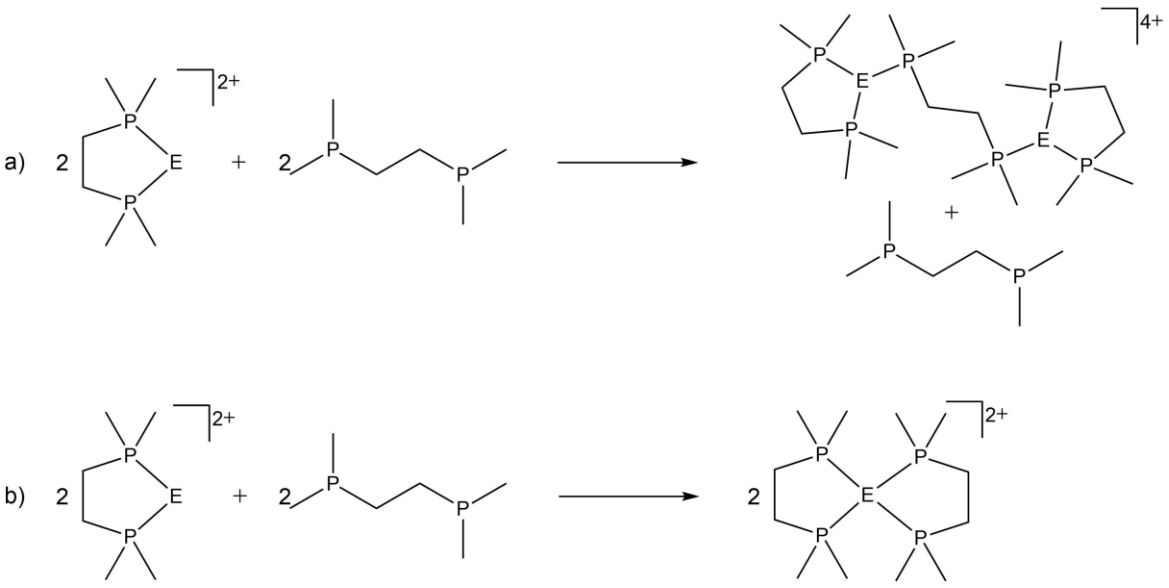

3.4 Summary

In summary, bipyridine and phosphine complexes of Ge(II) and Sn(II) cationic centres have been prepared and characterized crystallographically. The solid-state structures of $[(bipy)_2E][OTf]_2$ reveal a dication with a see-saw geometry at the tetrel centre, that have been modeled as minima in the gas phase. The LUMO exhibiting p-type character at the metal centre bodes well for behaviour as Lewis acids, and the tetrel based HOMO prompts investigation of nucleophilic behaviour. In terms of the phosphine complexes, the two possible outcomes for the reactions were identified through computational methods as viable

routes. However, only the tetracationic complex featuring both chelating and bridging interactions with diphosphines was isolated, and were found to be the enthalpically-preferred in the gas phase. These complexes represent prototypical coordination complexes of Ge(II) and Sn(II) cations, with future directions towards probing their ability to catalyze reactions akin to their transition metal analogues.

Chapter 4 - Reactivity of Cationic Ge(II) and Sn(II) Bipyridine Complexes

4.1 Introduction

The activation of small molecules by transition metal species has been studied extensively, and these are the primary compounds employed in catalytic and stoichiometric transformations of substrates today.[33,48,157] In contrast to this, the activation of small molecules by main group molecules, especially those featuring coordinatively unsaturated metal centres, has not attained the same level of recognition in terms of development on an industrial scale. However, this avenue has recently been a highly active area of research.[59] Of particular interest is using these species to activate and transform typically unreactive molecules into useful chemical feedstocks without the use of the commonly employed transition metals, which often add substantial cost to these processes. One such example is the activation of dihydrogen to generate main group hydrides, with the hope of using these to further transfer the equivalent of H_2 to an unsaturated substrate in a stoichiometric and, eventually, catalytic fashion.

At the forefront of these investigations have been reactive species such as carbenes, and their heavier group 14 (Si, Ge, Sn, Pb) analogues known collectively as the metallylenes.[158] These typically divalent compounds feature the central group 14 element in the +2 oxidation state, with each possessing a lone pair of electrons, and a formally empty *p*-type orbital (Scheme 4.1.1a). It is this implied ambiphilicity at the element centre which makes these attractive targets to use for molecule activations and transformation. The reactivity of these types of species can be broadly categorized into five groups: (i) oxidation, (ii) reduction,

(iii) insertion, (iv) cycloaddition, and (v) coordination reactions. Scheme 4.0.1b depicts an example of a group 14 metallylenes with each of these reactivity types.

Scheme 4.1.1: a) Generic orbital diagram of divalent germylenes, and b) examples of reactivity modes of metallylenes featuring (i) oxidation, (ii) reduction, (iii) insertion, (iv) cycloaddition, and (v) coordination.

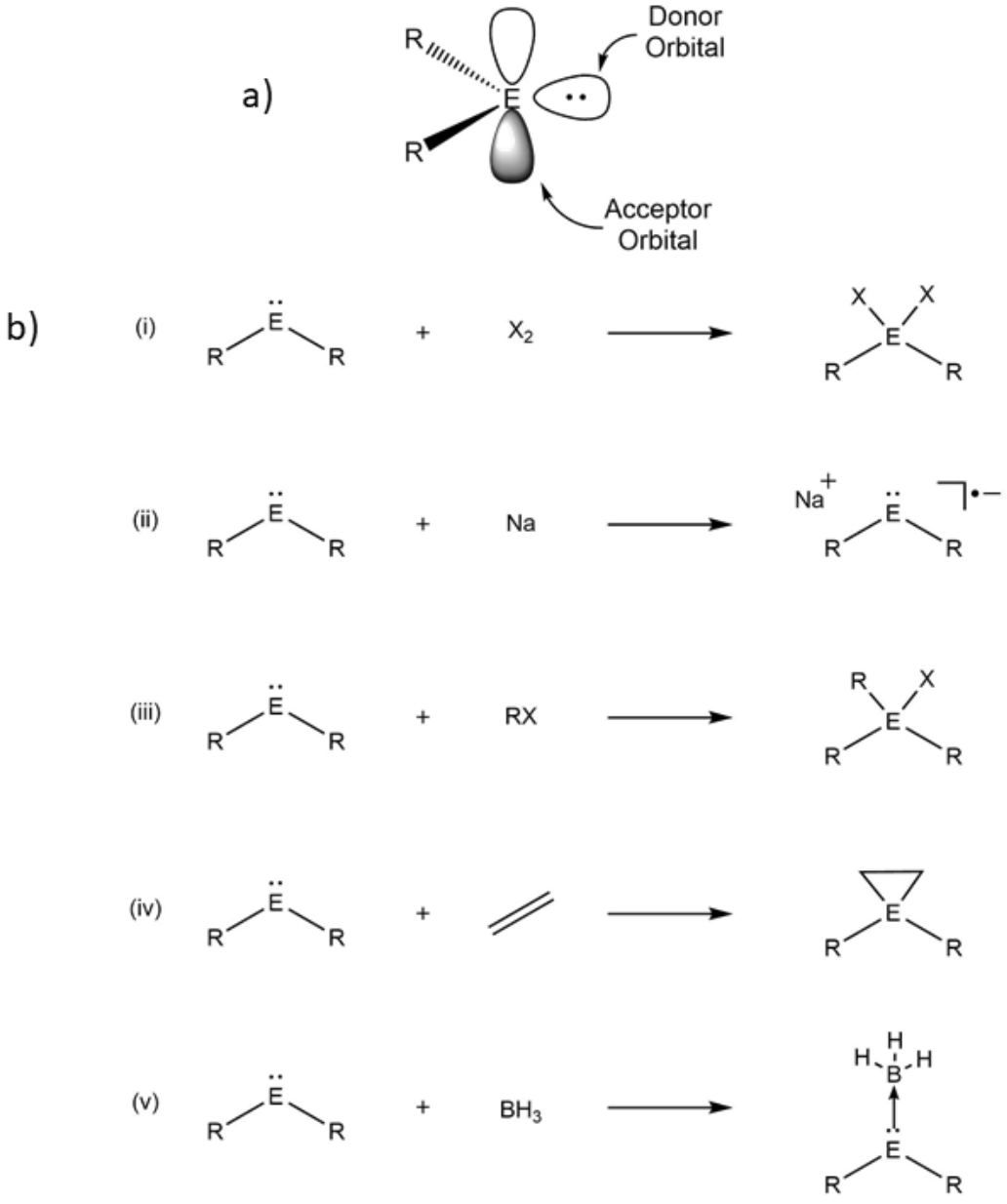

Examining these carbenoid derivatives as reagents towards small molecule activation, especially that of H_2, has been remarkably fruitful. The bond in dihydrogen is enthalpically strong and often requires harsh conditions or active transition metal catalysts to undergo activation. The first example of a group 14 carbenoid activating H_2 in a facile manner was discovered by Bertrand *et. al.* when both a cyclic and acyclic (alkyl)(amino) carbene were shown to undergo oxidative addition of H_2 at the carbon centre (Scheme 4.1.2).[159] Since then, several examples of divalent group 14 carbenoids have been found to activate small molecules such as H_2 in under mild conditions.[160–163]

Scheme 4.1.2: First example of a group 14 carbenoid activating H_2, reproduced with permission.[164]

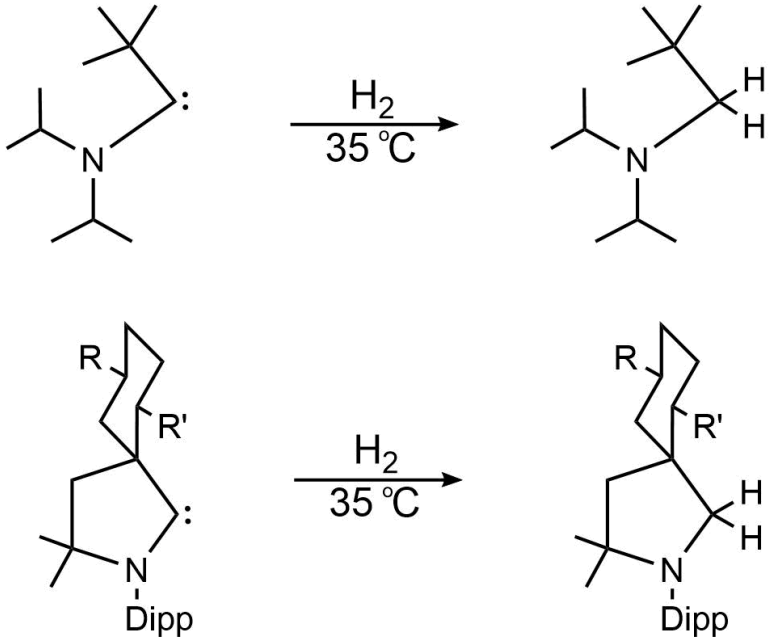

The reactivity of these compounds is dictated by the types of substituents at the divalent centre. As the mechanism of hydrogen activation proceeds through a bimolecular mechanism as presented in Chapter 1.3, with the lone pair at the carbenoid centre responsible for the perturbation of the H-H σ-bond through interaction with the σ* orbital, choosing

substituents that ensure the lone pair is energetically accessible is key to their activity. For example, a wider X-E-X bond angle (X = C, Si, Ge, Sn) resulting from bulky substituents typically decreases the HOMO s-orbital character, which increases the energy of the HOMO and consequently lowers the HOMO-LUMO gap while decreasing the X-E-X bond angle results in the opposite.[165] Additionally, employing substituents with increasing electronegativity results in a lowering of the HOMO through induction (σ-withdrawing) while substituents with π-donor character typically destabilize the LUMO and results in its elevation.[165] By tuning the influence of these steric and electronic factors, the reactivity of the metallylenes can be altered to perform a variety of reactions.

Compared to that of the neutral germylenes, the reactivity of cationic variants has not received nearly as much focus. Recently, the complexation of Ge(II) dications within a crown ether scaffold with water and ammonia was investigated.[166] Unsurprisingly, the Ge(II) dication behaves as a Lewis acid, and is coordinated by either H_2O or NH_3 in an axial position, while the Ge(II) centre remains encapsulated in the crown ether in an equatorial plane (Figure 4.1.1). However, to my knowledge there is only one example of a dicationic Ge(II) centre which directly coordinates to a transition metal centre through a donor-acceptor interaction.[167] As such, targeting complexes which attempt to employ the lone pair in these types of reactions is of great interest. Additionally, it is possible that the hemispherically-coordinated 2,2'-bipyridine ligands influence different reactivity at the Ge(II) or Sn(II) centre. The tetrel centre is less accessible than those in the crown ether complexes and so it is possible that the bipy complexes will show divergent reactivity towards substrates than their crown ether-ligated counterparts.

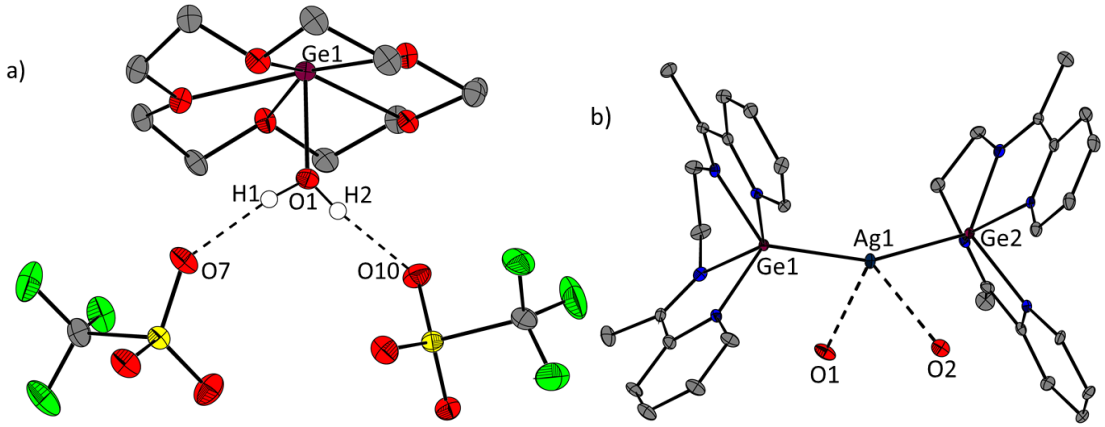

Figure 4.1.1: Examples of the potential ambiphilic nature Ge(II) dications, behaving as a a) Lewis acid and b) Lewis base.[166,167]

4.2 Assessing the Lone Pair Reactivity in Ge and Sn Dications

As described previously, the cations in $[(bipy)_2Ge][OTf]_2$ and $[(bipy)_2Sn][OTf]_2$ both feature the lone pair at the tetrel centre as the HOMO. It can be envisaged that these complexes could behave as nucleophilic species by engaging an acceptor centre. As such, it seemed reasonable to examine a variety of Lewis acidic acceptors with varying degrees of electrophilicity to probe whether the lone pair is accessible as a nucleophile. As methylation reactions were previously shown to be successful with the lone pair on phosphorus-based cations,[168–170] this seemed a reasonable starting point. Treatment of a CH_3CN solution of $[(bipy)_2Ge][OTf]_2$ and $[(bipy)_2Sn][OTf]_2$ with MeOTf resulted in immediate fuming, and with the retention of the yellow solution colours. After stirring overnight, the reaction mixtures were concentrated *in vacuo* and placed in a -35°C freezer, which yielded colourless prismatic crystals suitable for X-ray analysis. However, instead of the desired Ge- or Sn-methylation product (Scheme 4.2.1), the structure was elucidated to be that of [MeCN-Me][OTf] resulting from the *N*-methylation of acetonitrile. The structure is identical to that recently reported from the direct reaction of MeCN with MeOTf.[171] Unsurprisingly, the

acetonitrile is more basic towards the small $[CH_3]^+$ cation, likely due to the relative size of N vs Ge/Sn, as well as the resulting better orbital overlap forming a stronger interaction.

Scheme 4.2.1: Expected and observed reactivity of Ge(II) and Sn(II) dications with MeOTf.

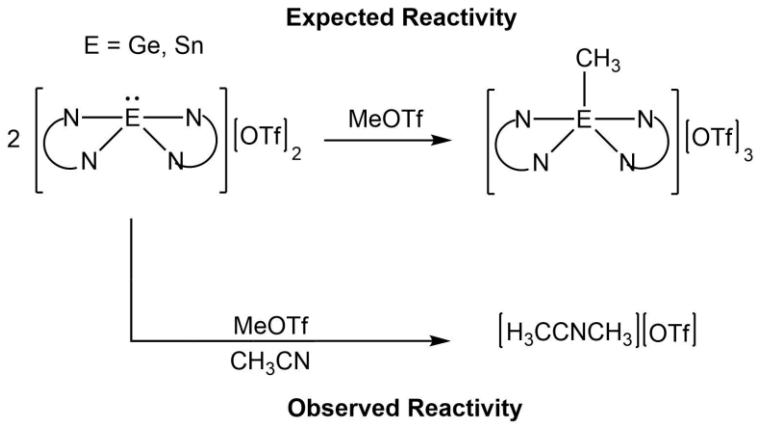

Additionally, the kinetic advantage of having MeCN in such a high concentration compared to the cations, as well as the large repulsive forces between $[CH_3]^+$ and the Ge/Sn cations means that the likelihood of collision is low. Identical reactions carried out in CH_2Cl_2 resulted in no reaction on the basis of ^1H and ^{119}Sn NMR spectroscopy. It should be noted that additional reactions of the dications with other small molecules that involve activation at the lone pair were also carried out. Substrates such as phenylacetylene, diphenylacetylene, 1,2-bis(trimethylsilyl)acetylene, and 2,3-dimethyl-2,3-epoxybutane were chosen as representative unsaturated compounds. However, reactions carried out at room temperature and at 70°C in a glass pressure reactor showed no evidence of activation of any of the substrates and the only species observed in the ^1H and ^{119}Sn NMR spectra were unreacted starting material, or protonated bipyridine.

Despite the lack of reactivity with this subset of small molecules and electrophiles, it is possible that using a larger, softer acceptor could undergo reactivity with the lone pair. As

only one complex which features direct coordination of a Ge(II) centre to a transition metal,[167] this was deemed a reasonable target to pursue. Addition of a CH_3CN solution of $[(bipy)_2Ge][OTf]_2$ and $[(bipy)_2Sn][OTf]_2$ to a slurry of $(COD)PtCl_2$ did not immediately result in an obvious reaction as the colourless $(COD)PtCl_2$ did not immediately dissolve, nor did the yellow supernatant appear any different. Upon stirring overnight however, each reaction mixture provided a yellow precipitate in the reaction mixture. The yellow supernatant was decanted from the yellow solid and was concentrated *in vacuo* and placed in a -35°C freezer overnight, which resulted in the formation of light yellow crystals for the germanium reaction.

Interestingly, the compound which crystallized was not that of the neutral adduct, but was instead formulated as $[(bipy)Pt(COD)][OTf]_2$. Evidently, the two chlorides were abstracted from the platinum centre by the Ge(II) dication, which effected a transfer of one bipyridine ligand to platinum, along with the triflate counterions. This implies that resulting germanium complex was the neutral complex $(bipy)GeCl_2$ (Scheme 4.2.2). Indeed, upon dissolving the yellow precipitate from which the reaction mixture was decanted in CD_3CN, the ^1H NMR spectrum corresponds to that of the previously characterized neutral adduct.[149] While attempts at crystallizing the Sn derivative was unsuccessful, ^1H NMR of the dark yellow solid, which was very sparingly soluble in CD_3CN, was in line with that for the previously reported neutral complex $(bipy)SnCl_2$.[172] Unfortunately, solubility of the complex precludes obtaining a ^{119}Sn NMR spectrum.

Scheme 4.2.2: Reaction of the Ge(II) and Sn(II) dications with (COD)$PtCl_2$

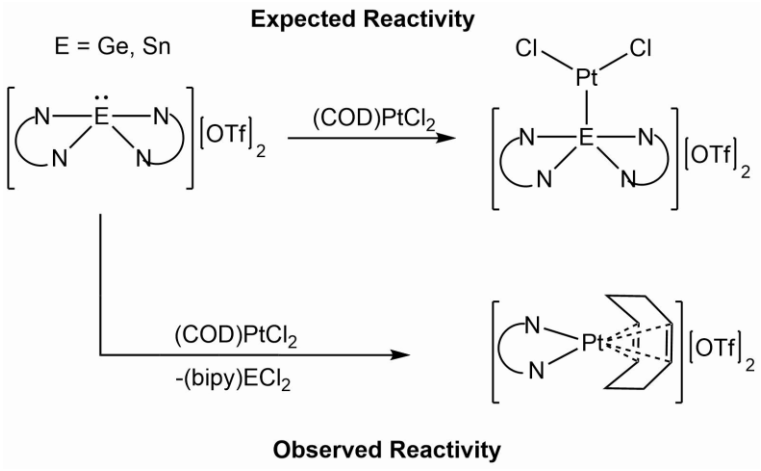

The complex [(bipy)Pt(COD)][OTf]$_2$ crystallizes in the triclinic space group *P-1* with two molecules in the unit cell. The structure reveals a slightly distorted square planar geometry at the platinum centre with the two nitrogen atoms and the centre point of the two η^2-double bonds forming the vertices of the distorted square (Figure 4.2.1). The two Pt-N bond lengths are essentially the same (Pt1-N1 = 2.058(3) Å; Pt1-N2 = 2.063(3) Å) with an N1-Pt-N2 angle of 79.83(14)°. The four Pt-C interactions are distributed in two distinguishable sets with average distances of 2.190(4) (averaged for Pt1-C1 and Pt1-C5) and 2.176(5) (averaged for Pt1-C2 and Pt1-C6). The asymmetric binding results from the Pt1-C1 and Pt1-C5 bonds being *trans* to the N1-Pt1 and N2-Pt1 bonds respectively. There is a close contact with one triflate anion, featuring a Pt1---O1 contact of 3.004(5), which is within the Pt-O van der Waals radii (Σ_{vdW} = 3.22 Å).[152,173,174] Selected structural parameters are presented in Table 4.1.1. Additionally, the gas-phase optimization of the complex at the PBE1PBE/def2TZVPP level in the absence of the triflate anions gave a structure that is essentially identical to that in the solid state. Overall, this suggests that the contact with the nearest triflate, while inside of the van der Waals radii of the two elements, does not impose any structural changes in the complex, at least to an observable extent. As such, the complex

can be described as a dicationic platinum centre, ligated by a 1,5-cyclooctadiene and 2,2'-bipyridine with two triflate counterions.

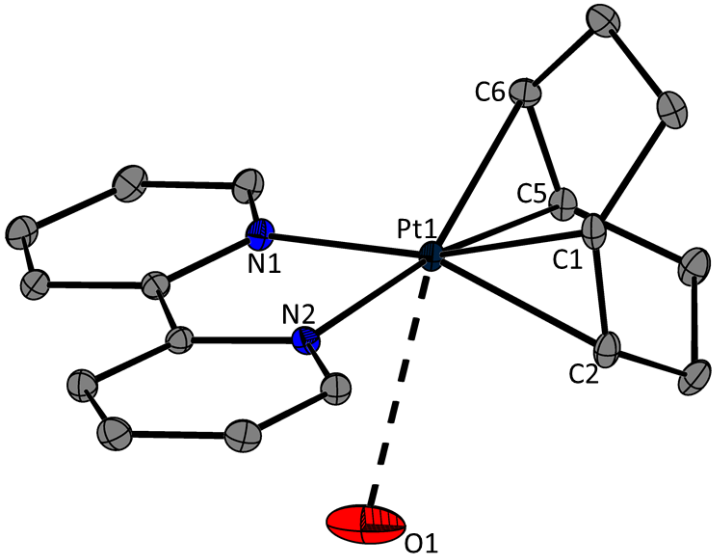

Figure 4.2.1: Solid-state structure of the cation in $[(bipy)Pt(COD)][OTf]_2$ with the closest triflate contact shown. Thermal ellipsoids are shown at the 50% probability level. Hydrogen atoms are omitted for clarity.

To try to understand why the reaction proceeds from an energetics point of view, free energies were calculated according to the reactions in Scheme 4.2.3. The reaction of $[(bipy)_2Ge]^{2+}$ and $[(bipy)_2Sn]^{2+}$ with $(COD)PtCl_2$ to displace the COD ligand and give the adducts $[(bipy)_2GePtCl_2]^{2+}$ and $[(bipy)_2SnPtCl_2]^{2+}$ (Scheme 4.2.3a) were found to be only slightly exergonic with ΔG_{rxn} = -11.2 kJ mol^{-1} and -8.1 kJ mol^{-1}. Interestingly, if the COD ligand is assumed to remain attached to the platinum centre, the reactions are slightly more exergonic with ΔG_{rxn} = -15.3 kJ mol^{-1} and -13.8 kJ mol^{-1} respectively, indicating that the additional, albeit weak, electron density donation from the COD to the platinum centre stabilizes the complex more than just the dication itself. In contrast to this, the reaction to give the crystallographically characterized $[(bipy)Pt(COD)]^{2+}$ with the formation of

(bipy)ECl_2 (Scheme 4.2.3b) was found, in the gas phase, to be endothermic with ΔH_{rxn} = 9.1 kJ mol^{-1} and 15.6 kJ mol^{-1} for the Ge(II) and Sn(II) derivatives, respectively, and was found to be significantly more exergonic than adduct formation with ΔG_{rxn} = 3.7 kJ mol^{-1} and 9.4 kJ mol^{-1} respectively.

Scheme 4.2.3: Possible reactivity investigated computationally leading to either a) direct metal coordination or b) halide abstraction of the $PtCl_2$(COD) by $[(bipy)_2E][OTf]_2$

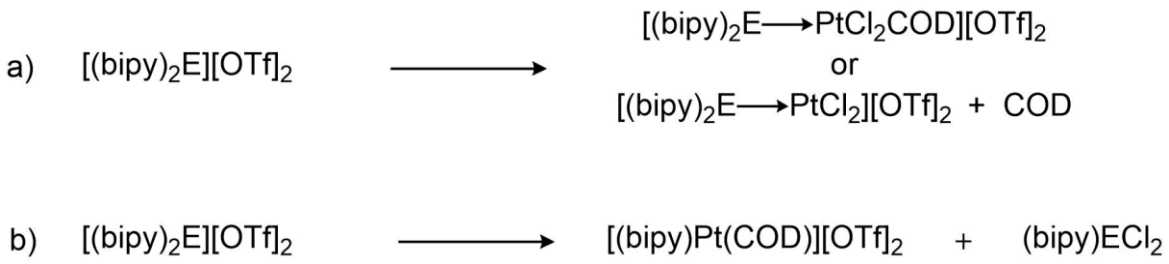

However, these calculations do not take into account the lattice energy responsible for the crystallization of the ionic salts. As lattice energy is inversely proportional to the size of the ions, the smaller ionic complex should have a larger lattice energy. Examining the CIF shows that the cell volume of the resulting platinum complex is smaller than both $[(bipy)_2Ge][OTf]_2$ and $[(bipy)_2Sn][OTf]_2$ meaning that the lattice energy should be larger and is likely a driving force for this reaction. As the coordination of the dication to the $PtCl_2$ moiety, with or without the COD remaining bound, would result in a very large cation, the lattice energy would likely be much smaller and this likely contributes to this complex not being formed despite being exothermic and exergonic in the gas phase. Also based on these data, it does appear that the Sn(II) dication derivative disfavours adduct coordination to the platinum centre more than the Ge(II) dication, which is in line with the lower nucleophilicity at the Sn(II) centre due to the higher *s*-orbital character of the lone pair. Overall, it appears that the dicationic complexes favour halide abstraction from the platinum metal centre rather

than coordination and these species appear more likely to behave as Lewis acids compared to Lewis bases. This could potentially lead to their use as bottleable sources of $E(OTf)_2$ Lewis acids, especially in the case of germanium as, unlike Sn, a stable equivalent of $Ge(OTf)_2$ is not currently commercially available.

4.3 Lewis Acid Behaviour of Ge(II) and Sn(II) Dications

As shown in the previous section, experimental and computational evidence supports that the dicationic Ge(II) and Sn(II) complexes prefer to behave as Lewis acids instead of Lewis bases, despite the presence of a stereochemically-active lone pair as the HOMO for each of the complexes. It is reasonable to assume that the lone pairs are likely too low in energy to engage the acceptor centre, augmented by the dicationic charge at the Ge(II) or Sn(II) centre. However, it was shown in Figure 3.2.2 that the dications do appear to have some potential acceptor character, evidenced by the presence of *p*-type orbital character as the LUMO. As such, it is desirable to explore the electrophilicity of these complexes, as well as their potential applications of soluble chloride abstracting agents. Unlike the reaction of main group halides with TMSOTf/bipy or AgOTf/bipy, the potential advantage of these systems is that the abstraction of the chlorides and transfer of a bipy ligand to the substrate happens in one pot, and potentially one step, without the need to filter off any AgCl by-product, and lacks any potential coordination of the ligand to the $[TMS]^+$ which has been previously shown to react with various donors in this regard.[175]

The first target of this potential avenue of reactivity was the previously characterized $[PhP(bipy)][OTf]_2$,[176] as the reaction could be easily monitored by ^{31}P NMR spectroscopy, and the known chemical shift could be compared to the experimentally obtained spectra. Dropwise treatment of a CD_3CN solution of $[(bipy)_2Ge][OTf]_2$ or $[(bipy)_2Sn][OTf]_2$ with

$PhPCl_2$ resulted in the formation of a yellow precipitate, which was found to be either (bipy)$GeCl_2$ or (bipy)$SnCl_2$. Upon collection of the $^{31}P\{^1H\}$ NMR spectra, it was apparent that in both cases, the reaction did indeed form [PhP(bipy)][OTf]$_2$, evidenced by a singlet at a chemical shift of δ = 132.6 ppm, an upfield shift of 28.4 ppm from the $PhPCl_2$ starting material at δ = 161.0 ppm.

In this vein, another reaction of interest was the reaction of the dications with a chloride source, that is, where only halide substituents are present, to see whether the reactivity presented above was a general outcome. Previously, it was shown that PPh_3 acts as a reductant towards [Ph_3P-P(Ph)Cl][OTf] in the presence of a substoichiometric amount of TMSOTf to give 2,3-diphosphino-1,4-diphosphonium ions.[109] The presence of a chloride at one of the phosphorus centres, due to the incomplete abstraction, results in oxidation of PPh_3 to [Ph_3PCl][OTf] (Scheme 4.3.1a) with concomitant reductive coupling of the other two phosphorus centres. Additionally, the *in situ* reduction of PCl_3 in the presence of phosphine ligand donors results in the phosphine-stabilized P(I) cationic salts (Scheme 4.3.1b).

Scheme 4.3.1: Examples of reductive coupling of phosphines to give the catenated a) tetraphosphorus dications and b) PPh_3-ligated P(I) cations from the oxidation of PPh_3 from a chloride-bearing phosphine.

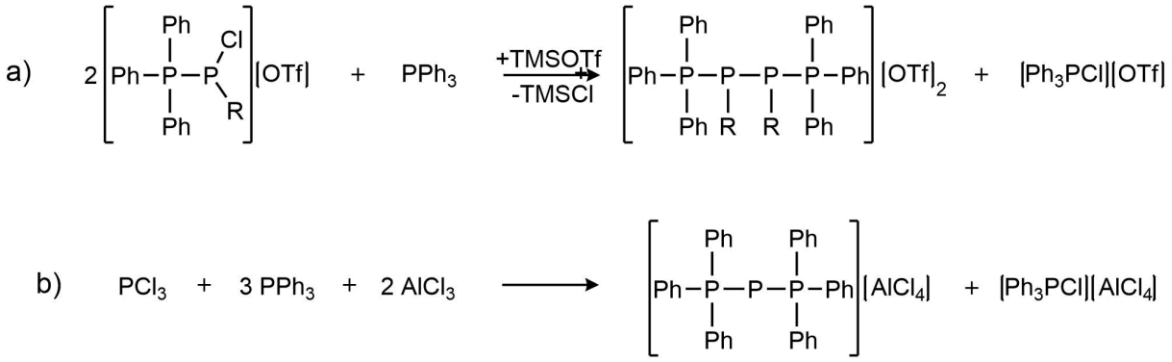

As the Ge(II) and Sn(II) cations have the potential to be oxidized to Ge(IV) and Sn(IV), reactivity with PCl_3 could result in the formation of either the previously unknown $[(bipy)PCl][OTf]_2$ through halide abstraction, or the postulated P(I) complex $[(bipy)P][OTf]$.[177] As such, dropwise treatment of a CD_3CN solution of the respective Ge or Sn dication with PCl_3 again results in the formation of $(bipy)GeCl_2$ or $(bipy)SnCl_2$. Examination of the $^{31}P\{^1H\}$ NMR spectrum shows the conversion to a singlet as the major product with a chemical shift of δ = 129.8 ppm, which is shifted upfield by approximately 90 ppm. This is significantly different than the proposed chemical shift for the bipy-ligated P(I) triflate salt identified recently from the reduction of $[(bipy)P][OTf]_3$ with zinc powder with a chemical shift of δ = 232.6 ppm (Scheme 4.3.2a).[178] Interestingly, while the major product is a singlet, roughly 15% of the spectrum shows the presence of a doublet and triplet resonance at δ = 237.9 ppm and δ = 83.8 ppm with a coupling constant of 403 Hz. This type of AX_2 spin system was seen previously in the reduction of $[(tBuBipy)_2P][OTf]_3$ with either magnesium or zinc metal, which was assigned as [(tBubipy)P-P-P(tBubipy)][OTf]$_5$ (Scheme 4.3.2b).[179] It is likely that this minor product results from the reduction of the P(III) centre of PCl_3 to a P(I) centre, which is ligated by one bipyridine. These P(I) centres, which

have been shown to be electron donors to metal centres,[180–183] are then likely acting as a donor towards a P(III) tricationic centre to give the AX_2 spin system and overall pentacationic salt.

Scheme 4.3.2: (a) Reduction of $[(bipy)P][OTf]_3$ to $[(bipy)P][OTf]$ and (b) reaction of $[(tBubipy)_2P][OTf]_3$ with magnesium.

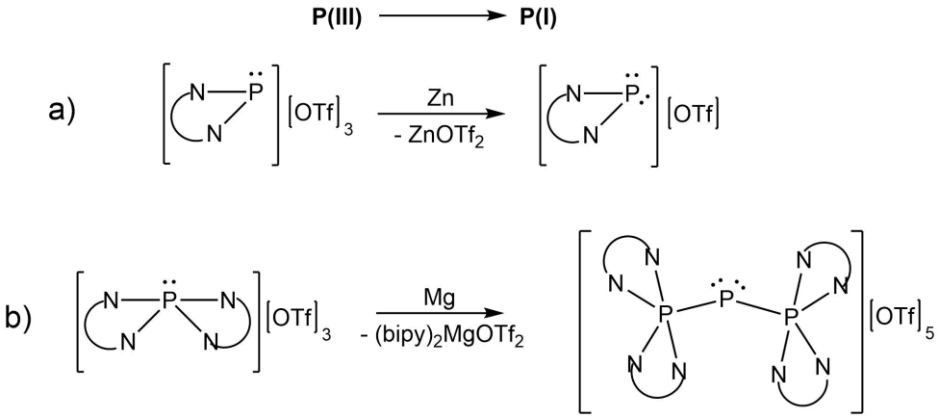

4.4 Reaction of a Ge(II) Dication with Water

It has previously been shown that crown ether complexes of Ge(II) dications are reactive towards small donor molecules such as water and ammonia, and result in the formation of the expected neutral adducts.[166] However, the nature of the crown ether complexes allows for the approach of the small molecule to one hemisphere of the complex, while the other hemisphere remains undisturbed. The coordination at one hemisphere means that the H_2O or NH_3 molecules do not inherently approach the lone pair, facilitating the coordination. Within the $[(bipy)_2E]^{2+}$ cations, as the two bipy ligands occupy one entire hemisphere, close approach at the germanium or tin must occur in close proximity to the lone pair. This interaction may either encourage reaction or preclude any reactivity at the tetrel centre, and was worthy of investigation.

Introduction of H_2O into a CH_3CN solution of either $[(bipy)_2Ge][OTf]_2$ or $[(bipy)_2Sn][OTf]_2$ resulted in the slow transition of the solution from yellow to pink solution resulting from formation of the protonated ligand salts [bipy-H][OTf] or $[bipy\text{-}H_2][OTf]_2$. In both cases, after stirring overnight, a colourless powder precipitated from the solution. The powders were filtered, washed with cold CH_3CN to remove any protonated ligand, dried *in vacuo*, and then redissolution was attempted in CH_3CN. After attempting to dissolve by stirring in acetonitrile for one hour, the solvent was filtered and removed *in vacuo* to quantify the amount of dissolved solid. However, no solid was evident for the tin derivative, and the germanium derivative was only sparingly soluble. The germanium product was redissolved in CH_3CN and placed in a -35°C freezer for two days, which deposited small, faintly yellow crystals suitable for X-ray analysis. Interestingly, the product that crystallized was formulated as $[(bipy)Ge\text{-}O(H)\text{-}Ge(bipy)][OTf]_3$ (Figure 4.4.1). It is possible that the initial step in the reaction is an interaction between H_2O and the germanium centre, which causes the weakening of the bipy-Ge interaction, or complete dissociation. The bipyridine likely then deprotonates the coordinated H_2O, as the O-H bond is weakened by interaction with the cationic Ge centre, leading to the protonated bipyridine salt and subsequent pink colour observed. The interaction of the Ge-O(H) with a second Ge centre likely leads to the displacement of a neutral bipyridine ligand from the $[(bipy)_2Ge]^{2+}$ dication to relieve steric strain, imposed from the coordination of the oxygen, as well as the lone pair. The preparation of this complex is somewhat surprising given the reactivity of a majority of divalent Ge(II) compounds, although not unheard of, as the first example of a "LGeOH"-type complex has been characterized previously, obtained upon coordination of water to a Ge(II) β-diketiminate complex, and subsequent deprotonation with a carbene.[184]

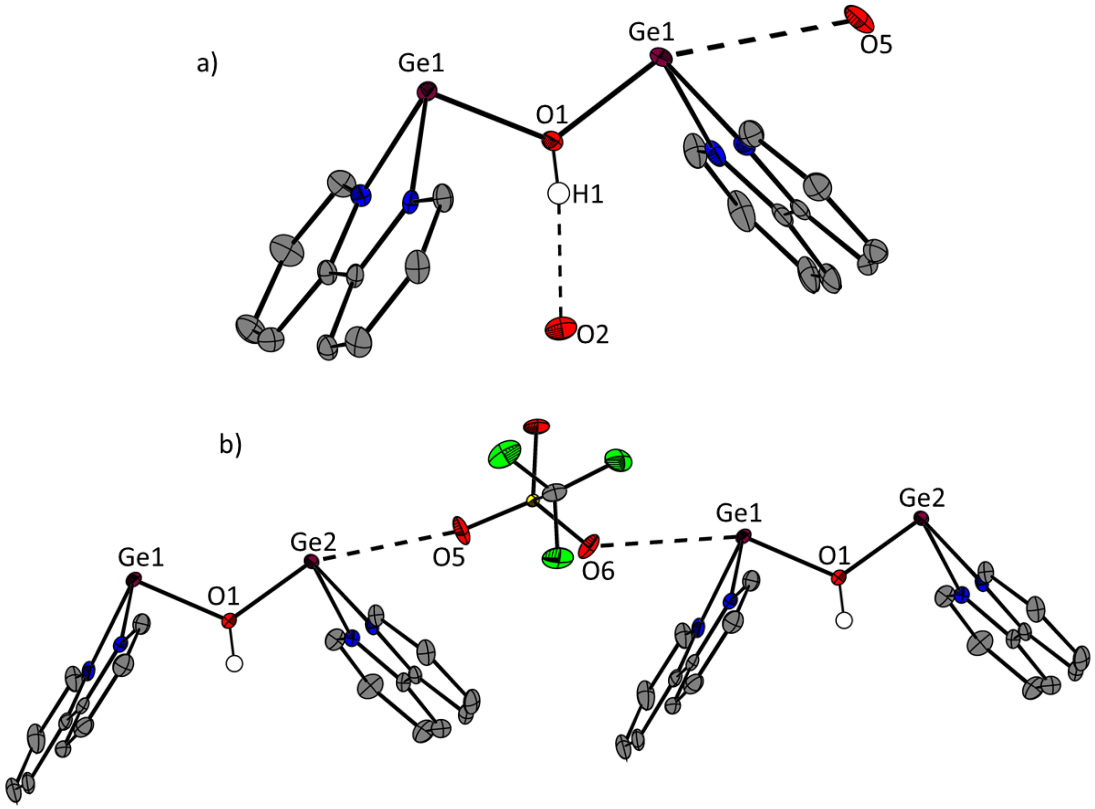

Figure 4.4.1: Solid-state structure of a) the cation in [(bipy)Ge-O(H)-Ge(bipy)][OTf]$_3$ with the closest triflate contact shown, and b) the coordination polymer formed in the solid state. Thermal ellipsoids are shown at the 50% probability level. Non-relevant hydrogen atoms are omitted for clarity.

In the solid state, the compound crystallizes in $P2_1/c$ space group with four molecules in the unit cell, and one as the asymmetric unit. The Ge-O(H)-Ge core appears to adopt an almost perfectly trigonal planar geometry, and the Ge-O-Ge angle is 121.81(14)° which is close to the idealized trigonal planar 120° angle. The Ge1-O1 and Ge2-O1 bond lengths are both similar with values of 1.923(3) Å and 1.940(3) Å respectively, suggesting a delocalized electronic structure, and a distribution of the 3+ charge around the entire Ge-O-Ge framework. The Ge-O_{OH} bonds are slightly outside of the sum of the Ge-O covalent radii (Ge-O Σ_{CR} = 1.84 Å),[151] and the Ge-N bonds (average: 2.060(4) Å) are significantly shorter

than those in $[(bipy)_2Ge]^{2+}$ (average *cis*-N-Ge bonds: 2.094(1) Å; average *trans*-N-Ge bonds: 2.233(1) Å), presumably due to the relief of steric pressure at the Ge centre, as well as there being no substituent *trans* to the N-Ge bonds. Overall in the solid state, one of the triflates acts as a bridge between Ge atoms of two adjacent asymmetric units, forming a coordination polymer in the solid state (Figure 4.4.1b).

The gas-phase geometry of the complex was computed at the PBE0-def2TZVPP level of theory, and reproduces the solid-state structure well. Additionally, NBO calculations were performed to investigate the bonding in the Ge-O-Ge core. It was found that the Ge atoms bear very similar positive charges at the metal centre of +1.12*e* and +1.15*e* on Ge1 and Ge2 respectively. The oxygen bears -0.47*e* and the proton on the OH has a charge of +0.29*e*. Looking at the orbital contributions to the bonding, it is evident that the bond is polarized towards the oxygen with the Ge1-O1 bond polarized by 76% and the Ge2-O1 bond polarized by 79%. Additionally, the WBI value shows that each of the bonds possess significant covalent bond character ($WBI_{Ge\text{-}O}$ = 0.413), and is in line with the values previously calculated for the crown ether Ge(II) system.[166] As there is significant positive charge still located on the germanium centres, it is possible to envisage these acting as significant electron-withdrawing groups, to the point of weakening the remaining O-H bond towards further deprotonation. However, this has not been realized experimentally as reactions with bipy, DMAP, and 1,3-bis(diisopropyl)imidazole-2-ylidene (^{i}PrNHC) appeared to result in no reaction, or only afford the coordination products at the germanium centre, as no protonated salts were detected in the ^{1}H NMR spectrum.

4.5 Attempted Oxidation of Ge(II) and Sn(II) Dications

While the lone pair of the Ge and Sn complexes were shown to be inactive towards electrophiles, it was postulated that they would still be active towards oxidants. It has been shown recently that Ge(II) cations can be oxidized by the powerful oxidant XeF_2.[185] However, it is worthy to investigate whether milder oxidants would be sufficient to access Ge(IV) and Sn(IV) cationic species. Based on the reactivity presented earlier in this chapter, it was desired to examine whether oxidation or halide abstraction would be preferred, or see whether it was reagent-dependant.

Treatment of a CD_3CN solution of the dication with a CD_3CN solution of PCl_5, a relatively mild oxidant, resulted in a dark orange solution with some precipitate formation in the case of the reaction of the Sn(II) complex. The $^{31}P\{^1H\}$ NMR spectrum of the reaction mixture for the germanium complex shows the major product as PCl_3, with a chemical shift of δ = 220.2 ppm, as a result of the reduction of the PCl_5. With the tin reaction, while PCl_3 is formed according the $^{31}P\{^1H\}$ NMR spectrum, the major signal is found at δ = 129.8 ppm, which is likely the result of the abstraction of chlorides from PCl_3. The reaction appears to lead to competing processes for Sn(II) between oxidation to Sn(IV) and abstraction from PCl_3 to remain Sn(II), while the germanium prefers oxidation to abstraction. As such, while milder reducing reagents are desired, those reagents or by-products which can participate as a chloride donor are likely to lead to undesired reactions and forego oxidation.

Contrary to the reaction with PCl_5, dropwise addition of SO_2Cl_2 to a CH_3CN solution of the constituent dication results in a clean conversion to colourless powders upon removal of the solvent *in vacuo*. Attempts to crystallize the $[(bipy)_2ECl_2][OTf]_2$ salts were unsuccessful, as the salts lack sufficient solubility and precipitate out of solution when placed in the freezer. However, by switching the ligand to the more soluble 4,4′-di-*tert*-butyl-2,2′-

bipyridine (tBubipy), facilitated crystallization of the complex $[(tBubipy)_2SnCl_2][OTf]_2$ (Figure 4.5.1). Reactions of the complex $[(tBubipy)_2Sn][OTf]_2$ with Br_2 and I_2 were also undertaken and appear to be complete by ^{119}Sn NMR spectroscopy, however crystals could not be obtained from these reactions.

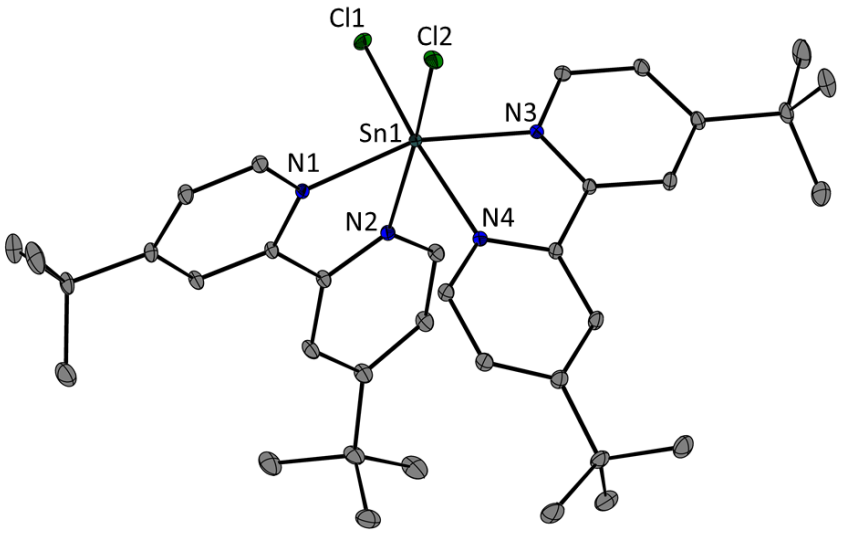

Figure 4.5.1: Solid-state structure of the cation in $[(tBubipy)_2SnCl_2][OTf]_2$. Thermal ellipsoids are shown at the 50% probability level. Non-relevant hydrogen atoms are omitted for clarity.

The $[(tBubipy)_2SnCl_2][OTf]_2$ compound crystallizes in the C2/c space group, with one half of the molecule in the asymmetric unit and four molecules in the unit cell. The Sn(IV) centre adopts a *pseudo*-octahedral bonding environment with four nitrogen atoms and two chlorine atoms forming the vertices. The N_{trans}-Sn bond lengths are 2.1870(12) Å, while the N_{cis}-Sn bond lengths are 2.2008(13) Å, both of which are significantly shorter than those found in the Sn(II) analogue $[(bipy)_2Sn][OTf]_2$ due to the greater Lewis acidity of Sn(IV) than Sn(II). The Sn-Cl bonds are 2.3488(4) Å, and are very similar to the previously reported Sn(IV) dication $[(Me_3P)_2SnCl_2][AlCl_4]_2$.[186] As the Sn(IV) centre is six-coordinate, there are no Sn---O contacts to the triflate counterions, and the closest approach is an H---$O_{triflate}$

interaction of 2.310 Å. The N_{trans}-Sn-N_{trans} angle is 160.77(7)° is much larger than that in the Sn(II) complex (143.1(2)°) due to the lack of the stereochemically-active lone pair, while the N_{axial}-Sn-N_{axial} angle of 82.52(7)° is closer to that of the Sn(II) derivative (77.1(2)°). The Cl-Sn-Cl angle is 96.93(2)°, which again is consistent with the phosphine-ligated Sn(IV) dicationic complex having an angle of larger than 90° (102.25(2)°).

4.6 Summary

In summary, the reactions of the dicationic salts $[(bipy)_2Ge][OTf]_2$ and $[(bipy)_2Sn][OTf]_2$ with a variety of substrates were examined. The reactions with electrophiles showed that the lone pair is likely not available to act as a Lewis base, likely due to the prevalent *s*-type character of the electrons, augmented by the cationic charge at the element centres. The ability of the dications $[(bipy)_2Ge][OTf]_2$ and $[(bipy)_2Sn][OTf]_2$ to act as halide abstracting agents, which sometimes occurs preferentially over oxidation, was explored. The new complex $[(bipy)Pt(COD)][OTf]_2$ was characterized crystallographically, and was found to exhibit a typical square planar geometry, despite a close approach of one triflate counterion. The NMR data presented for the reactions of $PhPCl_2$ and PCl_3 with the dications illustrates the ubiquity of the abstractions from both metal and non-metal substrates as a general reaction. However, through the reaction with water, it was demonstrated that these complexes can still behave as Lewis acids despite their high coordination numbers at the Ge or Sn centre. Ligand-facilitated deprotonation of the H_2O, likely *via* coordination to the metal centre, leads to the isolation of the hydroxyl-bridged digermanium tricationic complex. Unfortunately, attempts to further deprotonate this to access a cationic germyl ether were unsuccessful. Additionally, while the lone pairs are unavailable for bonding in a donor-acceptor sense, the oxidation of the complexes with X_2 sources cleanly afforded the

oxidation products, of which the chloride example was crystallographically characterized. These insights provide an entry point into developing the reactivity of cationic main group complexes and are of great interest from a fundamental perspective, as well as looking forward towards further exploring the utility of main group cations in application-based processes.

Chapter 5 - Complexes of High Oxidation-State Main Group Cations

5.1 Introduction

The preceding chapters have examined complexes of monocationic complexes of the group 13 elements, and dicationic complexes of the group 14 elements in the +2 oxidation state. In this chapter, the discussion turns to examine polycationic complexes (charges ≥ +3) in the highest oxidation state of these elements.

Highly electrophilic complexes are of interest for both their fundamental structure and bonding, but also for their potential to invoke reactivity in typically inert substrates due to their high charge. This principal has been exploited previously in the concept of Frustrated Lewis Pairs (FLPs), which rely on the synergistic activity of a highly electrophilic Lewis acid with a strongly nucleophilic Lewis base to initiate reactivity.[187] While the majority of these complexes which facilitate reactivity have focused on traditional Lewis acids and bases such as the electrophilic borane $B(C_6F_5)_3$, and the nucleophilic $P(tBu)_3$ or $P(Mes)_3$,[188] there have been a handful of examples which have employed less classical Lewis acids such as silylium ion $[(C_6Me_5)_3Si]^+$ and fluorophosphonium cation $[(C_6F_5)_3PF]^+$ (Figure 5.1.1).[93,95] As such, these complexes set a precedent for highly Lewis acidic main group cations having applications towards new reaction chemistry.

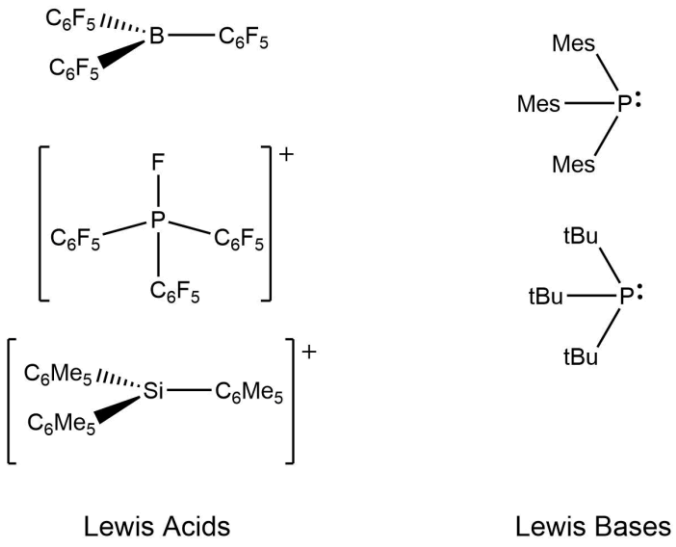

Figure 5.1.1: Examples of Lewis acids and Lewis bases used in FLP chemistry.

To facilitate the isolation of highly charged species, a variety of donors have potential to stabilize the cations. Pyridine-based donors such as bipy and 4-dimethylamino pyridine (dmap) are ubiquitous in transition metal coordination complexes, and have recently garnered interest towards stabilizing main group cations (Figure 5.1.2).[144,169,189,190] One potential complication that could arise is the reduction of the ligand, which has been seen in aluminum complexes of the type $Al(bipy)_3$,[191] and as predicted for some group 14 bipy complexes.[192] However, because of their omnipresence in coordination chemistry, pyridine-based donors represent useful reagents to assess at the outset of this project.

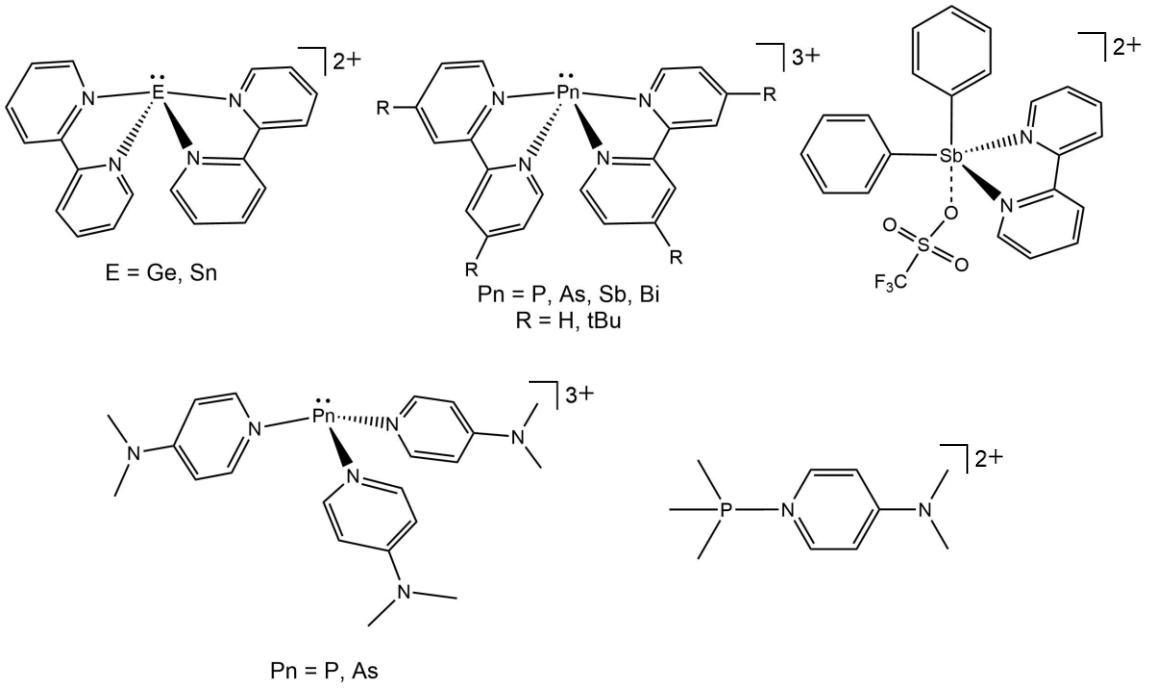

Figure 5.1.2: Recent examples of cationic complexes stabilized by bipy and dmap.[144,169,189,190]

In terms of starting materials, triel(III), tetrel(IV) and pnictogen(V) halides exist and are commercially available. These complexes themselves are known to act as Lewis acids, and the process of halide abstraction will certainly augment this. Due to the strong E-X bond strengths as a result of this Lewis acidity, the use of AgOTf will likely be required instead of TMSOTf. While TMSOTf has found generic use in halide abstraction from tetrel(II) and pnictogen(III) centres,[140,144,189] as well as facilitating the preparation of dicationic tetrel(IV) complexes,[186,193] the increased strength of the E-X bond as a result of increased charge build up will likely preclude activation with TMSOTf, and require the strong lattice enthalpy inherent in the formation of AgX using AgOTf. This leads to two potential reaction pathways to generate the desired cations. One route involves the direct reaction of the halide abstractor with the main group halide, filtration of the silver halide salt, and subsequent treatment of the solution with the ligand (Scheme 5.1.1a). The second viable option is the

mixture of all three components in a one-pot reaction, and subsequent filtration of all insoluble components (Scheme 5.1.1b). The advantage to method (a) is the removal of the insoluble silver salt precludes any undesired reactions of the ligand with the silver centre, forming silver coordination complexes. A complex of this type is presented in Figure 5.0.3, which resulted from the coordination of dmap to AgOTf rather than to the cationic centre. However, it is unknown whether AgOTf is strong enough to abstract four or five halides from a single element centre due to the E-X bond strength increasing with augmented charge, or is the coordination of a ligand required to induce E-X bond cleavage by decreasing the electrophilicity at the cationic centre. Method (b) is advantageous as the mixing of all components of the reaction shortens reaction time by removing the intermediary filtration step. However, if the resulting product exhibits low solubility, it may be removed with the AgX salt during the filtration, and separation of the two could prove difficult. Additionally, coordination of the ligand to the electrophilic Ag(I) cation may lower its reactivity and preclude complete halide abstraction. In general, it will likely be reaction dependent and the method should be adjusted as needed depending on the substrates, as well as after assessing whether undesired reactions occur with a particular route.

Scheme 5.1.1: (a) Reaction of halide precursor with AgOTf, with subsequent filtration of the insoluble silver salt, followed by addition of the ligand; (b) one-pot reaction of halide precursor, AgOTf, and the ligand to produce ionic salts.

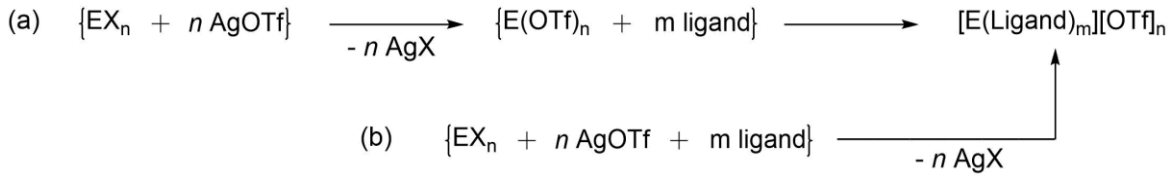

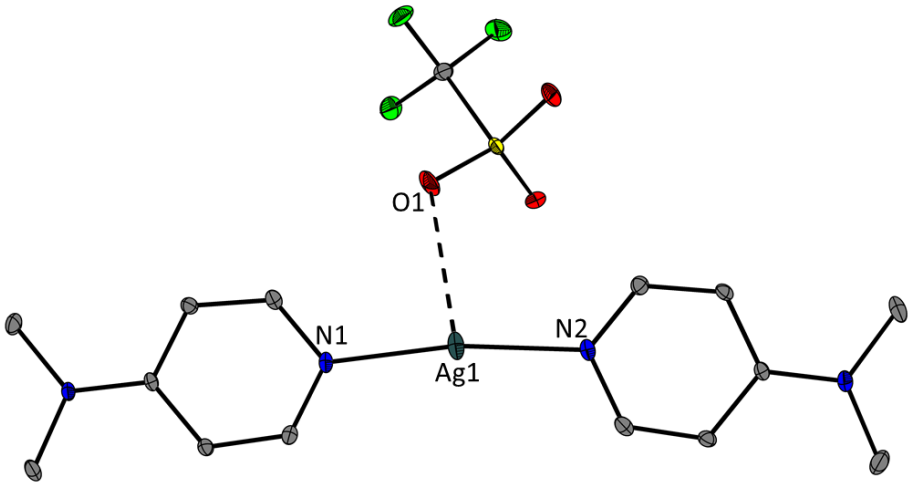

Figure 5.1.3: Complexation of silver(I) triflate with dmap obtained from a reaction mixture of AgOTf, $SeCl_4$ and dmap according to the method in Scheme 5.1.1b.

5.2 Preparation of an Octahedral Gallium Tricationic Complex

Treatment of a CH_3CN solution of $GaCl_3$ with three equivalents of AgOTf resulted in the immediate precipitation of a colourless AgCl, presumably forming $Ga(OTf)_3$ in solution, which has been characterized as a THF solvate previously.[194] To the suspension was added two equivalents of *tris*(1-methyl-imidazol-2-yl)phosphine (PIm_3) and the mixture was allowed to stir for 2 hours. Filtration of the solution led to a colourless solution, which when concentrated *in vacuo*, and placed in a -35°C freezer for two days, colourless prismatic crystals precipitated from the solution. Upon examination of the $^{31}P\{^1H\}$ NMR spectrum, there is a marked change in the chemical shift of the phosphorus atom (δ = -132.5 ppm) compared to the free ligand (δ = -61.2 ppm), indicative of coordination to a Lewis-acidic centre. The remaining crystals were analyzed using X-ray crystallography, and the complex was formulated as the octahedral *bis*-ligand complex $[(PIm_3)_2Ga][OTf]_3$, featuring a tricationic gallium core and three non-interacting triflate anions.

The complex crystallizes in the P-1 space group with two molecules in the unit cell, and the asymmetric unit contains two $[PIm_3Ga]^{3+}$ ions with the other PIm_3 ligand being

generated by the inversion centre at each gallium centre. The local structure at each gallium centre features an octahedral coordination, with an overall C_{3v} symmetry enforced by the trifold symmetry of the coordinated ligand (Figure 5.2.1a and b). The average N-Ga bond distances are 2.0523(15) Å, which is outside of the N-Ga covalent radii (Σ_{CR} (N-Ga) = 1.95 Å)[151], but in this case is likely due to the steric repulsion of the two PIm_3 ligands crowding at the gallium centre. Additionally, where each nitrogen is approximately 180° from another nitrogen donor, this likely enforces a *trans*-effect which elongates the N-Ga bonds. The same trend was observed in $[(bipy)_3Ga][I]_3$, which had slightly longer average N-Ga bonds at 2.064(6) Å.[195] The complex also features a pronounced pyramidalization at the phosphorus centre (Avg $\Sigma_{P(complex)}$ = 287.9(1)°), which is significantly more pyramidalized compared to the relaxed free ligand ($\Sigma_{P(ligand)}$ = 302.95(7)°),[196] indicating more *s*-character to the lone pair at phosphorus in the complex. Additional structural parameters are presented in Table 5.1.1, including a comparison with the indium derivative $[(PIm_3)_2In][OTf]_3$ which has also been structurally characterized.[197]

Table 5.2.1: Comparison of average metrical parameters of $[(PIm_3)_2Ga][OTf]_3$ and $[(PIm_3)_2In][OTf]_3$, along with their ^{31}P NMR chemical shifts.

	$[(PIm_3)_2Ga][OTf]_3$	**$[(PIm_3)_2In][OTf]_3$**
Average N-M distance (Å)	2.0523(15)	2.212(19)
M-P Distances (Å)	3.502(3) and 3.486(3)	3.603(3) and 3.589(3)
$\Sigma_{P(ligand)}$ (°)	287.9(1)	293.09(10)
^{31}P Chemical Shift (ppm)	-132.5	-125.9

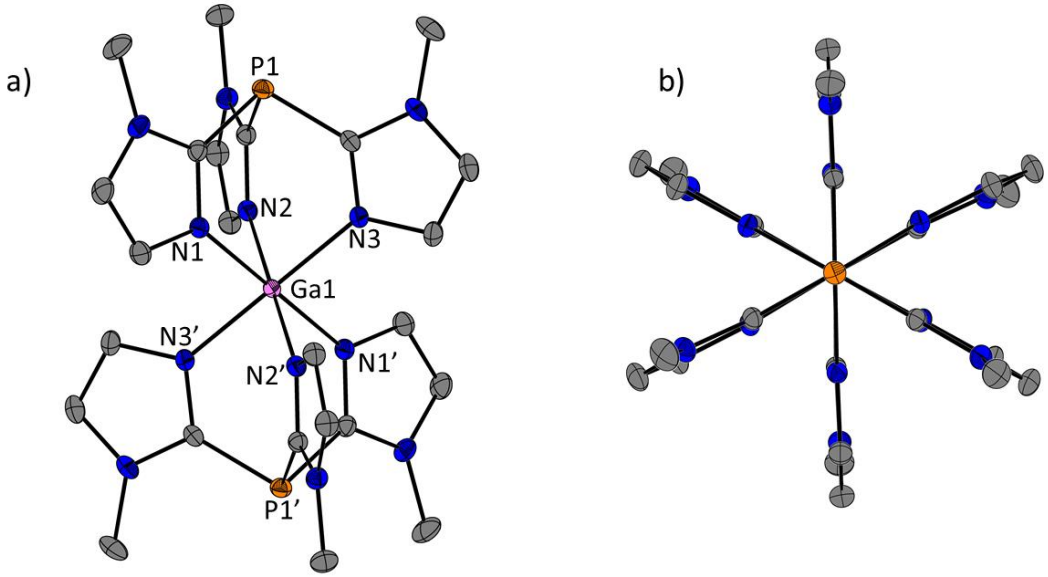

Figure 5.2.1: (a) Crystal structure of the cation $[(PIm3)_2Ga]^{3+}$ showing the octahedral arrangement around the Ga atom and (b) perspective view showing the C3v nature of the ligand coordination environment. Ellipsoids presented at the 50% level and hydrogen atoms and anions have been omitted for clarity.

To assess whether there was any potential for reactivity, including whether there was any degree of lability to the binding of the PIm_3 ligand, the complex was dissolved in CD_3CN and to this was added three equivalents of 2,2'-bipyridine to examine whether ligand exchange would occur at the gallium centre. After letting the reaction stir, a $^{31}P\{^1H\}$ NMR spectrum was collected, which showed the unreacted *bis*-ligand complex as the only phosphorus-containing complex, with no free ligand evident in the spectrum. The same outcome was found when dmap was added to the reaction mixture as well. Finally, Et_3PO was also added to a CD_3CN solution of the complex to examine whether there would be any interaction with the Lewis acidic centre using the Gutmann-Beckett method.[198,199] Unsurprisingly, examination of the $^{31}P\{^1H\}$ NMR spectrum showed no change in the chemical shift of the Et_3PO moiety (^{31}P δ = 49.5 ppm in CD_3CN) indicating no interaction,

likely due to the gallium centre being fully encapsulated by the two phosphine ligands, and no evidence of ligand dissociation in solution has been found. As such, these complexes in and of themselves do not exhibit significant Lewis acidity in solution.

5.3 Targeting Tricationic Aluminum Complexes

Like the tricationic gallium complexes, aluminum also makes an attractive target for pursuing highly charged complexes. Aluminum is a prototypical Lewis acid for many organic transformations and is often engaged by a variety of basic neutral donors.[118,200,201] However, in order to engage less classical donors with hopes of catalytic activity, higher Lewis acidity is desired at the aluminum centre. This approach has worked in the application of phosphorus towards small molecule activation using Frustrated Lewis Pairs (FLPs) by enhancing the phosphorus centre with a cationic charge, as well as electrophilic fluorine atoms.[202,203] The potential for aluminum to adopt a +3 charge provides opportunity to improve on traditional aluminum-based Lewis acid catalysis.

The incorporation of a phosphorus atom into the ligand scaffold, as was the case with the gallium complex, enabled efficient reaction monitoring with ^{31}P NMR spectroscopy. As such, the use of the *tris*(1-methyl-imidazol-2-yl)phosphine ligand was desired for this purpose. Additionally, as aluminum(III) trifluoromethanesulfonate, $Al(OTf)_3$ is commercially available, the hope was that the intermediary filtering of AgCl from the reaction with AgOTf could be avoided. Treatment of a suspension of $Al(OTf)_3$ in CH_3CN with the PIm_3 ligand immediately resulted in the formation of a yellow solution, common with acetonitrile solvates of main group cations.[144] However, upon collection of the $^{31}P\{^1H\}$ NMR spectrum, it was immediately apparent that the mixing of the two chemicals caused the degradation of the ligand, likely due to $Al(OTf)_3$ being a potent Lewis acid. It was

decided to approach the synthesis with the same halide abstraction methodology with AgOTf, despite the extra filtration step. To the CH_3CN solution of $AlCl_3$ was added solid PIm_3, in hopes of generating a donor-acceptor adduct, which would ideally lower the Lewis acidity of the cation as it is formed from the chloride abstraction. Upon addition of AgOTf, immediate precipitation of AgCl occurred, along with formation a yellow supernatant. Again, the $^{31}P\{^1H\}$ NMR spectrum showed many peaks (>8 total) and indicated the degradation of the ligand due to the lack of signal for the free ligand (δ = -61.4 ppm), likely through a P-C bond activation process facilitated by the cationic aluminum centre (Figure 5.3.1). This type of bond activation has been seen previously with highly electrophilic boranes and diaryl(phenylethynyl)phosphine.[204]

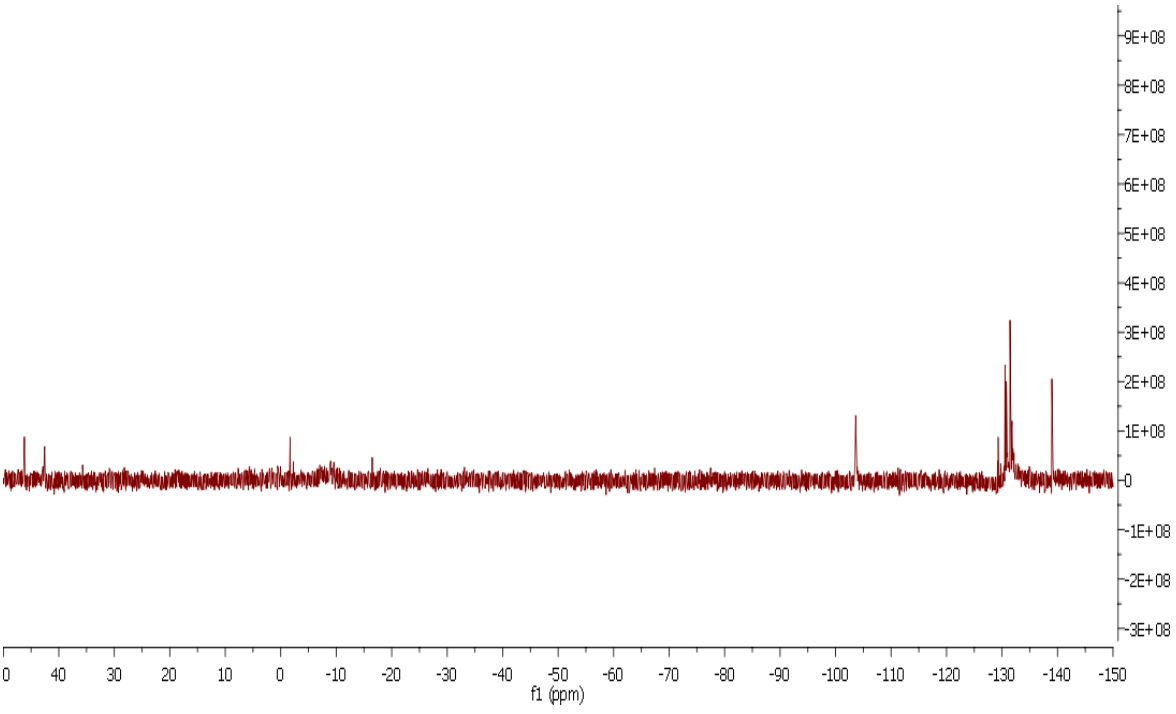

Figure 5.3.1: $^{31}P\{^1H\}$ NMR spectrum of the reaction mixture of $Al(OTf)_3$ with PIm_3, resulting in Lewis acid-induced ligand degradation.

To prevent this unwanted P-C bond activation, the ligand 4,4′,4″-Tri-*tert*-butyl-2,2′:6′,2″-terpyridine (tBu_3terpy) was investigated as an alternative. The presence of three pyridine functionalities ensures strong donor centres similar to the imidazoles in PIm_3, and the lack of P-C bonds precludes activation of the ligand. Additionally, the presence of the *tert*-butyl (tBu) groups should improve solubility of these highly charged salts. Treatment of a mixture of CH_3CN and the tBu_3terpy ligand with solid $AlCl_3$, followed by three equivalents of AgOTf, led to the formation of a yellow solution, which when the solvent was removed *in vacuo*, produced a light yellow solid. The ^{1}H NMR showed the preservation of the ligand scaffold, and no extraneous signals were present. Additionally, the $^{27}Al\{^{1}H\}$ NMR spectrum showed a single peak at 3.1 ppm. Upon redissolution of the solid in CH_3CN and cooling to -35°C for 48 hours, light yellow X-ray quality crystals precipitated from solution, which were formulated as the tricationic salt $[(tBu_3terpy)Al][OTf]_3$.

The complex crystallizes in the orthorhombic space group $Pna2_1$ with four molecules in the unit cell. The complex adopts a six-coordinate *pseudo*-octahedral geometry at the aluminum centre with the three nitrogen atoms of the tBu_3terpy ligand occupying three of the equatorial positions, and contacts to the three triflate ions occupying the fourth equatorial and two axial positions (Figure 5.3.2). The N-Al bond distances average 1.981(3) Å which is greater than the sum of the N-Al covalent radii (Σ_{CR} (N-Al) = 1.97 Å).[151] The average O-Al bond distance is 1.882(2) Å, with the shortest O-Al bond being the equatorial triflate interaction, which is within the sum of the Al-O covalent radii (Σ_{CR} (O-Al) = 1.89 Å).[151] The short O-Al interactions are likely due to the strong electrostatic component of the electronegative oxygen with the cationic aluminum centre. The triflate anions appear to be fully dissociated in solution, as in the ^{19}F NMR spectrum, there is only one signal at -79.8

ppm. The interligand *cis*-N-Al-N bite angles are 80.05(11)° and 79.73(11)° with the *trans*-N-Al-N angle being 178.74(11)°. Additionally, the planarity of the ligand is essentially unchanged with a total torsion between all three pyridine rings of 2.4°. Similar structural features are seen in the analogous complex (tBu_3terpy)$FeCl_3$.[205]

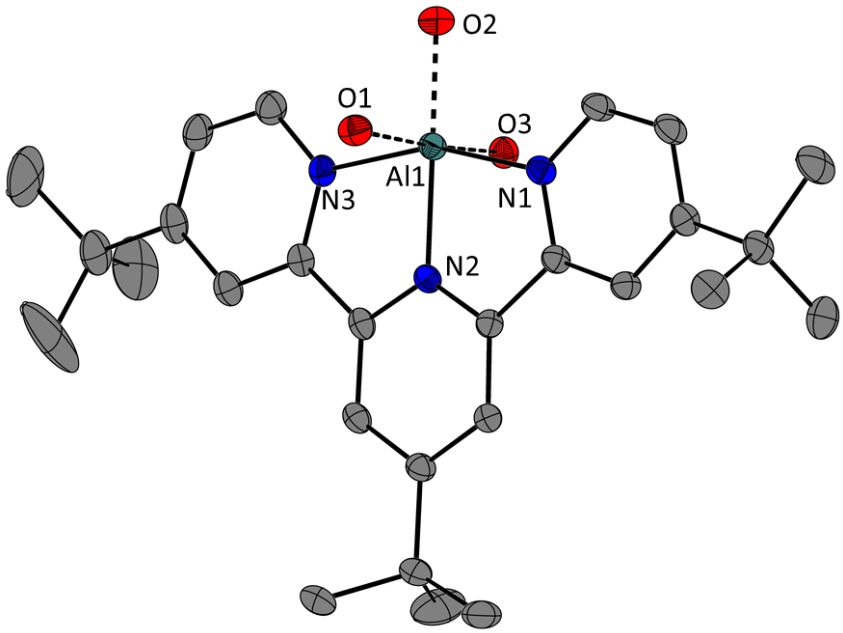

Figure 5.3.2: Crystal structure of the salt [tBu_3terpyAl][OTf]$_3$ showing the octahedral arrangement around the Al atom incorporating the Al---O contacts to the triflate anions. Ellipsoids presented at the 50% level and hydrogen atoms have been omitted for clarity.

The difference in Lewis acidity between aluminum and gallium can often be pronounced, depending on the nature of the substituents at the metal centre. The values presented in Table 5.3.1 show the difference in dissociation energies between various group 13 complexes and a subset of neutral and anionic donors.[206] By affixing electron-withdrawing substituents to the metal centre, the enhancement of Lewis acid character is greatly influenced. However, these data do not examine how dissociation energies are influenced by molecular charge at the metal centre. To probe the difference, the model compounds $[PIm_3M]^{3+}$ (M = Al, Ga)

were computed at the PBE1PBE/def2TZVPP, along with their Et_3PO-complexed derivatives, to determine the energetics of complexation to the metal centre. The aluminum derivative shows a dissociation energy of 620 kJ mol^{-1} while the gallium complex was found to favour complexation by 567 kJ mol^{-1}. As aluminum is a harder Lewis acid than gallium, it likely prefers the harder oxygen donor than gallium does. This is likely exacerbated by the strong Al-O bond formation, and better orbital overlap with the smaller aluminum centre. Experimentally, adding Et_3PO to a solution of $[(tBu_3terpy)Al][OTf]_3$ in CD_3CN resulted in a ^{31}P chemical shift of δ = 70.4 ppm, which is significantly different than that of the free ligand in CD_3CN (δ = 49.5 ppm), indicating the aluminum is significantly Lewis acidic, and the coordination of only one terpyridine ligand does not impede the coordination of the phosphine oxide as it does in the case of the gallium complex $[(PIm_3)_2Ga][OTf]_3$. This is in line with employing the Gutmann-Beckett method with other examples of main group Lewis acids,[207,208] however, it should be noted that solvent effects are an important consideration and care should be taken when comparing absolute values across different solvents.

Table 5.3.1: Gas-phase dissociation energies (kJ mol^{-1}) of selected donor-acceptor complexes at the RI-BP86/def2TZVPP level of theory. Reproduced with permission.[206]

	NH_3	**H_2O**	**PH_3**	**H^-**	**CH_3^-**	**F^-**
BCl_3	89.3	15.8	13.5	451.2	458.7	426.5
$B(C_6H_5)_3$	45.8	10.1	----	383.8	367.7	344.7
$B(C_6H_4F)_3$	40.7	4.8	----	405.2	389.1	366
$B(C_6F_5)_3$	97.1	36.5	24	528.1	487.5	454
$AlCl_3$	143.9	97.4	66.4	482.7	496.8	523
$Al(C_6H_5)_3$	94.4	63.8	34.8	395.6	401.1	442.7
$Al(C_6H_4F)_3$	94.6	63.7	34.9	420.2	425.9	467.2
$Al(C_6F_5)3$	145.5	112	63.9	513.6	521.5	552.1
$GaCl_3$	118.3	68.9	56.7	502.4	507.5	456.2
$Ga(C_6H_5)_3$	66.1	23.1	23.1	382.5	376.2	356.1
$Ga(C_6H_4F)_3$	66.3	37.4	22.8	407.5	401.1	379.8
$Ga(C_6F_5)_3$	114.9	74.9	52.9	510.7	506.6	464.7

5.4 Synthesis of Highly-Charged Group 14 E(IV) Complexes

While the fundamental chemistry of preparing highly charged cations is interesting from a chemical curiosity point-of-view, the lack of characterization data for these elusive complexes represents a missing piece of our knowledge of the behaviour of main group Lewis acids. By tailoring the synergistic properties of the ligand of choice and the cationic centre, it should be possible to stabilize these species so they can be isolated while still retaining significant Lewis acidity. Employing nitrogen-based donors has served this type of chemistry well in the past, and the application of these pyridine-type donors was determined to be a viable starting point to investigate their ability to stabilize highly charged group 14-based cations.

Prototypical pyridine-based donors such as bipy and dmap have recently been used to stabilize tetrel dications of the form $[Me_2E(donor)][OTf]_2$ (E = Si, Ge, Sn),[209] and have also been investigated for stabilizing pnictogen(III) trications.[144] Upon addition of solid bipy to a mixture of SiI_4 or $SnCl_4$ in CH_3CN, a yellow solution becomes apparent over the precipitated AgX. However, filtering the AgX and placing in the freezer overnight results in a light pink coloured solution over colourless crystals. The pink colour is indicative of protonation of bipyridine, and the ^1H NMR spectrum of the crystals indicated this with a broadened downfield signal of +12 ppm. The identical reaction using dmap, a monodentate pyridine donor, was also found to form protonated dmap with the downfield signal in the ^1H NMR spectrum. Originally, it was suspected that the CH_3CN or reagents were contaminated with adventitious water. The reaction was repeated with CH_3CN which was rigorously dried over CaH_2 and freshly distilled into a Strauss flask to be immediately used in the glovebox. Despite the care taken to ensure dry solvent, the conjugate acid of the ligand, resulting from

protonation, was still present in the solution. Additionally, addition of bipyridine or dmap to a solution of SiI_4 or SnX_4 does not result in a pink solution, ruling out HX presence in the reagents. The most plausible explanation suggests that the protonated ligand originates from the acetonitrile solvent. Acetonitrile is reasonably acidic and has been shown to react with strong bases previously.[210] However, even after isolation, no evidence of the reaction product containing the $[CH_2CN]^-$ or equivalent was found in either the ^1H or ^{13}C NMR spectra.

The reactivity of the bipy or dmap ligand with CH_3CN is likely due to the coordination of the CH_3CN to the Si centre upon addition of SiI_4 to the solution. It is well known that $SnCl_4$ forms neutral coordination complexes with CH_3CN, and the product has been structurally characterized.[211,212] This coordination to SiI_4 in itself may allow a strong ligand to deprotonate the CH_3CN, or more likely, the deprotonation occurs after one or more abstraction events augmenting the electrophilicity at the silicon centre. This would initiate an Umpolung effect which withdraws electron density from the CH_3 group of acetonitrile and weakens the C-H bonds. The CH_3 can then be deprotonated by the basic pyridine ligand. It is possible that the ligand would coordinate to the Si centre first, then deprotonate the CH_3 by dissociating from silicon. As such, using a ligand with a higher denticity may mitigate the formation of the protonated ligand if the process is based on a dissociative mechanism, as multiple dissociation events are required to completely dissociate the ligand, which would be entropically disfavoured.

The use of the tBu_3terpy ligand presented in Chapter 5.2, as well as the ligand tris(1-ethyl-benzoimidazol-2-ylmethyl)amine ($BIMEt_3$), are good candidates as tricationic aluminum complexes of tBu_3terpy, as well as the recently reported cationic [$BIMEt_3$Ge(II)] and

[BIMEt_3Ge(IV)] complexes, have been characterized.[185] Combination of the ligand with AgOTf and SiI_4 in CH_3CN resulted in a bright orange supernatant along with precipitation of yellow AgI. After filtration and concentrating *in vacuo*, the solutions were placed in the freezer and after 72 hours, orange crystals had precipitated which were suitable for X-ray analysis. Unexpectedly, the complexes characterized crystallographically were found to be silicon cations each featuring an anionic β-diketiminate substituent resulting from the deprotonation, and subsequent trimerization, of CH_3CN. While the data obtained BIMEt_3 complex was only suitable for establishing the connectivity, the tBu_3terpy complex is of higher quality and can be discussed in terms of structural parameters.

The salt [(tBu_3terpy)Si(NacNacCN)][OTf]$_3$ crystallizes in the $P2_1/n$ space group with the tBu_3terpy ligand occupying three of the four equatorial positions, with the acetonitrile trimer occupying the other equatorial position and one of the axial position (Figure 5.4.1a). One coordinating triflate occupies the other axial position. The average length of the N-Si bond distance for the bound tBu_3terpy ligand is 1.908(2) Å, outside of the sum of the N-Si covalent radii (Σ_{CR} (N-Si) = 1.87 Å). The average for the acetonitrile trimer N_{NacNac}-Si bonds is much shorter than for the tBu_3terpy ligand at 1.807(2) Å. These are also within the sum of the N-Si covalent radii presumably due to the delocalized negative charge on the trimer moiety. As for the aluminum complex, the terpyridine ligand is essentially planar with a total deformation of 4.2°. The imide C-N bond distances are, on average, 1.329(2) Å, and are shorter than those found in the pyridine fragments of the tBu_3terpy ligand, further evidencing the delocalized π-bonding within the trimer. The $O_{triflate}$-Si interaction is 1.831(2) Å, which is slightly outside of the sum of the van der Waals radii (Σ_{CR} (O-Si) = 1.79 Å). The interaction of the triflate with the silicon centre has a marked effect on the geometry, as the complex would be expected to adopt a *pseudo*-

trigonal bipyramidal geometry consistent with a AX_5 VSEPR model and no lone pair at the silicon centre. These complexes prefer to adopt an octahedral geometry, as evidence by the anion coordination in $[(tBu_3terpy)Si(NacNacCN)][OTf]_3$, as well as the six nitrogen atoms around the silicon in $[(BIMEt_3)SiNacNac][OTf]_3$ (Figure 5.4.1b)

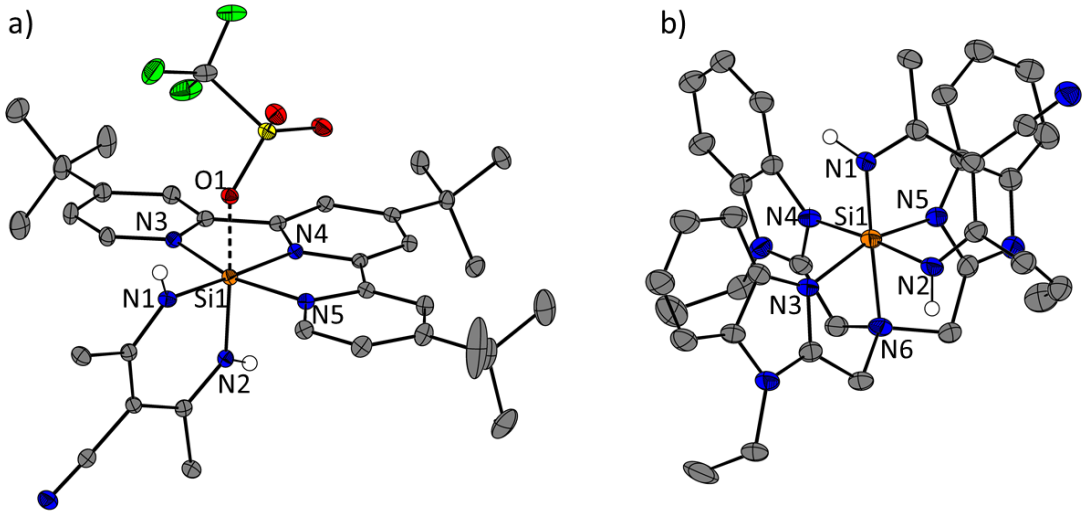

Figure 5.4.1: (a) X-ray structure of the cation in$[(tBu_3terpy)Si(NacNacCN)][OTf]_3$ showing the close contact to one triflate anion, and the NacNacCN coordination to the silicon centre. (b) X-ray structure of the cation in $[(BIMEt_3)SiNacNac][OTf]_3$ showing the six-coordinate silicon centre with no triflate contact. Ellipsoids presented at the 50% level and non-important hydrogen atoms have been omitted for clarity.

To examine the nature of the charge and bonding in these cations, DFT calculations were carried to examine the gas-phase electronic structures of the model complexes $[(terpy)M]^{n+}$ for M = Al, Si, Ge, Sn, and P. For the aluminum and silicon example, there is significant charge localized on the element centre (+2.19*e* for Al, +2.37*e* for Si) and both complexes retain their +3 and +4 oxidation states. Interestingly, for Ge, Sn, and P, it appears that these complexes appear to prefer their lower oxidation states of +2 and +3 respectively. The

Natural Population Analysis (NPA) shows that there is significant electron density (between 1.79*e* and 1.94*e*) in a valence orbital with lone pair character while those for the Al and Si centre are much less than one in any given valence orbital. For the geometry optimization of the Ge, Sn, and P complexes, there is a marked puckering of the terpy framework to accommodate the lone pair (Figure 5.4.2).

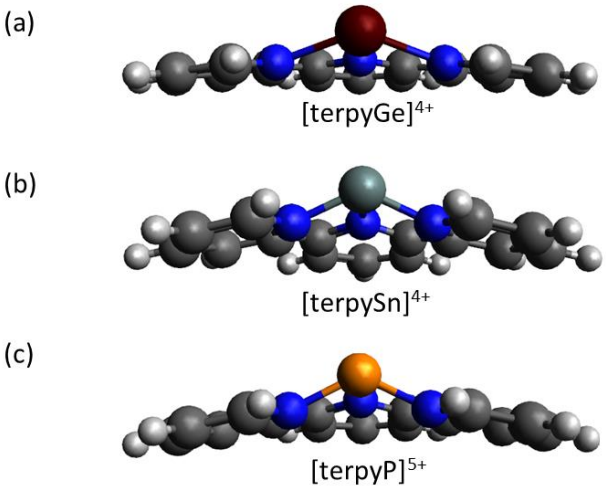

Figure 5.4.2: Optimized gas-phase geometries for a) $[terpyGe]^{4+}$, b) $[terpySn]^{4+}$, and c) $[terpyP]^{5+}$ at the PBE1PBE/def2TZVPP level of theory showing the puckering of the terpy ligand

These findings are consistent with a previous experiment in which the reaction of PCl_5 with AgOTf and the $BIMEt_3$ was found to give the P(III) tricationic complex $[(BIMEt_3)P][OTf]_3$. In the Al and Si examples, the HOMO is the π-system on the terpyridine ligand and the LUMO is an empty orbital at the Al or Si centre, which in the case of the silicon complex, likely facilitates coordination of CH_3CN which initiates the C-H bond activation process (Figure 5.4.3). There is obvious π-bonding character between the Al or Si centre and the nitrogen atoms on the terpyridine ligand. The similar orbital arrangement, yet differing

reactivity of the aluminum and silicon complexes shows how the charge impacts the overall reaction chemistry.

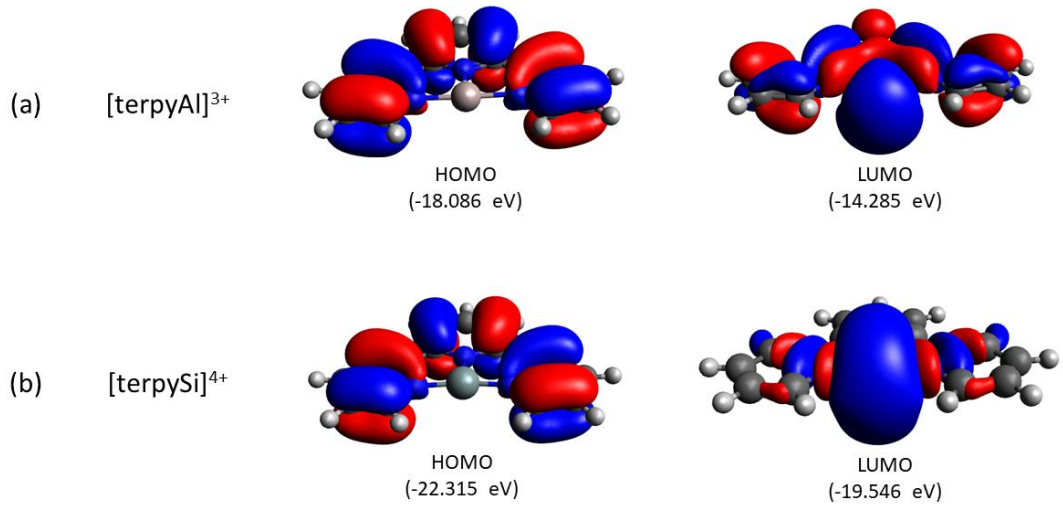

Figure 5.4.3: HOMO and LUMO of a) $[terpyAl]^{3+}$ and b) $[terpySi]^{4+}$.

Additionally, calculations were carried on the complex $[(terpy)Si(NacNacCN)]^{3+}$ to reveal several bonding characteristics in the cation without the triflate contact. The LUMO is primarily based at the silicon centre, and it is apparent that the triflate coordination in the solid-state occurs via interaction with this vacant orbital. The vacant orbital at the silicon also features some conjugation to the π-system of the terpy ligand. The HOMO is mainly the π-type orbital based on carbon backbone of the NacNacCN moiety. Interestingly, the HOMO-3 and HOMO-4, along with being part of the π-system of the terpy ligand, are also the lone pair based at the exocyclic -CN moiety, indicating that the ligand itself could retain some Lewis base character. This opens up the potential to use this nucleophilic moiety to link these cationic complexes to other electrophiles through a coordinative interaction. The N-Si σ-bonding orbitals of the three terpy nitrogen atoms and the in-plane nitrogen of the NacNacCN fragment are based in the HOMO-11

while the other out-of-plane N-Si σ-interaction for the NacNacCN moiety are the HOMO-8 HOMO-15. These orbitals are presented in Figure 5.4.4.

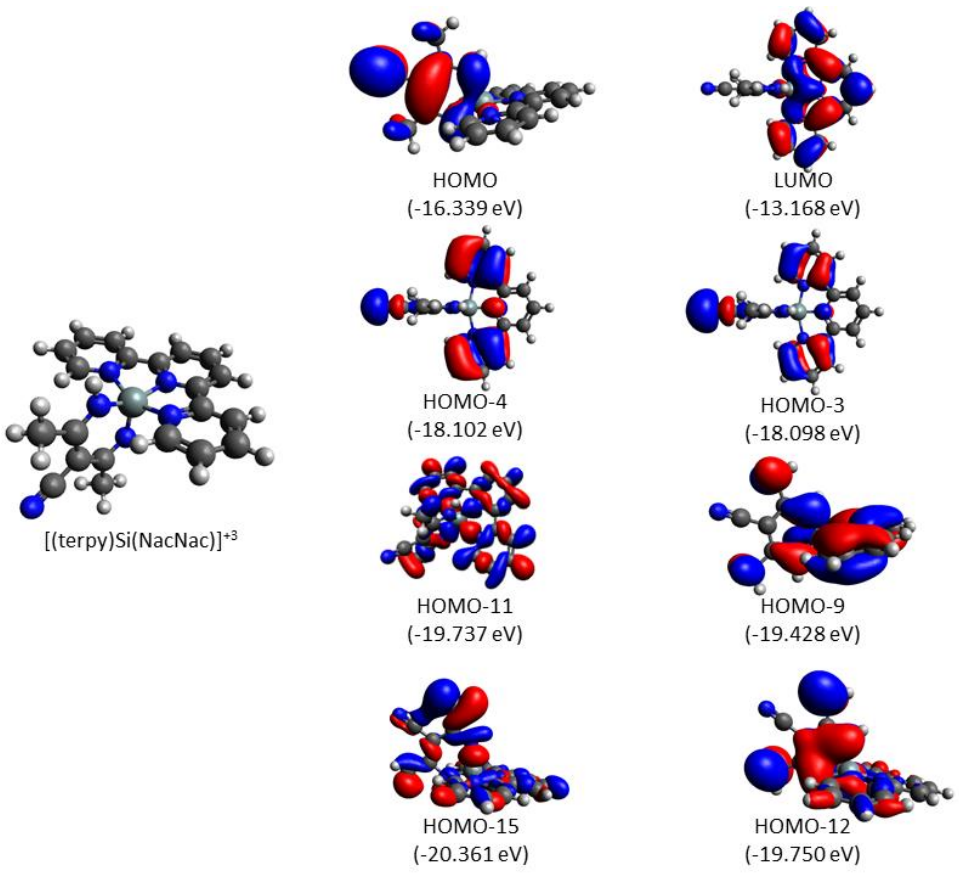

Figure 5.4.4: Relevant bonding orbitals in $[(terpy)Si(NacNacCN)]^{3+}$ with isovalues = 0.05

While the gas-phase calculations show that the tetracationic complex of Sn is less stable with respect to reduction than the silicon complex, it was still desired to investigate whether Sn(IV) tetracationic complexes were synthetically accessible. However, it was difficult to continue to use the *tert*-butyl-substituted terpyridine ligand as its economic feasibility to prepare these complexes on a large scale was low due to its cost of $650 for 5g. As such,

another ligand which features the same coordination environment was sought and it appeared that the ligand 2,6-bis(1-ethylbenzimidazol-2-yl)pyridine ($BIMEt_2Pyr$) would be easy to synthesize on a large scale and invoke the same *tris*-chelation.[213] Treatment of $SnBr_4$ with AgOTf and two equivalents of the $BIMEt_2Pyr$ led to the formation of a yellow solution along with AgBr, which was subsequently filtered off. Placing into the freezer for 72 hours produced yellow prismatic crystals suitable for X-ray analysis. Despite the prediction of the Sn(II)-type complex being more stable, the complex characterized crystallographically was found to be $[(BIMEt_3Pyr)_2Sn][OTf]_4$, and no reaction with CH_3CN was observed through spectroscopic means. To our knowledge, this is only the second characterized example of a Sn(IV) tetracationic complex.

The compound crystallizes in the C2/c space group with four molecules in the unit cell and half of the molecule in the asymmetric unit. The complex adopts a *pseudo*-octahedral geometry with the two pyridines occupying the axial positions and the nitrogen atoms of the four benzimidazole units occupying the equatorial plane (Figure 5.4.5). The N_{pyr}-Sn bond lengths average 2.161(4) Å while the N_{benz}-Sn bonds average 2.118(3) Å. Both are outside of the sum of the covalent radii (Σ_{CR} (N-Sn) = 2.01 Å), likely due to the sterics of the ligand around the tin centre precluding any closer approach. The N_{pyr}-Sn-N_{pyr} angle is linear at 180° while the two *trans*-N_{benz}-Sn-N_{benz} angles are 150.30(18)°. One of the ligands is significantly more distorted from the planar arrangement (approximately 16°) than the second ligand (approximately 4.8°). As the tin atom is completely surrounded by the ligand, there is likely no way for another molecule to approach the tin centre and take advantage of the Lewis acidity. In this vein, addition of Et_3PO to the solution does not result in any chemical shift change in the ^{31}P

NMR spectrum, indicating no interaction with the tin centre, and suggesting there is no ligand dissociation in solution, and implying the compound itself is not Lewis acidic.

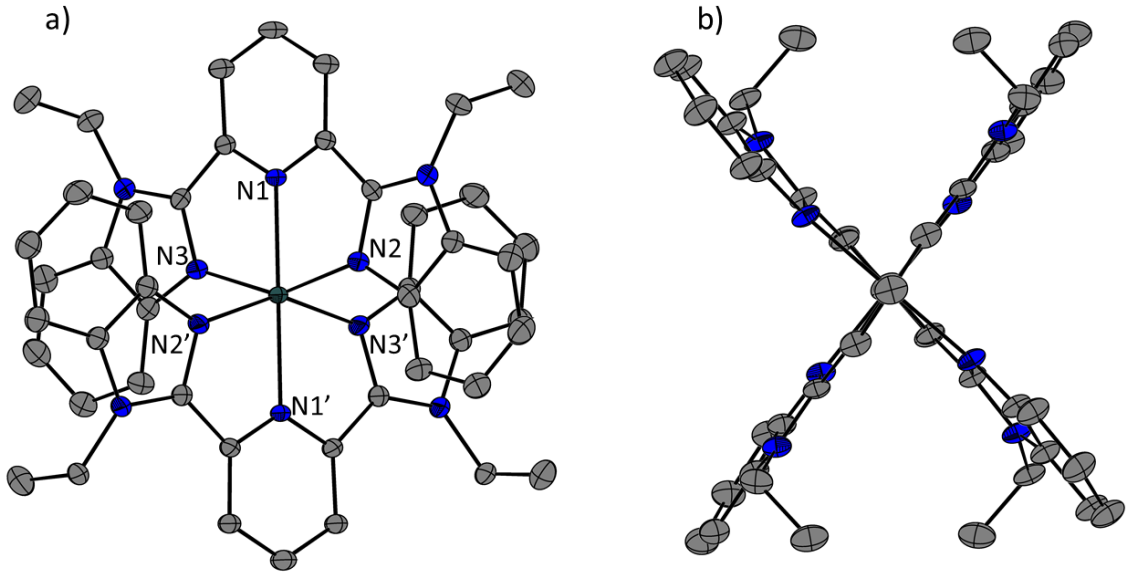

Figure 5.4.5: (a) Crystal structure of the cation in the salt $[(BIMEt_2Pyr)_2Sn][OTf]4$ showing the pseudo-octahedral geometry and (b) perspective view showing the two distinct ligand planes in the cation. Ellipsoids presented at the 50% level. Anions and important hydrogen atoms have been omitted for clarity.

5.5 Attempted Synthesis of P(V) Pentacationic Complexes

Attempts to generate examples of P(V) pentacations are expected to be difficult to isolate due to the build-up of cationic charge at the phosphorus centre. The highly electrophilic centre, coupled with the basicity of nitrogen based donors, is likely to lead to further examples of protonated ligand through the activation of acetonitrile. Indeed, every attempt

to isolate complexes of the type $[(dmap)_nP][OTf]_5$ or $[(bipy)_3P][OTf]_5$ (where n = 5 or 6) led only to crystals which were analyzed by X-ray crystallography to be the protonated ligand salts of [dmapH][OTf] or [bipyH][OTf]. Interestingly, the ^{1}H NMR spectrum of the reaction mixture for $[(dmap)_5P][OTf]_5$ shows the presence of two distinct sets aromatic pyridine signals in a 3:2 ratio. Likewise the equivalent reaction to produce $[(dmap)_6P][OTf]_5$ shows only one set of aromatic signals in the ^{1}H NMR spectrum. Both of these reactions indicate that the desired complexes are likely forming in solution but when exposed to CH_3CN for a longer period of time, reaction with the solvent forms the protonated ligand. Thus, alternative ligands which are less basic, but still afford coordinative stabilization, are desired to allow isolation of these electrophilic species.

Recently, pyridine-*N*-oxides have been shown to be good donors for the stabilization of Sb(V) monocations and trications.[147,214] In this vein, their ability to stabilize these high oxidation state cations could be applied to the analogous phosphorus cations. However, because of their monodentate coordination mode, the compounds resulting from their use could adopt a variety of geometries. A systematic study of the coordination would be useful in determining the preferred coordination environment of these complexes. Addition of 4, 5, 6, and excess equivalents of solid 4-methylpyridine-*N*-oxide (MePyrO) to a mixture of AgOTf and either PCl_5 or PBr_5 results in the formation of increasingly dark red supernatants with the concomitant formation of AgCl or AgBr. After filtration, a $^{31}P\{^1H\}$ spectrum of all four reaction mixtures showed multiple products (Figure 5.5.1a-d). It appears that the relative integrations of the signals correspond to the amount of ligand in the reaction mixture. Additionally, it is apparent that as the concentration of ligand increases, the relative integration of the most upfield signal at -4.2 ppm increases, until once a two-fold excess (12

eq) is added (Figure 5.5.1d), when that signal becomes the only peak in the spectrum. However, crystallization of the complexes was unsuccessful in most cases, yielding only brown-coloured powders. However, in the case of the reaction of 5 equivalents of MePyrO, after two weeks at -35°C, brown crystals precipitated from solution which were suitable for X-ray analysis. The isolated complex was found to be formulated as the tetracationic salt $[(MePyrO)_5PCl][OTf]_4$ (Figure 5.5.2). More importantly, when the isolated crystals are redissolved, a single signal at -61.2 ppm is apparent in the $^{31}P\{^1H\}$ NMR spectrum (Figure 5.5.1e), which corresponds to the postulated signal corresponding to 5 equivalents in Figure 5.5.1a-c.

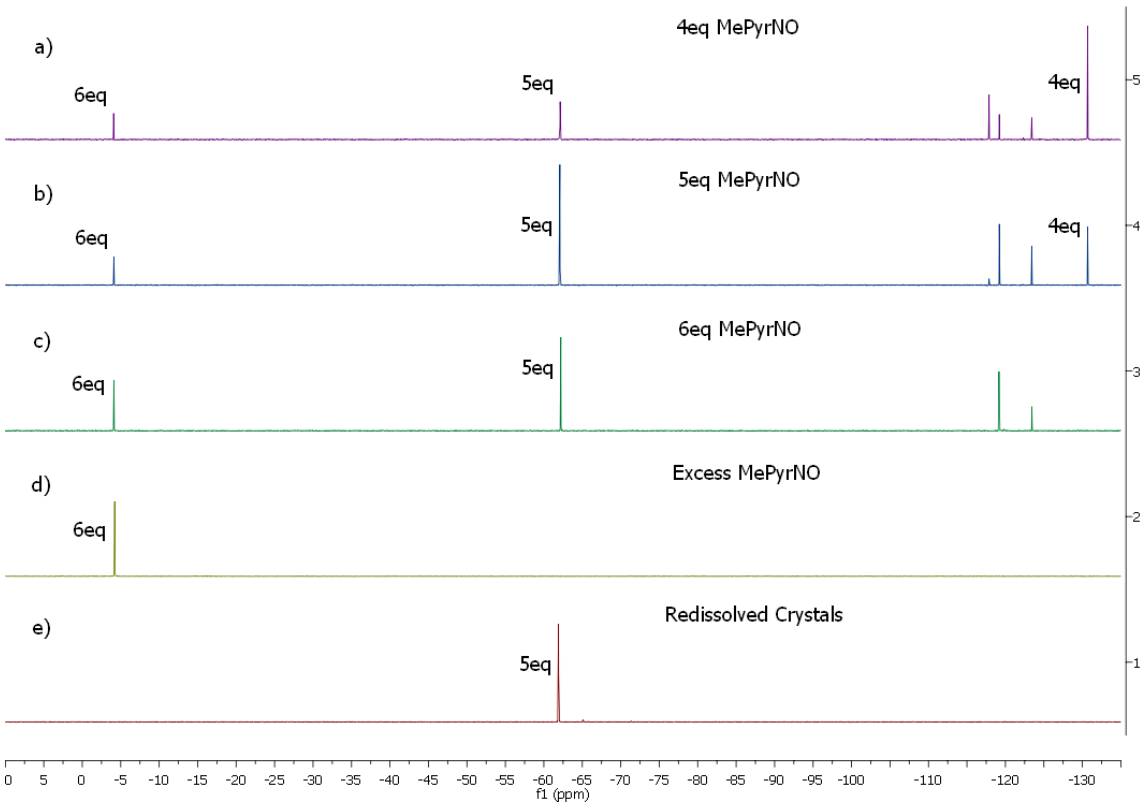

Figure 5.5.1: $^{31}P\{^1H\}$ NMR spectra of the reactions of a) 4 equivalents, b) 5 equivalents, c) 6 equivalents, and d) excess MePyrO with PCl_5 and AgOTf. Redissolution of the crystals obtained from the 5 equivalent reaction is shown in e).

The compound $[(MePyrO)_5PCl][OTf]_4$ crystallizes in the $P2_1/n$ space group and features five O-P interactions with the MePyrO ligands (Figure 5.5.2). The average O-P bond distance in the cation is 1.719(1) Å, which is inside the sum of the O-P covalent radii (Σ_{CR} (O-P) = 1.74 Å). The longest O-P interaction is 1.747(1) Å which is *trans* to the remaining chloride. This lengthened interaction is likely due to the steric interference with the four equatorial MePyrO ligands, as well as the *p*-type orbital which would be involved in the bonding of both the axial MePyrO and chloride is partially occupied and is not as available for donation from the ligand. The average O-P-O angle is 172.40(6)°, and the O-P-Cl angle is 172.42(5)°, indicating an overall slightly distorted *pseudo*-octahedral geometry at the phosphorus centre. It is apparent that having the oxygen between the bulk of the ligand and the small phosphorus centre allows the approach of a greater number of ligands, and may mitigate the dissociation of ligands in solution which is prevalent with bipy and dmap. There is an obvious bend at the oxygen centre of 123.33(9)°, which allows greater freedom for the ligands to adopt a conformation which minimizes steric interactions with the other ligands. In addition to their usefulness from a steric point-of-view, these ligands are also redox resistant[214] and could potentially find use in stabilizing these cationic complexes in conformations which allow redox chemistry to occur controllably at the element centre while still maintaining a degree of coordinative saturation.

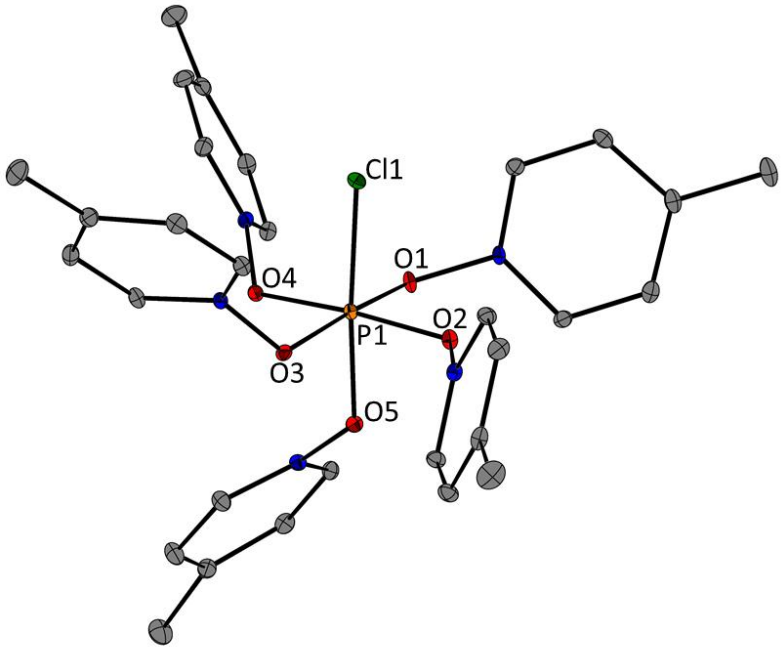

Figure 5.5.2: Crystal structure of the cation in $[(MePyrO)_5PCl][OTf]_4$ showing the *pseudo*-octahedral coordination environment at phosphorus. Ellipsoids presented at the 50% level. Anions and hydrogen atoms have been omitted for clarity.

5.6 Summary

The preparation of examples of high oxidation state cations of group 13-15 were found to be possible with judicious choice of ligands. The use of traditional pyridine-based donors such as dmap and bipy do not allow for the isolation of the cationic complexes, although evidence of their formation in solution is obtained, and instead typically result in the isolation of protonated ligand salts. The combination of solvent concentration, as well as steric interference, likely leads to the dissociation of the pyridine moiety from the cationic centre, allowing the coordination of CH_3CN. The coordination allows for the deprotonation of the CH_3 group as a result of a possible Umpolung process, leading to the protonated pyridine. As such, the use of other ligands allows for a multidentate interaction, which entropically disfavor dissociation, were desired. Using the PIm_3 ligand, useful for

monitoring reactions via ^{31}P NMR spectroscopy, the tricationic gallium complex $[(PIm_3)_2Ga][OTf]_3$ was successfully synthesized and characterized. By employing the terpyridine framework, the isolation of tricationic aluminum and silicon complexes were realized. The $BIMEt_3$ ligand also allowed the isolation of a silicon tricationic complex. In the silicon complexes, the activation of acetonitrile yields a β-diketiminate acetonitrile trimer which subsequently coordinates to the electrophilic centre. Interestingly, using the $BIMEt_2Pyr$ ligand, which is analogous in denticity to the terpyridine ligand, facilitated the isolation of the tetracationic tin complex $[(BIMEt_2Pyr)_2Sn][OTf]_4$.

Calculations of *mono*-terpyridine complexes $[(terpy)M]^{n+}$ in the gas phase reveals that these complexes for aluminum and silicon are stable with respect to redox chemistry. However, the analogous complexes of germanium, tin, and phosphorus prefer reduction to the +2 and +3 oxidation states respectively, as evidenced by the NPA occupancies of close to two electrons in the valence shell as a lone pair. Examining the bonding in $[(terpy)Si(NacNacCN)][OTf]_3$ reveals that there is significant delocalization throughout the π-system of the terpy ligand as well as the NacNacCN trimer. There is conjugation of the LUMO at the silicon centre to the terpyridine ligand, which likely lowers the electrophilicity slightly. The coordination of the triflate anion to the silicon centre through interaction with the LUMO is evident in the solid-state structure.

While the reactions to attempt to generate terpyridine-ligated P(V) pentacationic complex are expected to result in P(V) to P(III) reduction based on computational data, the use of the pyridine-*N*-oxide donors MePyrO enabled the isolation of the tetracationic complex $[(MePyrO)_5PCl][OTf]_4$, containing the tetracation. To my knowledge, this is one of the first structurally characterized complex featuring a main group polycation with a

charge >+3, where the charge can be envisaged to originate from a single atomic centre. The inclusion of an oxygen atom spacer in the donor molecule likely enables greater conformational freedom and allows closer approach of more donors and precludes dissociation of the ligands on the basis of steric interference which is likely a contributing factor in the protonation of dmap and bipy complexes. Within the broader context of coordination chemistry, these highly cationic complexes represent a new class of main group coordination complexes and continued investigation should target the design of a ligand scaffold which increases the availability of more coordination sites at the element centres to should lead to higher Lewis acidity. This would potentially lead towards new applications in Lewis acid catalysis, Frustrated Lewis Pair chemistry, and small molecule activation.

Chapter 6 – Summary

The work presented in this dissertation explored the synthesis of a wide variety of main group cations stabilized through coordinative interactions with N-, P-, and O-based ligands. The preparation of these molecules highlights the utility of halide abstracting agents to generate Lewis acidic cations, which are easily engaged by a variety of ligands. Judicious ligand choice has shown to be important, as unwanted degradation or insolubility results from the high electrophilicity in some cases. The majority of complexes presented herein were successfully characterized by X-ray crystallography, which allows for an in-depth study of their structure and bonding, as well as the ability to draw comparison between main group donor-acceptor complexes and their transition metal counterparts.

Chapter 2 highlights the synthesis of unique dmpe-stabilized octahedral cations of aluminum and gallium halides. The reactions proceed in a straight-forward reaction to give the characterized salts. These cations were investigated computationally to show that while other structural outcomes are possible in the gas phase, mainly based on neutral structures, it is the strong lattice enthalpy from the formation of ionic salts that drives the reactions forward. Additionally, this chapter also highlights the differences that donor atoms invoke within the complexes as the use of tmeda as a ligand, which is essentially identical to dmpe save the N- vs. P-donor atom, does not result in octahedral cation formation but rather forms neutral adducts with aluminum halides and gallium chloride, but tetrahedral cations with gallium bromide and iodide. Further investigations into similar compounds with other anionic groups, such as alkyl groups or hydridic groups, would be fruitful as abstraction with an alkyl or hydride abstracting agent (e.g. $[Ph_3C][B(C_6F_5)_4]$) may yield higher charges than possible with halide abstraction.

Chapter 3 examined the synthesis of cationic complexes of Ge(II) and Sn(II) with bipy and dmpe donor ligands. The use of bipy led to mono- and dicationic triflate salts which were structurally characterized. The monocations are shown to be coordination dimers in the solid state, and the dications were found to be exhibit disphenoidal structures at the Ge or Sn centre and can be considered ligated sources of $E(OTf)_2$. However, when the conformationally-labile dmpe ligand is used instead, tetracationic salts featuring both bridging and chelating Ge-P and presumably Sn-P interactions are formed. These phosphine systems were found to be labile in solution, which could potentially allow for the generation of open coordination sites and prove to be useful reagents towards Lewis acid catalysis as soluble "$E(OTf)_2$" sources.

Chapter 4 explores the reactivity of the bipy-ligated dications from Chapter 3 with several classes of molecules. The reaction of the dications with $(COD)PtCl_2$ results not in the coordination to the Pt centre, but rather halide abstraction from the metal and bipy transfer to form the salt $[(bipy)Pt(COD)][OTf]_2$. Additionally, on reaction with $PhPCl_2$ and PCl_3, again, halide abstraction occurs showing how these complexes can act as Lewis acids by accepting two X^- moieties. The reaction with H_2O also furnishes new complexes, of which $[(bipy)Ge\text{-}OH\text{-}Ge(bipy)][OTf]_3$ was structurally characterized, and featured a bridging Ge-OH-Ge interaction. This is considerably different than the coordination of neutral water to the systems stabilized by macrocyclic ethers, presumably due to the high coordination number of the element centres in these complexes.[166] This series of reactivity speaks towards these complexes being inherently Lewis acidic, despite the presence of the stereochemically-active lone pair as the HOMO. Further investigations into their reactivity as Lewis acids would be useful and comparison to well known reactions catalyzed by Lewis acids (e.g. β-

caprolactone polymerization) would be intriguing. Finally, oxidation with sources of X_2 cleanly affords the oxidation products, of which $[(tBubipy)_2SnCl_2][OTf]_2$ was structurally characterized, and could potentially be used towards accessing higher charged main group cations through further abstraction.

Chapter 5 discusses the synthesis and characterization of highly-charged ($\leq$+3) main group cations. Tricationic complexes of $Al(OTf)_3$ and $Ga(OTf)_3$ were generated using the terpy or PIm_3 ligand respectively. When the central element is changed to silicon(IV), the cations are able to undergo *in situ* C-H activation of acetonitrile, resulting in the trimerization of CH_3CN to form a CN-substituted β-diketiminate substituent which attaches to the Si(IV) centre. However, this does not occur with Sn(IV) and instead the complexes $[(ligand)_2Sn][OTf]_4$ are obtained with both the tBu_3terpy and $BIMEt_2Pyr$ ligands. These represent two of the first examples of tetracationic main group salts where the charge can be considered to reside on a single central element. Additionally, while employing nitrogen-based ligands to isolate examples of P(V) polycations, the O-based donor MePyrO was successfully used to stabilize the first example of a P(V) tetracationic centre in the complex $[(MePyrO)_5PCl][OTf]_4$. While most of these compounds do not feature significant Lewis acidity themselves due to their coordination environments, the activation of CH_3CN in the Si-based system does show that these systems have the potential to behave as strong Lewis acids, given the appropriate ligand scaffolds. Targeting a ligand scaffold which exhibits strong donor moieties, but also allows open coordination sites to facilitate substrate interaction, could lead towards more useful complexes which behave as strong, yet bottleable, Lewis acids.

In general, a series of cationic donor-acceptor complexes of the Group 13-15 elements have been characterized, and in some cases, their preliminary reactivity has been examined. These complexes represent additions to the evolving library of main group complexes which structurally mimic their transition metal counterparts, featuring examples of octahedral and tetrahedral coordination environments. While these results are primarily fundamental in nature, the chemistry presented serves as a motivation towards exploring the utility of main group cations in synthesis, whether it be as novel halide abstraction agents, or as precursors to functional materials, and further investigations into their reactivity will likely be fruitful.

Chapter 7 – Future Work

7.1 New Ligands in Transition Metal Catalysis

The assessment of the reactivity of $[(bipy)_2Ge][OTf]_2$ and $[(bipy)_2Sn][OTf]_2$ showed that when halides are present, halide abstraction is likely to occur. However, it was recently shown that Ge(II) dications can coordinate silver(I) triflate.[167] It is likely that employing $[(bipy)_2Ge][OTf]_2$ and $[(bipy)_2Sn][OTf]_2$ could also potentially lead to coordination complexes. However, the weakly- or non-coordinating nature of triflate ions will likely preclude abstraction from the metal centre by the Ge(II) or Sn(II) centre and should allow isolation of a cation-ligated Ag(I) cation (Scheme 7.1.1). The same type of complexes should theoretically be accessible by using Au(I) sources instead of Ag(I) sources.

Scheme 7.1.1: Potential use of Ge(II) and Sn(II) cations as ligands in a silver complexes.

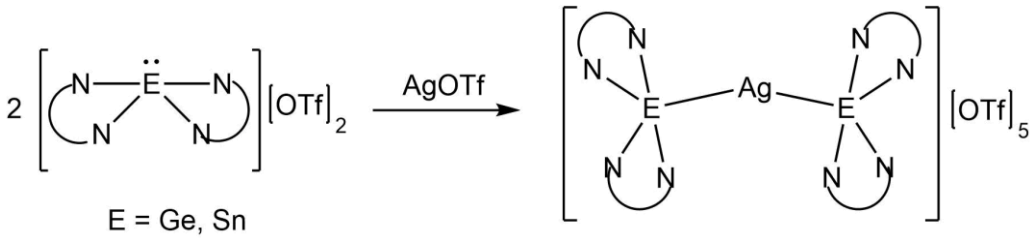

Silver(I) and gold(I) have been shown to catalyze various organic transformations including cyclopropanation,[215] hydration of allenes,[216] and oxidation of aldehydes.[217] In these cases, the activity of Ag(I) and Au(I) is related to its Lewis acidity. It is reasonable to assume that coordination of cationic Ge(II) and Sn(II) centres, as is the case with cationic phosphine ligands, would enhance the Lewis acidity at the Ag(I) or Au(I) centre and potentially increase its activity.[218,219] The Lewis acidity of the ligand can be modulated through using either monocationic or dicationic ligands.

Another potential avenue of reactivity to explore is the application of these dicationic systems as Z-type ligands on transition metals. The Lewis acidity of these complexes lends itself to the idea of acting as an acceptor from a metal centre. While typical Z-type ligands are typically electron deficient boranes or other group 13 elements,[220,221] examples of silicon and tin Z-type ligands have been realized.[222,223] More recently, Gabbai *et. al.* have shown that dicationic Sb(V) centres also act as Z-type ligands towards transition metals such as gold and platinum.[224,225] In these cases, the coordination to the electrophilic antimony centre enhanced the Lewis acidity at the gold and platinum centres, and augmented the catalytic activity of the metal centres. It is possible to envisage this phenomenon occurring with the dicationic germanium and tin complexes, as coordination as a Z-type ligand is likely to lead to increased electrophilicity at the corresponding transition metal centre.

Ligand choice could play an important role in the reactivity of these complexes. While bipy has shown to be effective in stabilizing these cations, using stronger donor ligands such as NHCs or carbodiphosphoranes, could promote coordination by putting more electron density at the Ge(II) or Sn(II) centre and facilitate donation to the metal centre. Additionally, along with an almost endless number of substituted bipyridines, the ability to use NHCs with a variety of substituents at the N-atom opens the door for potential asymmetric or chiral catalysis.

7.2 C-F Bond Activation by Main Group Cations

One obvious extension towards the application of main group Lewis acids in synthesis is to develop synthetic routes to controlled C-F bond activation. The thermodynamic and kinetic stability of these bonds, while facilitating their widespread use in materials applications, limits the ability to reliably functionalize molecules without harsh conditions

and often leads to improper treatment at the end of their lifetimes from an environmental standpoint. Exploiting the Lewis acidity of these complexes could potentially lead to new reagents for these transformations.

As presented in Chapter 5.3, sources of $[(\text{ligand})\text{Si}]^{4+}$ are capable of facilitating C-H bond activation of CH_3CN. However, silicon also exhibits a very strong C-F bonds and it is reasonable to envisage these complexes participating in this type of chemistry. As $[\text{Si}]^{4+}$ complexes appear to be too potent to be isolated without reaction with solvent, using $[\text{RSi}]^{3+}$ complexes would likely still exhibit enough Lewis acidity to be reactive, but should be stable enough to isolate. The depending on the desired transformation, the choice of co-reactant would be important. For example, to transform a C-F bond to a C-H bond, adding a hydride source such as Et_3SiH would be needed (Scheme 7.2.1).

Scheme 7.2.1: C-F bond activation by a silicon(IV) tricationic salt.

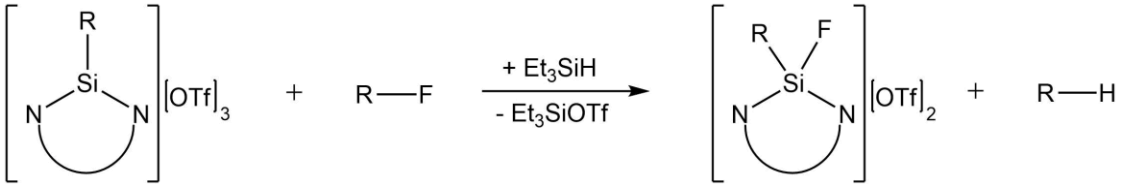

Chapter 8 – Experimental

8.1 General Procedures

Most of the compounds presented in this dissertation are sensitive to oxygen and moisture. As such, manipulations of these compounds were carried out under an inert atmosphere of nitrogen or argon gas. The preparation of these compounds were carried out in rigorously air- and moisture-free conditions using either a Schlenk/vacuum line or within a glovebox. The glovebox syntheses were performed in one of three gloveboxes: an Innovative Technologies box under nitrogen working gas and using titanocene tests for atmosphere purity, an MBraun Labmaster 110 box with nitrogen working gas and H_2O/O_2 levels < 0.5 ppm, and an MBraun Labmaster DP glovebox with nitrogen working gas and H_2O/O_2 levels < 0.1 ppm. Reactions were carried out in glass vials using dry and deoxygenated solvents stored over activated molecular sieves. Schlenk Line syntheses were carried using a dual vacuum-gas manifold with at least 10^{-2} mbar of pressure under vacuum, and using high-purity nitrogen gas. Standard reagent transfer and manipulations were employed (cannula transfer, fritted glass filtration, etc.).

All halide reagents presented in the syntheses herein were purchased from Sigma Aldrich with the exception of SiI_4 (99.999% Trace Metals Basis) which was purchased from Strem Chemicals and used as received. All commercial ligands were also purchased from Sigma Aldrich, with the exception of dmpe which was purchased from Strem Chemicals. All liquid reagents were purified by vacuum distillation prior to use. Bipy was recrystallized from CH_2Cl_2 and dmap was sublimed prior to use. The ligands $P(Im)_3$, $BIMEt_3$, and $BIMEt_2Pyr$ were prepared using literature methods.

All solvents with the exception of CH_3CN were refluxed over CaH_2 or Na/benzophenone and distilled into Strauss flasks under nitrogen, and were subsequently transferred to VWR or Fisherbrand glass bottles and stored over 4 Å molecular sieves inside the glovebox for a minimum of 48 hours prior to use. Anhydrous CH_3CN was purchased from Sigma Aldrich and stored over 3 Å molecular sieves inside the glovebox for a minimum of 48 hours prior to use. Deuterated solvents (CD_2Cl_2, CD_3CN, C_6D_6 and $CDCl_3$) were purchased from Sigma Aldrich and were dried CaH_2 or Na/benzophenone, distilled under nitrogen, and stored over molecular sieves prior to use. In(OTf), $P(Im)_3$[S2] was synthesized following literature procedures.

NMR tubes fitted with either Teflon-sealed plastic caps or J-Young valves were charged and sealed inside the glovebox. ^{1}H NMR spectra were recorded on Bruker spectrometers operating at 300, 360 MHz, ^{13}C NMR spectra were recorded at 76 MHz, ^{19}F NMR spectra were recorded at 282.3 MHz, ^{27}Al NMR spectra were recorded at 93.8 MHz, ^{31}P NMR spectra were recorded at 121.6 MHz, and ^{119}Sn NMR spectra were recorded at 134.3 MHz. All ^{1}H and ^{13}C NMR chemical shifts are reported relative to $SiMe_4$ using the ^{1}H (residual) and ^{13}C chemical shifts of the solvent as a secondary standard. All ^{31}P and ^{19}F NMR spectra were externally referenced to 85% H_3PO_4 (δ = 0.00 ppm) and $CFCl_3$ (δ = 0.00 ppm) respectively. Infrared spectra were obtained on a Perkin Elmer Frontier instrument. Elemental analyses were carried out by Canadian Microanalytical Ltd. in Delta, British Columbia, Canada. Yields were measured after isolation and washing of the solid obtained from the reaction mixture. NMR spectra of the resulting solids were used to ensure the bulk material corresponded to the compound of interest prior to this purification.

Single crystals suitable for X-ray diffraction were coated with paratone oil in a glovebox, transferred to a nylon loop and then transferred to the goniometer of a Bruker D8 APEX2, equipped with a molybdenum (λ = 0.71073 Å) or copper (λ = 0.71073 Å) X-ray tube. Preliminary data was collected to determine the crystal system. The space group was identified, and the data were processed using the Bruker SAINT program and corrected for absorption using SADABS. The structures were solved using Intrinsic Phasing (SHELXT) on OLEX2 completed by Fourier synthesis and refined by full-matrix least-squares procedures.

Quantum chemical calculations were performed using the Gaussian-09[226] (Chapter 2 and 3) or Gaussian-16[227] (Chapter 4 and 5) suite of programs as implemented on the Grex cluster within the WestGrid high-performance computing system, or on the Graham cluster within the SHARCNet high-performance computing system. To establish suitability of basis sets and functionals, structural features (bond lengths and angles) were benchmarked at a variety of levels of theory to determine suitability towards modelling the complexes in the gas-phase. NBO calculations and WBI values were determined with the NBO6 software implemented in Gaussian-16.[228]

8.2 Compounds in Chapter 2

8.2.1 Synthesis of $[(dmpe)_2AlCl_2][AlCl_4]$

$AlCl_3$ (0.133 g, 1.00 mmol) was suspended in CH_2Cl_2 (5 mL). To this was added dmpe (167 µL, 1.00 mmol) which caused the immediate precipitation of some colourless solid. The reaction was stirred for 2 h at room temperature and the solid isolated by removal of the solvent under reduced pressure and washing with Et_2O. Colourless crystals suitable for

structural analysis were obtained by layering 3 mL of a concentrated CH_2Cl_2 solution with 0.5 mL Et_2O and standing in a -35°C freezer.

Yield: 0.244 g (86%): ^{1}H NMR, ppm (CD_2Cl_2, 295 K): δ = 1.42 (br s, 24H, CH_3), 1.93 (s, 8H, CH_2). ^{27}Al{^{1}H} NMR, ppm (CD_2Cl_2, 295 K): δ = 102.9 (s), δ = -0.1 (quintet, $^1J_{PAl}$ = 160 Hz). ^{31}P{^{1}H} NMR, ppm (CD_2Cl_2, 295 K): δ = −40.9 (sextet, $^1J_{AlP}$ = 161 Hz). ^{13}C NMR, ppm (CD_2Cl_2, 295 K): δ = 10.4 (d, $^1J_{PC}$ = 26 Hz), 22.1 (d, $^1J_{PC}$ = 24 Hz).

8.2.2 Synthesis of $[(dmpe)_2AlBr_2][AlBr_4]$

$AlBr_3$ (0.267 g, 1.00 mmol) was dissolved in CH_2Cl_2 (5 mL) to form a light yellow solution. To this was added dmpe (167 µL, 1.00 mmol) which caused the immediate precipitation of a colourless solid. The reaction was stirred for 2 h at room temperature and the solid isolated by removal of the solvent under reduced pressure and washing with Et_2O. Colourless crystals suitable for structural analysis were obtained by layering 3 mL of a CH_2Cl_2 solution with 0.5 mL Et_2O and standing in a -35°C freezer.

Yield: 0.379 g (91%). ^{1}H NMR, ppm (CD_2Cl_2, 295 K): δ = 1.49 (br s, 24H, CH_3), 1.98 (br s, 8H, CH_2). ^{27}Al{^{1}H} NMR, ppm (CD_2Cl_2, 295 K): δ = 79.8 (s), δ = -11.9 (br, assumed pentet). ^{31}P{^{1}H} NMR, ppm (CD_2Cl_2, 295 K): δ = −38.2 (br, sextet). ^{13}C NMR, ppm (CD_2Cl_2, 295 K): δ = 10.6 (br s), 22.6 (br s).

8.2.3 Synthesis of $[(dmpe)_2AlI_2][AlI_4]$

AlI_3 (0.408 g, 1.00 mmol) was dissolved in CH_2Cl_2 (5 mL) to form a light yellow solution. To this was added dmpe (167 µL, 1.00 mmol) which caused the immediate precipitation of a colourless solid. The reaction was stirred for 2 h at room temperature and the solid isolated

by removal of the solvent under reduced pressure and washing with Et_2O. Colourless crystals were obtained by layering 3 mL of a CH_2Cl_2 solution with 0.5 mL Et_2O and standing in a -35°C freezer.

Yield: 0.502 g (90%). ^{1}H NMR, ppm (CD_2Cl_2, 295 K): δ = 1.51 (br s, 24H), 2.03 (s, 8H). $^{27}Al\{^{1}H\}$ NMR, ppm (CD_2Cl_2, 295 K): δ = -27.9 (s), δ = -33.3 (br, assumed pentet). $^{31}P\{^{1}H\}$ NMR, ppm (CD_2Cl_2, 295 K): δ = −41.0 (br, assumed sextet). ^{13}C NMR, ppm (CD_2Cl_2, 295 K): δ = 10.9 (br, s), 22.8 (br, s).

8.2.4 Synthesis of $[(dmpe)_2GaCl_2][GaCl_4]$

$GaCl_3$ (0.176 g, 1.00 mmol) was dissolved in CH_2Cl_2 (5 mL) to form a colourless solution. To this was added dmpe (167 µL, 1.00 mmol) which caused the immediate precipitation of a colourless solid. The reaction was stirred for 2 h at room temperature and the solid isolated by removal of the solvent under reduced pressure and washing with Et_2O. Colourless crystals suitable for structural analysis were obtained by layering 3 mL of a CH_2Cl_2 solution with 0.5 mL Et_2O and standing in a -35°C freezer.

Yield: 0.292 g (87%): ^{1}H NMR, ppm (CD_2Cl_2, 295 K): δ = 1.40 (br s, 24H, CH_3), 1.89 (s, 8H, CH_2). $^{31}P\{^{1}H\}$ NMR, ppm (CD_2Cl_2, 295 K): δ = −35.8 (br s). ^{13}C NMR, ppm (CD_2Cl_2, 295 K): δ = 10.1 (br s, CH_3), 21.8 (br s, CH_2); IR ATR, cm^{-1}, (relative intensities): 2911 (w), 1418 (s), 1291 (m), 947 (s), 929 (s), 900 (m), 868 (m), 841 (m), 755 (m), 718 (m); Anal. Calc. for $C_{12}H_{32}Ga_2Cl_6P_4$ (%): C, 22.09; H, 4.94. Found for crystalline sample with yield of 0.091g: C, 21.83; H, 4.96.

8.2.5 Synthesis of $[(dmpe)_2GaBr_2][GaBr_4]$

$GaBr_3$ (0.309 g, 1.00 mmol) was dissolved in CH_2Cl_2 (5 mL) to form a colourless solution. To this was added dmpe (167 µL, 1.00 mmol) which caused the immediate precipitation of a colourless solid. The reaction was stirred for 2 h at room temperature and the solid isolated by removal of the solvent under reduced pressure and washing with Et_2O. Colourless crystals suitable for structural analysis were obtained by layering 3 mL of a CH_2Cl_2 solution with 0.5 mL Et_2O and standing in a -35°C freezer.

Yield: 0.405 g (88%). ^{1}H NMR, ppm (CD_2Cl_2, 295 K): δ = 1.38 (br s, 24H), 1.89 (s, 8H). $^{31}P\{^1H\}$ NMR, ppm (CD_2Cl_2, 295 K): δ = −39.4 (br s). ^{13}C NMR, ppm (CD_2Cl_2, 295 K): δ = 10.0 (s), 21.6 (br, s); IR ATR, cm^{-1}, (relative intensities): 2966 (w), 1416 (m), 1291 (w), 951 (s), 929 (s), 899 (w), 868 (s), 775 (w), 753 (w), 721 (w). Anal. Calcd. for $C_{12}H_{32}Ga_2Br_6P_4$ (%): C, 15.68; H, 3.51. Found for crystalline sample with yield of 0.154g: C, 15.48; H, 3.52.

8.2.6 Synthesis of $[(dmpe)_2GaI_2][GaI_4]$

GaI_3 (0.450 g, 1.00 mmol) was dissolved in CH_2Cl_2 (5 mL) to form a light yellow solution. To this was added dmpe (167 µL, 1.00 mmol) which caused the immediate precipitation of a colourless solid. The reaction was stirred for 2 h at room temperature and the solid isolated by removal of the solvent under reduced pressure and washing with Et_2O. Colourless crystals were obtained by layering 3 mL of a CH_2Cl_2 solution with 0.5 mL Et_2O and standing in a -35°C freezer.

Yield: 0.506 g (84%). ^{1}H NMR, ppm (CD_2Cl_2, 295 K): δ = 1.33 (br s, 24H), 1.91 (s, 8H). $^{31}P\{^1H\}$ NMR, ppm (CD_2Cl_2, 295 K): δ = −41.5 (br s). ^{13}C NMR, ppm (CD_2Cl_2, 295 K): δ

= 9.2 (br, s), 21.3 (br, s); IR, ATR, cm^{-1}, (relative intensities): 2961 (m), 2880 (m), 1403 (m), 1291 (s), 1230 (w), 1123 (w) 951 (s), 908 (s), 866 (s), 770 (m).

8.2.7 Synthesis of (tmeda)$AlCl_3$

$AlCl_3$ (0.137 g, 1.00 mmol) was suspended in CH_2Cl_2 (5 mL) to form a colourless solution. To this was added tmeda (149 µL, 1.00 mmol) which caused the immediate precipitation of some colourless solid. The reaction was stirred for 2 h at room temperature and the solid isolated by removal of the solvent under reduced pressure and washing with Et_2O. Colourless crystals suitable for structural analysis were obtained by layering 3 mL of a concentrated CH_2Cl_2 solution with 0.5 mL Et_2O and standing in a -35°C freezer.

Yield: 0.212 g (85%). ^{1}H NMR, ppm (CD_2Cl_2, 295 K): δ = 2.58 (s, 24H), 2.83 (s, 8H). ^{13}C NMR, ppm (CD_2Cl_2, 295 K): δ = 49.3 (s), 56.0 (s); $^{27}Al\{^{1}H\}$ NMR, ppm (CD_2Cl_2, 295 K): δ = 74.3 (s).

8.2.8 Synthesis of (tmeda)$AlBr_3$

$AlBr_3$ (0.267 g, 1.00 mmol) was suspended in CH_2Cl_2 (5 mL) to form a colourless solution. To this was added tmeda (149 µL, 1.00 mmol) which caused the immediate precipitation of some colourless solid. The reaction was stirred for 2 h at room temperature and the solid isolated by removal of the solvent under reduced pressure and washing with Et_2O. Colourless crystals suitable for structural analysis were obtained by layering 3 mL of a concentrated CH_2Cl_2 solution with 0.5 mL Et_2O and standing in a -35°C freezer.

Yield: 0.310 g (81%). ^{1}H NMR, ppm (CD_2Cl_2, 295 K): δ = 2.74 (s, 24H), 3.01 (s, 8H). ^{13}C NMR, ppm (CD_2Cl_2, 295 K): δ = 48.9 (s), 55.6 (s); ^{27}Al{^{1}H} NMR, ppm (CD_2Cl_2, 295 K): δ = 71.9 (s).

8.2.9 Synthesis of (tmeda)AlI_3

AlI_3 (0.408 g, 1.00 mmol) was suspended in CH_2Cl_2 (5 mL) to form a colourless solution. To this was added tmeda (149 µL, 1.00 mmol) which caused the immediate precipitation of some colourless solid. The reaction was stirred for 2 h at room temperature and the solid isolated by removal of the solvent under reduced pressure and washing with Et_2O. Colourless crystals suitable for structural analysis were obtained by layering 3 mL of a concentrated CH_2Cl_2 solution with 0.5 mL Et_2O and standing in a -35°C freezer.

Yield: 0.434 g (83%). ^{1}H NMR, ppm (CD_2Cl_2, 295 K): δ = 2.86 (s, 24H), 3.37 (s, 8H). ^{13}C NMR, ppm (CD_2Cl_2, 295 K): δ = 49.5 (s), 55.5 (s); ^{27}Al{^{1}H} NMR, ppm (CD_2Cl_2, 295 K): δ = 70.0 (s).

8.2.10 Synthesis of (tmeda)$GaCl_3$

$GaCl_3$ (0.176 g, 1.00 mmol) was suspended in CH_2Cl_2 (5 mL) to form a colourless solution. To this was added tmeda (149 µL, 1.00 mmol) which caused the immediate precipitation of some colourless solid. The reaction was stirred for 2 h at room temperature and the solid isolated by removal of the solvent under reduced pressure and washing with Et_2O. Colourless crystals suitable for structural analysis were obtained by layering 3 mL of a concentrated CH_2Cl_2 solution with 0.5 mL Et_2O and standing in a -35°C freezer.

Yield: 0.257 g (88%). ^{1}H NMR, ppm (CD_2Cl_2, 295 K): δ = 2.55 (s, 24H), 2.87 (s, 8H). ^{13}C NMR, ppm (CD_2Cl_2, 295 K): δ = 46.1 (s), 55.1 (s)

8.2.11 Synthesis of [(tmeda)GaBr$_2$][GaBr$_4$]

$GaBr_3$ (0.309 g, 1.00 mmol) was dissolved in CH_2Cl_2 (5 mL) to form a colourless solution. To this was added tmeda (149 µL, 1.00 mmol) which caused the immediate precipitation of some colourless solid. The reaction was stirred for 2 h at room temperature and the solid isolated by removal of the solvent under reduced pressure and washing with Et_2O. Colourless crystals suitable for structural analysis were obtained by layering 3 mL of a concentrated CH_2Cl_2 solution with 0.5 mL Et_2O and standing in a -35°C freezer.

Yield: 0.305 g (83%). ^{1}H NMR, ppm (CD_2Cl_2, 295 K): δ = 2.48 (s, 24H), 2.87 (s, 8H). ^{13}C NMR, ppm (CD_2Cl_2, 295 K): δ = 45.1 (s), 54.5 (s)

8.2.12 Synthesis of [(tmeda)GaI$_2$][GaI$_4$]

GaI_3 (0.450 g, 1.00 mmol) was dissolved in CH_2Cl_2 (5 mL) to form a colourless solution. To this was added tmeda (149 µL, 1.00 mmol) which caused the immediate precipitation of some colourless solid. The reaction was stirred for 2 h at room temperature and the solid isolated by removal of the solvent under reduced pressure and washing with Et_2O. Colourless crystals suitable for structural analysis were obtained by layering 3 mL of a concentrated CH_2Cl_2 solution with 0.5 mL Et_2O and standing in a -35°C freezer.

Yield: 0.458 g (90%). ^{1}H NMR, ppm (CD_2Cl_2, 295 K): δ = 2.79 (s, 24H), 3.23 (s, 8H). ^{13}C NMR, ppm (CD_2Cl_2, 295 K): δ = 47.5 (s), 55.3 (s).

Table 8.2.1: Crystallographic information for compounds in Chapter 2.

	$[(dmpe)_2AlCl_2][AlCl_4]$	**$[(dmpe)_2AlBr_2][AlBr_4]$**	**$[(dmpe)_2GaCl_2][GaCl_4]$**	**$[(dmpe)_2GaBr_2][GaBr_4]$**	**$(tmeda)AlCl_3$**
formula	$C_{12}H_{32}Cl_6Al_2P_4$	$C_{12}H_{32}Br_6Al_2P_4$	$C_{12}H_{32}Cl_6Ga_2P_4$	$C_{12}H_{32}Br_6Ga_2P_4$	$C_6H_{16}AlCl_3N_2$
mw (g mol^{-1})	566.96	833.66	652.44	919.15	249.54
space group	P21/n	P21/n	Pbca	P-1	P21/c
***a* (Å)**	10.6271(5)	10.6749(4)	19.6815(7)	7.7324(4)	10.5569(4)
***b* (Å)**	17.9625(8)	18.1319(8)	16.2217(5)	13.2442(7)	7.9019(3)
***c* (Å)**	16.3668(7)	16.5596(7)	34.8372(11)	14.0461(8)	13.7446(5)
α (°)	90	90	90	85.0400(10)	90
β (°)	100.8960(10)	100.0682(6)	90	87.7980(10)	95.9275(4)
γ (°)	90	90	90	88.0280(10)	90
***V* (Å^3)**	3067.9(2)	3155.9(2)	11122.4(6)	1431.31(13)	1140.44(7)
Z	4	4	16	2	4
ρ (g cm^{-3})	1.411	1.933	1.558	2.133	1.453
radiation (Å)	0.71073	0.71073	0.71073	0.71073	0.71073
T (K)	173	173	173	173	173
G.O.F	1.036	1.053	1.035	1.040	1.081
R_1 (I ≥ 2σI))	0.0335	0.0778	0.0419	0.0297	0.0220
wR_2 (all data)	0.0828	0.2574	0.1080	0.0729	0.0603

Table 8.2.2: Crystallographic information for compounds in Chapter 2 continued

	(tmeda)AlBr$_3$	**(tmeda)AlI$_3$**	**(tmeda)GaCl$_3$**	**[(tmeda)GaBr$_2$] [GaBr$_4$]**	**[(tmeda)GaI$_2$] [GaI$_4$]**
formula	$C_6H_{16}AlBr_3N_2$	$C_6H_{16}AlI_3N_2$	$C_6H_{16}GaCl_3N_2$	$C_6H_{16}Ga_2Br_6N_2$	$C_6H_{16}Ga_2I_6N_2$
mw (g mol^{-1})	382.90	523.90	292.29	735.07	1017.08
space group	P21/c	P21/n	P21/c	P21/n	P421/c
***a* (Å)**	10.7346(4)	7.8650(2)	10.5600(3)	13.2390(5)	10.8262(6)
***b* (Å)**	8.0948(3)	13.8185(4)	7.9543(2)	10.7417(4)	10.8262(6)
***c* (Å)**	14.0662(5)	12.6015(3)	13.7784(4)	14.2566(5)	15.7148(9)
α (°)	90	90	90	90	90
β (°)	95.4329(5)	90.4928(3)	95.9926(3)	111.4043(4)	90
γ (°)	90	90	90	90	90
***V* (Å^3)**	1216.78(8)	1369.51(6)	1151.03(5)	1887.59(12)	1841.9(2)
Z	4	4	4	4	2
ρ (g cm^{-3})	2.090	2.541	1.687	2.587	2.856
radiation (Å)	0.71073	0.71073	0.71073	0.71073	0.71073
T (K)	173	173	173	173	173
G.O.F	1.047	1.191	1.117	1.021	1.100
***R*$_1$ (I ≥ 2σI))**	0.0328	0.0190	0.0158	0.0247	0.0205
***wR*$_2$ (all data)**	0.0930	0.0430	0.0417	0.0542	0.0476

8.3 Compounds in Chapter 3

8.3.1 Synthesis of [(bipy)GeCl][OTf]

Method A: $GeCl_2$·dioxane (2 mmol, 0.463g), TMSOTf (2 mmol, 362 µL) and 2,2'-bipyridine (2 mmol, 0.312 g) were combined in 5 mL CH_3CN to obtain a colourless, cloudy mixture which was stirred for 2 hours. Removal of the solvent under reduced pressure gave the product as a fine colourless powder. The powder was washed with CH_2Cl_2 and Et_2O and re-dissolved in a minimum volume of CH_3CN. The resulting solution was filtered, layered with Et_2O, and placed in a freezer at -35°C for 48 hours to obtain colourless crystalline material.

Method B: $GeCl_2$·dioxane (2 mmol, 0.463g) and 2,2'-bipyridine (2 mmol, 0.312 g) were combined in 5 mL CH_2Cl_2 to immediately give a bright yellow suspension, which was stirred for 1 hour. Removal of the solvent under reduced pressure gave a dark yellow powder as the previously characterized neutral adduct. The powder was subsequently re-suspended in CH_3CN, and to this mixture was added TMSOTf (2 mmol, 362 µL), giving a slightly cloudy, colourless mixture after 2 hours. Removal of the solvent gave the title product as a colourless powder. The powder was washed with CH_2Cl_2 and Et_2O and re-dissolved in a minimum volume of CH_3CN. The resulting solution was filtered, layered with Et_2O, and placed in a freezer at -35°C for 48 hours to obtain colourless crystalline material. Yield: 0.726 g (88%); ^{1}H NMR, ppm (CD_3CN, 298K) δ = 8.05 (ddd, J_{HH} = 7.6, 5.6, 1.2 Hz, 2H), 8.55 (td, J_{HH} = 7.6, 1.5 Hz, 2H), 8.66 (*pseudo dt*, J_{HH} = 8.1, 1.1 Hz, 2H), 9.12 (ddd, J_{HH} = 5.6, 1.5, 0.9 Hz, 2H; ^{13}C{^{1}H} NMR, ppm (CD_3CN, 298K): δ = 124.3 (s), 128.9 (s), 144.8 (s), 146.0 (s), 148.8 (s); ^{19}F{^{1}H} NMR, ppm (CD_3CN, 298K) δ = -79.2 (s); Melting point: 205-206°C; IR, Nujol mull, cm^{-1}: 3118, 2921, 2853, 2325, 1621, 1605, 1581, 1576,

1506, 1480, 1466, 1453, 1441, 1377, 1326, 1291, 1276, 1266, 1248, 1219, 1185, 1150, 1109, 1058, 1049, 1039, 1024, 1019, 984, 921, 776, 770, 726, 658, 649, 635, 576, 572;

8.3.2 Synthesis of $[(bipy)_2Ge][OTf]_2$

Method A: $GeCl_2$·dioxane (2 mmol, 0.463g), TMSOTf (4 mmol, 724 µL) and 2,2'-bipyridine (4 mmol, 0.624 g) were combined in 5 mL CH_3CN to obtain a clear, yellow solution which was stirred for 2 hours. Removal of the solvent under reduced pressure gave a fine yellow powder. The powder was washed with CH_2Cl_2 and Et_2O and re-dissolved in a minimum volume of CH_3CN. The resulting solution was filtered, layered with Et_2O, and placed in a freezer at -35°C for 48 hours to obtain yellow crystalline material.

Method B: $GeCl_2$·dioxane (2 mmol, 0.463g) and 2,2'-bipyridine (2 mmol, 0.312 g) were combined in 5 mL CH_2Cl_2 to immediately give a bright yellow suspension, which was stirred for 1 hour. Removal of the solvent under reduced pressure gave a dark yellow powder as the previously characterized neutral adduct. The powder was subsequently re-suspended in CH_3CN, and to this mixture was added TMSOTf (4 mmol, 724 µL), giving first a cloudy, colourless mixture, turning to a clear, yellow solution which was stirred for 2 hours. Removal of the solvent under reduced pressure gave a fine yellow powder. The powder was washed with CH_2Cl_2 and Et_2O and re-dissolved in a minimum volume of CH_3CN. The resulting solution was filtered, layered with Et_2O, and placed in a freezer at -35°C for 48 hours to obtain yellow crystalline material.

Yield: 1.175 g (86%); ^{1}H NMR, ppm (CD_3CN, 298K) δ = 7.89 (t, broad, J_{HH} = 6.5 Hz, 4H), 8.48 (td, broad, J_{HH} = 7.9, 1.2 Hz, 4H), 8.69 (d, broad, J_{HH} = 8.2 Hz, 4H), 8.86 (d, broad, J_{HH} = 4.9 Hz, 4H; $^{13}C\{^1H\}$ NMR, ppm (CD_3CN, 298K) : δ = 124.5 (s), 128.5 (s),

143.9 (s), 147.4 (s), 159.1 (s); $^{19}F\{^{1}H\}$ NMR, ppm (CD_3CN, 298K) δ = -79.3 (s); Melting point: 195-196°C; (dec) IR, Nujol mull, cm^{-1}: 3091, 2953, 2921, 2853, 2342, 1610, 1604, 1594, 1583, 1562, 1509, 1462, 1446, 1377, 1317, 1281, 1254, 1234, 1224, 1191, 1152, 1112, 1099, 1088, 1031, 1021, 971, 943, 819, 772, 757, 734, 723, 654, 648, 637, 630, 612, 573; Elemental Analysis including 0.75 molecules of CH_2Cl_2 (Calc/Exp): C (36.59/36.52); H (2.36/2.13); N (7.50/7.53) for crystalline sample with yield of 0.093g.

8.3.3 Synthesis of [(bipy)SnCl][OTf]

Method A: $SnCl_2$ (2 mmol, 0.379g), TMSOTf (2 mmol, 362 μL) and 2,2'-bipyridine (2 mmol, 0.312 g) were combined in 5 mL CH_3CN to obtain a colourless suspension which was stirred for 2 hours. Removal of the solvent under reduced pressure gave the product as a fine colourless powder. The powder was washed with CH_2Cl_2 and Et_2O and pumped dry. Due to it's low solubility in CH_2Cl_2 and CH_3CN, crystalline material suitable for x-ray analysis could not be isolated. However, the analysis of the bulk material was consistent with the title compound.

Method B: $SnCl_2$ (2 mmol, 0.379g) and 2,2'-bipyridine (2 mmol, 0.312 g) were combined in 5 mL CH_2Cl_2 to immediately give a bright yellow suspension, which was stirred for 1 hour. Removal of the solvent under reduced pressure gave a dark yellow powder as the previously characterized neutral adduct. The powder was subsequently re-suspended in CH_3CN, and to this mixture was added TMSOTf (2 mmol, 362 μL), giving a colourless suspension after 2 hours. Removal of the solvent gave the title product as a colourless powder. The powder was washed with CH_2Cl_2 and Et_2O and pumped dry. Due to it's low solubility in CH_2Cl_2 and CH_3CN, crystalline material suitable for x-ray analysis could not

be isolated. However, the analysis of the bulk material was consistent with the title compound.

Yield: 0.827 g (90%); ^{1}H NMR, ppm (CD_3CN, 298K) δ = 7.63 (ddd, J_{HH} = 7.6, 5.3, 1.2 Hz, 2H), 8.11 (td, J_{HH} = 7.8, 1.8 Hz, 2H), 8.45 (*pseudo dt*, J_{HH} = 7.9, 1.1 Hz, 2H), 8.91 (ddd, J_{HH} = 5.3, 1.8, 0.9 Hz, 2H;. ^{13}C{^{1}H} NMR, ppm (CD_3CN/DMSO, 298K): δ = 123.3 (s), 126.8 (s), 141.0 (s), 149.3 (s), 153.6 (s); ^{19}F{^{1}H} NMR, ppm (CD_3CN/DMSO, 298K) δ = -79.2 (s); ^{119}Sn{^{1}H} NMR, ppm, (CD_3CN/DMSO, 298K) δ = -577.0 (s); Melting point: 211-212°C; IR, Nujol mull, cm^{-1}: 3113, 2921, 2853, 2724, 2364, 1610, 1601, 1576, 1567, 1502, 1463, 1448, 1377, 1324, 1292, 1271, 1250, 1219, 1188, 1160, 1151, 1114, 1108, 1074, 1064, 1044, 1019, 979, 909, 771, 767, 757, 730, 671, 654, 638, 633, 576, 572; Elemental Analysis (Calc/Exp): C (28.76/28.56); H (1.76/1.68); N (6.10/5.98).

8.3.4 Synthesis of [(bipy)$_2$Sn][OTf]$_2$]

Method A: $SnCl_2$ (2 mmol, 0.379g), TMSOTf (4 mmol, 724 μL) and 2,2'-bipyridine (4 mmol, 0.624 g) were combined in 5 mL CH_3CN to obtain a clear, yellow solution which was stirred for 2 hours. Removal of the solvent under reduced pressure gave a fine yellow powder. The powder was washed with CH_2Cl_2 and Et_2O and re-dissolved in a minimum volume of CH_3CN. The resulting solution was filtered, layered with Et_2O, and placed in a freezer at -35°C for 48 hours to obtain yellow crystalline material.

Method B: $SnCl_2$ (2 mmol, 0.379g) and 2,2'-bipyridine (2 mmol, 0.312 g) were combined in 5 mL CH_2Cl_2 to immediately give a bright yellow suspension, which was stirred for 1 hour. Removal of the solvent under reduced pressure gave a dark yellow powder as the previously characterized neutral adduct. The powder was subsequently re-suspended in

CH_3CN, and to this mixture was added TMSOTf (4 mmol, 724 µL), giving first a colourless suspension, turning to a clear, yellow solution which was stirred for 2 hours. Removal of the solvent under reduced pressure gave a fine yellow powder. The powder was washed with CH_2Cl_2 and Et_2O and re-dissolved in a minimum volume of CH_3CN. The resulting solution was filtered, layered with Et_2O, and placed in a freezer at -35°C for 48 hours to obtain yellow crystalline material.

Yield: 1.283 g (88%); ^{1}H NMR, ppm (CD_3CN, 298K) δ = 7.79 (ddd, J_{HH} = 7.8, 5.3, 1.2 Hz, 4H), 8.33 (td, J_{HH} = 7.9, 1.6 Hz, 4H), 8.51 (*pseudo dt*, J_{HH} = 8.1, 1.0 Hz, 4H), 8.74 (ddd, J_{HH} = 5.3, 1.8, 0.9 Hz, 4H;. ^{13}C{^{1}H} NMR, ppm (CD_3CN, 298K) : δ = 125.3 (s), 129.0 (s), 143.7 (s), 149.3 (s), 151.5 (s); ^{19}F{^{1}H} NMR, ppm (CD_3CN, 298K) δ = -79.5 (s); ^{119}Sn{^{1}H} NMR, ppm, (CD_3CN, 298K) δ = -728.6 (s); Melting point 192°C (dec): IR, Nujol mull, cm^{-1}: 3068, 2924, 2853, 2725, 2258, 1605, 1598, 1578, 1567, 1495, 1467, 1445, 1377, 1321, 1276, 1296, 1276, 1238, 1222, 1158, 1135, 1025, 1013, 1004, 908, 808, 756, 748, 732, 653, 634, 627, 572; Elemental Analysis (Calc/Exp): C (36.24/35.89); H (2.21/2.07); N (7.68/7.51) for crystalline sample with yield of 0.113g.

8.3.5 Synthesis of [(dmpe)GeCl][OTf]

$GeCl_2$·dioxane (1 mmol, 0.231g), TMSOTf (1 mmol, 191 µL) and dmpe (167 µL, 1.00 mmol) were combined in 5 mL CH_2Cl_2, immediately forming a colourless precipitate, and the mixture was stirred for 2 hours. Removal of the solvent under reduced pressure gave a fine colourless powder. The powder was washed with Et_2O and re-dissolved in a minimum volume of CH_3CN. The solution was then layered with Et_2O and placed in a -35°C freezer overnight, giving colourless crystals suitable for X-ray analysis.

Yield: 0.322 g (79%); ^{1}H NMR, ppm (CD_3CN, 298K) δ = 1.72 (d, $^{2}J_{HP}$ = 12.6 Hz, 12H), 2.35 (m, 4H); $^{13}C\{^{1}H\}$ NMR, ppm (CD_3CN, 298K) : δ = 7.1 (d, $^{1}J_{CP}$ = 28 Hz, CH_3), δ = 23.7 (dd, $^{1}J_{CP}$ = 26 Hz, $^{2}J_{CP}$ = 10 Hz, CH_3); $^{19}F\{^{1}H\}$ NMR, ppm (CD_3CN, 298K) δ = -79.2 (s); $^{31}P\{^{1}H\}$ NMR, ppm (CD_3CN, 298K): δ = 18.7 (s)

8.3.6 Synthesis of $[(dmpe)_3Ge_2][OTf]_4$

$GeCl_2$·dioxane (1 mmol, 0.231g), TMSOTf (2 mmol, 382 µL) and dmpe (334 µL, 2.00 mmol) were combined in 5 mL CH_2Cl_2, immediately forming a colourless precipitate, and the mixture was stirred for 2 hours. Removal of the solvent under reduced pressure gave a fine colourless powder. The powder was washed with Et_2O and re-dissolved in a minimum volume of CH_3CN. The solution was then layered with Et_2O and placed in a -35°C freezer overnight, giving colourless crystals suitable for X-ray analysis.

Yield: 0.489 g (82%); ^{1}H NMR, ppm (CD_3CN, 298K) δ = 1.72 (br s, 36H), 2.33 (br d, 12H); $^{13}C\{^{1}H\}$ NMR, ppm (CD_3CN, 298K) : δ = 7.5 (br s, CH_3), δ = 24.2 (br s, CH_3); $^{19}F\{^{1}H\}$ NMR, ppm (CD_3CN, 298K) δ = -79.3 (s); $^{31}P\{^{1}H\}$ NMR, ppm (CD_3CN, 298K): δ = -13.1 (s)

8.3.7 Synthesis of [(dmpe)SnCl][OTf]

$SnCl_2$ (2 mmol, 0.189g), TMSOTf (1 mmol, 191 µL) and dmpe (167 µL, 1.00 mmol) were combined in 5 mL CH_2Cl_2, immediately forming a colourless precipitate, and the mixture was stirred for 2 hours. Removal of the solvent under reduced pressure gave a fine colourless powder. The powder was washed with Et_2O and re-dissolved in a minimum volume of

CH_3CN. The solution was then layered with Et_2O and placed in a -35°C freezer overnight, giving colourless crystals suitable for X-ray analysis.

Yield: 0.385 g (85%); ^{1}H NMR, ppm (CD_3CN, 298K) δ = 1.63 (d, $^2J_{HP}$ = 11.2 Hz, 12H), 2.21 (m, 4H); $^{13}C\{^1H\}$ NMR, ppm (CD_3CN, 298K) : δ = 7.3 (d, $^1J_{CP}$ = 25 Hz, CH_3), δ = 23.7 (dd, $^1J_{CP}$ = 24 Hz, $^2J_{CP}$ = 11 Hz, CH_3); $^{19}F\{^1H\}$ NMR, ppm (CD_3CN, 298K) δ = -79.4 (s); $^{31}P\{^1H\}$ NMR, ppm (CD_3CN, 298K): δ = 7.6 (s with satellites, $^1J_{P\text{-}117Sn}$ = 1765 Hz, $^1J_{P\text{-}119Sn}$ = 1848 Hz); $^{119}Sn\{^1H\}$ NMR, ppm (CD_3CN, 298K): -594 (br m)

8.3.8 Synthesis of $[(dmpe)_3Sn_2][OTf]_4$

$SnCl_2$ (1 mmol, 0.189g), TMSOTf (2 mmol, 191 µL) and dmpe (334 µL, 2.00 mmol) were combined in 5 mL CH_2Cl_2, immediately forming a colourless precipitate, and the mixture was stirred for 2 hours. Removal of the solvent under reduced pressure gave a fine colourless powder. The powder was washed with Et_2O and re-dissolved in a minimum volume of CH_3CN. The solution was then layered with Et_2O and placed in a -35°C freezer overnight, however only microcrystalline powders were obtained.

Yield: 0.462 g (72%); ^{1}H NMR, ppm (CD_3CN, 298K) δ = 1.63 (d overlapped with br s, $^2J_{HP}$ = 9.7 Hz, 36H), 2.23 (br d, 12H); $^{13}C\{^1H\}$ NMR, ppm (CD_3CN, 298K) : δ = 7.4 (br s, CH_3), δ = 23.9 (br s, CH_3); $^{19}F\{^1H\}$ NMR, ppm (CD_3CN, 298K) δ = -79.3 (s); $^{31}P\{^1H\}$ NMR, ppm (CD_3CN, 298K): δ = -11.6 (br s); $^{119}Sn\{^1H\}$ NMR, ppm (CD_3CN, 298K): -606 (br m).

Table 8.3.1: Crystallographic information for compounds in Chapter 3 continued.

	[(bipy)GeCl][OTf]	**[(bipy)$_2$Ge][OTf]$_2$**	**[(bipy)$_2$Sn][OTf]$_2$**	**[(dmpe)GeCl][OTf]**
formula	$C_{11}H_8ClGeN_2F_3O_3S$	$C_{22}H_{16}GeN_4F_6O_6S_2$	$C_{22}H_{16}SnN_4F_6O_6S_2$	$C_7H_{16}ClGeP_2F_3O_3S$
mw (g mol^{-1})	413.35	683.15	729.22	407.30
space group	$P2_1/n$	P-1	$P2_1/n$	$Pna2_1$
***a* (Å)**	7.5779(7)	9.6827(5)	9.3539(4)	20.6441(8)
***b* (Å)**	16.7991(14)	12.2345(7)	19.7280(9)	19.8941(8)
***c* (Å)**	11.0317(10)	13.5264(8)	17.8782(8)	7.3795(3)
α (°)	90	105.9780(10)	90	90
β (°)	93.030(3)	96.5280(10)	103.627(2)	90
γ (°)	90	109.6380(10)	90	90
***V* (Å^3)**	1402.4(2)	1412.75(14)	3206.3(2)	3030.7(2)
Z	4	2	4	8
ρ (g cm^{-3})	1.957	1.702	1.786	1.785
radiation (Å)	0.71073	0.71073	0.71073	0.71073
T (K)	296	296	296	296
G.O.F	1.047	1.045	1.206	0.950
***R*$_1$ (I ≥ 2σI))**	0.0320	0.0244	0.0567	0.0210
***wR*$_2$ (all data)**	0.0715	0.0614	0.1135	0.0411

Table 8.3.2: Crystallographic information for compounds in Chapter 3 continued.

	$[(dmpe)_3Ge_2][OTf]_2$	**[(dmpe)SnCl][OTf]**
formula	$C_{22}H_{48}Ge_2P_6F_{12}O_{12}S_4$	$C_7H_{16}ClSnP_2F_3O_3S$
mw (g mol^{-1})	1191.97	453.37
space group	$P2_1/n$	C2/c
***a* (Å)**	11.4161(6)	19.599(2)
***b* (Å)**	8.2595(4)	13.0543(15)
***c* (Å)**	17.8265(9)	19.515(2)
α (°)	90	90
β (°)	104.813(3)	92.864(2)
γ (°)	90	90
***V* (Å^3)**	1625.02(14)	4986.8(10)
Z	4	4
ρ (g cm^{-3})	1.853	1.697
radiation (Å)	0.71073	0.71073
T (K)	296	296
G.O.F	1.096	1.031
***R*1 (I ≥ 2σI))**	0.0303	0.0450

8.4 Compounds in Chapter 4

8.4.1 Attempted Synthesis of $[(bipy)_2EMe][OTf]_3$

$[(bipy)_2Ge][OTf]_2$ (0.25 mmol, 0.171 g) or $[(bipy)_2Sn][OTf]_2$ (0.25 mmol, 0.182 g) were dissolved in 3 mL of CD_3CN to give yellow solutions. To the solution was added MeOTf (0.25 mmol, 28.3 µL) with no apparent colour change. Layering with Et_2O and placing in a -35°C freezer for 48 hours gave colourless crystals suitable for X-ray analysis. The resulting compound was found to be $[H_3CCN\text{-}CH_3][OTf]$.

Crystalline yield: 0.045 g. ^1H NMR, ppm (CD_3CN, 298K) δ = 2.05 (br s, 3H), 4.11 (br s, 3H); ^{19}F NMR, ppm (CD_3CN, 298K) δ = -79.6 (s).

8.4.2 Reactions of $[(bipy)_2EMe][OTf]_3$ with Small Molecules

$[(bipy)_2Ge][OTf]_2$ (0.25 mmol, 0.171 g) or $[(bipy)_2Sn][OTf]_2$ (0.25 mmol, 0.182 g) were dissolved in 3 mL of CD_3CN to give yellow solutions. To the solution was added 1 eq of phenylacetylene, diphenylacetylene, 1,2-bis(trimethylsilyl)acetylene, and 2,3-dimethyl-2,3-epoxybutane and the mixtures were stirred at room temperature overnight. No change in the ^1H NMR were detected in all cases so the reaction mixtures were heated overnight at 70°C and upon examining the ^1H NMR specra, it was evident that no reaction with the substrates took place and only protonated bipyridine was present in addition to the starting materials.

8.4.3 Synthesis of $[(bipy)Pt(COD)][OTf]_2$

$[(bipy)_2Ge][OTf]_2$ (0.25 mmol, 0.171 g) or $[(bipy)_2Sn][OTf]_2$ (0.25 mmol, 0.182 g) were dissolved in 3 mL of CD_3CN to give yellow solutions. To the solution was added solid $(COD)PtCl_2$ (0.25 mmol, 0.094g) and stirred overnight. A small amount of yellow solid,

which was determined to be (bipy)ECl_2, had precipitated from solution with a light yellow supernatant. The yellow solution was decanted from the precipitate and placed in a -35°C freezer overnight, giving light yellow X-ray quality crystals.

Yield: 0.477 g (63%). ^{1}H NMR, ppm (CD_3CN, 298K): δ = 8.52 (br s, 2H), 8.31 (br s, 2H), 8.05 (br s, 2H), 7.68 (br s, 2H), 6.41 (br s, 4H), 3.08 (br s, 4H), 2.52 (br s, 4H); $^{13}C\{^{1}H\}$ NMR, ppm (CD_3CN, 298K) : δ = 163.1 (s), 156.5 (s), 151.3(s), 128.7 (s), 123.9 (s), 118.8 (s), 37.1 (s); ^{19}F NMR, ppm (CD_3CN, 298K) δ = -79.4 (s).

8.4.4 Synthesis of [(bipy)PPh][OTf]$_2$

[(bipy)$_2$Ge][OTf]$_2$ (0.25 mmol, 0.171 g) or [(bipy)$_2$Sn][OTf]$_2$ (0.25 mmol, 0.182 g) were dissolved in 3 mL of CD_3CN to give yellow solutions. To the solutions, $PhPCl_2$ (0.25 mmol, 33.9 µL) was added dropwise and immediately the solution went orange, with simultaneous precipitation of a yellow solid. The solid was filtered and the solution was placed in a -35°C which gave colourless crystals.

Yield: 0.287 g (51%). ^{1}H NMR, ppm (CD_3CN, 298K) δ = 9.41-9.33 (m, 2H), 9.18 (dt, J_{HH} = 7.9, 1.3 Hz, 2H), 8.93 (td, 8.0, 1.2 Hz, 2H), 8.39-8.33 (m, 2H) 7.85-7.54 (m, 5H); ^{19}F NMR, ppm (CD_3CN, 298K) δ = -79.3 (s); $^{31}P\{^{1}H\}$ NMR, ppm (CD_3CN, 298K): 136.5 (s).

8.4.5 Reactions of [(bipy)$_2$E][OTf]$_2$ with PCl_3

[(bipy)$_2$Ge][OTf]$_2$ (0.25 mmol, 0.171 g) or [(bipy)$_2$Sn][OTf]$_2$ (0.25 mmol, 0.182 g) were dissolved in 3 mL of CD_3CN to give yellow solutions. To the solutions, PCl_3 (0.25 mmol, 33.9 µL) was added dropwise and immediately the solution went orange, with simultaneous

precipitation of a yellow solid. The solid was filtered and $^{31}P\{^{1}H\}$ NMR spectra of the reaction mixture were taken.

$^{31}P\{^{1}H\}$ NMR, ppm (CD_3CN, 298K): 237.6 (d, $^{1}J_{PP}$ = 404 Hz, [bipy**P**-P-**P**bipy]), 129.8 (s, [bipy**P**Cl]$^{2+}$ or [bipy**P**]$^{3+}$), 83.8 (t, $^{1}J_{PP}$ = 404 Hz, [bipy**P**-P-**P**bipy]).

8.4.6 Synthesis of [(bipy)Ge-O(H)-Ge(bipy)][OTf]$_3$

$[(bipy)_2Ge][OTf]_2$ (0.25 mmol, 0.171 g) was dissolved in 5 mL of CH_3CN to give a yellow solution. H_2O (0.25 mmol, 4.5 µL) was added via micropipette and stirred overnight. The resulting colourless precipitate was separated from the pink supernatant, washed with Et_2O and CH_2Cl_2, and dried under vacuum. The powder, which was only sparingly soluble in CH_3CN, was stirred overnight in CH_3CN, and the resulting supernatant was separated and placed in a -35°C freezer for 48 hours, giving small colourless crystals suitable for X-ray analysis.

Yield: 0.664 g (72%). ^{1}H NMR, ppm (CD_3CN, 298K) δ = 7.79 (br d, J_{HH} = 7.8 Hz, 4H), 8.33 (br t, J_{HH} = 7.7 Hz, 4H), 8.51 (*br d*, J_{HH} = 7.9 Hz, 4H), 8.74 (br s, 4H), 12.02 (br s, 1H); ^{19}F NMR, ppm (CD_3CN, 298K) δ = -79.3 (s);

8.4.7 Synthesis of [(bipy)$_2$GeCl$_2$][OTf]$_2$

$[(bipy)_2Ge][OTf]_2$ (0.25 mmol, 0.171 g) was dissolved in 5 mL of CH_3CN to give a yellow solution. To the solution was added SO_2Cl_2 (0.25 mmol, 250 µL of 1M solution in CH_2Cl_2). The reaction mixture was stirred for one hour and the volatiles removed giving a colourless solid. Attempted recrystallizations were unsuccessful at producing X-ray-quality crystals.

Yield: 0.664 g (72%). ^{1}H NMR, ppm (CD_3CN, 298K) δ = 7.96 (br s, 4H), 8.46 (br s, 4H), 8.71 (br s, 4H), 8.92 (br s, 4H); ^{19}F NMR, ppm (CD_3CN, 298K) δ = -78.9 (s);

8.4.8 Synthesis of $[(bipy)_2SnCl_2][OTf]_2$

$[(bipy)_2Sn][OTf]_2$ (0.25 mmol, 0.182 g) was dissolved in 5 mL of CH_3CN to give a yellow solution. To the solution was added SO_2Cl_2 (0.25 mmol, 250 µL of 1M solution in CH_2Cl_2). The reaction mixture was stirred for one hour and the volatiles removed giving a yellow solid. Attempted recrystallizations were unsuccessful at producing X-ray-quality crystals.

Yield: 0.158 g (79%). ^{1}H NMR, ppm (CD_3CN, 298K) δ = 7.79 (br s, 4H), 8.33 (br s, 4H), 8.51 (br s, 4H), 8.74 (br s, 4H); ^{19}F NMR, ppm (CD_3CN, 298K) δ = -79.1 (s);

8.4.9 Synthesis of $[(tBubipy)_2SnCl_2][OTf]_2$

$[(tBubipy)_2Sn][OTf]_2$ (0.25 mmol, 0.245 g) was dissolved in 5 mL of CH_3CN to give a yellow solution. To the solution was added SO_2Cl_2 (0.25 mmol, 250 µL of 1M solution in CH_2Cl_2). The reaction mixture was stirred for one hour and the volatiles removed giving a light yellow solid. Redissolution in CH_3CN and layering with Et_2O gave colourless crystals of X-ray quality.

Yield: 0.197 g (75%). ^{1}H NMR, ppm (CD_3CN, 298K) δ = 1.51 (s, 36H), 8.01 (d, J_{HH} = 5.9 Hz, 4H), 8.54 (br s, 4H), 8.98 (br d, J_{HH} = 5.9 Hz, 4H); ^{19}F NMR, ppm (CD_3CN, 298K) δ = -79.3 (s); ^{119}Sn{^{1}H} NMR, ppm, (CD_3CN, 298K) δ = -535 (br s)

8.4.10 Synthesis of $[(tBubipy)_2SnBr_2][OTf]_2$

$[(tBubipy)_2Sn][OTf]_2$ (0.25 mmol, 0.171 g) was dissolved in 5 mL of CH_3CN to give a yellow solution. To the solution was added a solution of Br_2 (0.25 mmol, 12.8 µL) in 2 mL of CH_3CN. The orange colour of the bromine faded after the reaction mixture was stirred for one hour and the volatiles were removed giving a yellow solid. Attempted recrystallizations were unsuccessful at producing X-ray-quality crystals.

Yield: 0.197 g (69%). ^{1}H NMR, ppm (CD_3CN, 298K) δ = 1.53 (s, 36H), 7.99 (br d, J_{HH} = 5.7, Hz, 4H), 8.51 (br s, 4H), 8.92 (br d, J_{HH} = 5.8 Hz, 4H); ^{19}F NMR, ppm (CD_3CN, 298K) δ = -79.4 (s); ^{119}Sn{^{1}H} NMR, ppm, (CD_3CN, 298K) δ = -973 (br s)

8.4.11 Synthesis of $[(tBubipy)_2SnI_2][OTf]_2$

$[(tBubipy)_2Sn][OTf]_2$ (0.25 mmol, 0.171 g) was dissolved in 5 mL of CH_3CN to give a yellow solution. To the solution was added I_2 (0.25 mmol, 0.064 g). The brown colour of the iodine had faded significantly after reaction mixture was stirred for one hour and the volatiles removed giving a yellow solid. Attempted recrystallizations were unsuccessful at producing X-ray-quality crystals.

Yield: 0.250 g (81%) ^{1}H NMR, ppm (CD_3CN, 298K) δ = 1.52 (s, 36H), 8.00 (br d, J_{HH} = 5.4, Hz, 2H), 8.48 (br s, 4H), 8.89 (br d, J_{HH} = 5.4 Hz, 4H); ^{19}F NMR, ppm (CD_3CN, 298K) δ = -79.1 (s); ^{119}Sn{^{1}H} NMR, ppm, (CD_3CN, 298K) δ = -973 (br s)

Table 8.4.1: Crystallographic information for compounds in Chapter 4.

	$[CH_3CNCH_3][OTf]$	**$[(bipy)Pt(COD)][OTf]_2$**	**$[(bipy)Ge\text{-}OH\text{-}Ge(bipy)][OTf]_3$**	**$[(tBubipy)_2SnCl_2][OTf]_2$**
formula	$C_3H_6F_3NO_3S$	$C_{20}H_{20}F_6N_2O_6PtS_2$	$C_{23}H_{17}F_9Ge_2N_4O_{10}S_3$	$C_{38}H_{48}Cl_2F_6N_6O_6S_2Sn$
mw (g mol^{-1})	193.14	757.59	921.86	1052.56
space group	$P2_1/c$	P-1	$P2_1/c$	C2/c
***a* (Å)**	6.3879(4)	9.5041(9)	11.4858(6)	11.8106(5)
***b* (Å)**	13.1064(8)	11.2954(9)	13.2167(7)	23.2792(11)
***c* (Å)**	9.6743(6)	11.5212(10)	24.0444(13)	18.4844(8)
α (°)	90	104.331(2)	90	90
β (°)	94.5400(10)	93.557(2)	93.566(2)	91.6220(10)
γ (°)	90	94.130(2)	90	90
***V* (Å^3)**	807.41(9)	1191.14(18)	3643.0(3)	5080.1(4)
Z	1	2	4	8
ρ (g cm^{-3})	1.712	2.112	1.754	1.447
radiation (Å)	0.71073	0.71073	0.71073	0.71073
T (K)	296	296	296	296
G.O.F	1.092	1.034	1.217	1.041
***R*1 (I ≥ 2σI))**	0.0361	0.0350	0.0606	0.0258
***wR*2 (all data)**	.01077	0.0799	0.1367	0.0614

8.5 Compounds in Chapter 5

8.5.1 Synthesis of $[(PIm_3)_2Ga][OTf]_3$

PIm_3 (0.276 g, 1 mmol) was suspended in 5 mL of CH_3CN. To the reaction mixture, solid $GaCl_3$ (0.088 g, 0.5 mmol) and AgOTf (368 mg, 1.5 mmol) was added. The suspension was stirred for 1 hour and the resulting mixture was filtered to remove AgCl. The solution was then layered with Et_2O and placed in a -35°C freezer overnight, giving colourless crystals suitable for X-ray analysis.

Yield: 0.378 g (71%). ^{1}H NMR (CD_3CN, 298K): δ = 4.01 (s, CH_3, 18 H), 6.51 (d, *J* = 1.3 Hz, 6H), 7.21 (dd, *J* = 4.0, 1.4 Hz, 6H); ^{19}F NMR (CD_3CN, 298K): δ = - 79.4 (s); ^{31}P{^{1}H} NMR (CD_3CN, 298K): δ = -132.5 (s)

8.5.2 Attempted Synthesis of $[(PIm_3)_2Al][OTf]_3$

PIm_3 (0.276 g, 1 mmol) was suspended in 5 mL of CH_3CN. To the reaction mixture, solid $Al(OTf)_3$ (0.238 g, 0.5 mmol) was added. The suspension was stirred for 1 hour and the volatiles were removed under reduced pressure, giving a yellow solid. Analyzing the solid in CD_3CN with ^{31}P{^{1}H} NMR spectroscopy showed more than six signals so the solid was discarded.

8.5.3 Synthesis of $[(tBu_3terpy)Al][OTf]_3$

$AlCl_3$ (0.067g, 0.5 mmol) was suspended in 4 mL CH_3CN. To the solution was added AgOTf (368 mg, 1.5 mmol) and tBu_3terpy (0.200g, 0.5 mmol) and the mixture was stirred for 1 hour. The mixture was filtered to remove AgCl and the resulting yellow solution was

layered with Et_2O and placed in a -35°C freezer overnight, giving yellow crystals suitable for X-ray analysis.

Yield: 0.362 g (79%). ^{1}H NMR (CD_3CN, 298K): 1.37 (s, 18H), 1.76 (s, 9H), 8.26 (dd, *J* = 6.2, 1.9 Hz, 2H), 9.05 (m, 2H), 9.20 (s, 2H), 9.40 (d, *J* = 6.2 Hz, 2H); ^{19}F NMR (CD_3CN, 298K): -79.6 (s); ^{27}Al NMR (CD_3CN, 298K): -25.3 (s).

8.5.4 Synthesis of [(tBu$_3$terpy)Si(NacNacCN)][OTf]$_3$

SiI_4 (0.268g, 0.5 mmol) was dissolved in 4mL of CH_3CN. To the solution was added AgOTf (490 mg, 2 mmol) and tBu_3terpy (0.400g, 1 mmol) and the mixture was stirred for 1 hour. The mixture was filtered to remove AgI and the resulting red solution was layered with Et_2O and placed in a -35°C freezer overnight, giving dark orange crystals suitable for X-ray analysis.

Yield: 0.359 g (72%) ^{1}H NMR (CD_3CN, 298K): 1.41 (s, 18H), 1.82 (s, 9H), 2.11 (s, 3H) 2.88 (s, 3H) 8.31-8.40 (br m, 4H), 8.58-8.71 (br m, 5H), 8.95 (s, 1H); ^{19}F NMR (CD_3CN, 298K): -79.2.

8.5.5 Synthesis of [(BIMEt$_3$)Si(NacNacCN)][OTf]$_3$

SiI_4 (0.268g, 0.5 mmol) was dissolved in 4mL of CH_3CN. To the solution was added AgOTf (0.49 g, 2 mmol) and $BIMEt_3$ (0.5 g, 1 mmol) and the mixture was stirred for 1 hour. The mixture was filtered to remove yellow AgI and the resulting red solution was layered with Et_2O and placed in a -35°C freezer overnight, giving dark orange crystals suitable for X-ray analysis.

Yield: 0.365 g (67%). ^{1}H NMR (CD_3CN, 298K): 1.32 (t, *J* = 7.3 Hz, 3 H), 1.56 (t, *J* = 7.4 Hz, 6H), 2.31 (s, 3H), 3.10 (s, 3H), 4.07 (q, *J* = 8.5 Hz, 2H), 4.44 (m, 4H), 5.27 (s, 2H), 5.74 (d, *J* = 17.8 Hz, 2H), 5.84 (d, *J* = 17.8 Hz, 2H), 7.55-7.87 (m, 11H), 8.26 (br s, 1H), 8.50-8.56 (m, 2H): $^{13}C\{^{1}H\}$ NMR(CD_3CN, 298K): 13.5 (s), 14.4 (s), 25.5 (s), 27.9 (s), 42.4 (s), 42.6 (s), 57.9 (s), 61.4 (s), 90.2 (s), 114.4 (s), 114.6 (s), 116.0 (s), 116.2 (s), 127.8 (s), 127.9 (s), 128.3 (s), 132.6 (s), 134.0 (s), 135.7 (s), 136.2 (s), 147.7 (s), 151.0 (s), 179.2 (s), 181.0 (s); ^{19}F NMR (CD_3CN, 298K): -79.6 (s).

8.5.6 Synthesis of $[(BIMEt_2Pyr)_2Sn][OTf]_4$

$SnBr_4$ (0.219 g, 0.5 mmol) was dissolved in 5 mL of CH_3CN. To the solution was added $BIMEt_2Pyr$ (0.367 g, 1.0 mmol) and AgOTf (490 mg, 2 mmol) were added to the solution. The mixture was stirred for 1 hour and was filtered to remove tan AgBr. The resulting orange solution was layered with Et_2O and placed in a -35°C freezer overnight, giving dark orange crystals suitable for X-ray analysis.

Yield: 0.565 g, (78%). ^{1}H NMR (CD_3CN, 298K): 2.54 (br s, 12H), 2.61 (br s, 3H), 7.51-7.76 (br m, 8H) 7.84 (br s, 2H), 8.52-8.65 (br m, 8H), 8.73 (br s, 2H); ^{19}F NMR (CD_3CN, 298K): -79.1. ^{119}Sn NMR (CD_3CN, 298K): -762 (s)

8.5.7 Synthesis of $[(MePyrO)_5PCl][OTf]_5$

PCl_5 (0.104 g, 0.5 mmol) was dissolved in 4mL of CH_3CN. To the solution was added AgOTf (0.514 g, 2 mmol) and MePyrO (0.273 g, 2.5 mmol) and the mixture was stirred for 1 hour. The mixture was filtered to remove tan AgBr and the resulting brown solution was

layered with Et_2O and placed in a -35°C freezer overnight, giving brown crystals suitable for X-ray analysis.

Crystalline yield: 0.093 g. ^{1}H NMR (CD_3CN, 298K): 2.54 (br s, 12H), 2.61 (br s, 3H), 7.51-7.76 (br m, 8H) 7.84 (br s, 2H), 8.52-8.65 (br m, 8H), 8.73 (br s, 2H); $^{31}P\{^{1}H\}$ NMR (CD_3CN, 298K): -61.2 (s); ^{19}F NMR (CD_3CN, 298K): -79.1.

Table 8.5.1: Crystallographic information for compounds in Chapter 5.

	[(PIm$_3$)$_2$Ga][OTf]$_3$	**[(tBu$_3$terpy)Al][OTf]$_3$**	**[(BIMEt$_3$)Si(NacNacCN)][OTf]$_3$**	**[(tBu$_3$terpy)Si(NacNacCN)][OTf]$_3$**
formula	$C_{27}H_{30}F_9GaN_{12}O_9P_2S_3$	$C_{32}H_{38}N_4O_9F_9AlS_3$	$C_{39}H_{41}N_{10}SiF_9O_9S_3$	$C_{36}H_{42}N_6SiF_9O_9S_3$
mw (g mol^{-1})	1065.45	916.83	1089.27	998.02
space group	P-1	$Pna2_1$	P-1	$P2_1/n$
***a* (Å)**	12.4155(5)	21.4255(4)	11.7454(13)	17.1170(5)
***b* (Å)**	12.6255(6)	12.1288(2)	14.901(2)	11.9641(4)
***c* (Å)**	16.6030(7)	16.0966(3)	19.242(2)	25.2998(7)
α (°)	98.8550(10)	90	107.553(9)	90
β (°)	101.1220(10)	90	107.683(9)	102.5870(10)
γ (°)	116.5990(10)	90	94.576(8)	90
***V* (Å^3)**	2196.08(17)	4182.95(13)	3004.3(7)	5056.6(3)
Z	2	4	2	4
ρ (g cm^{-3})	1.673	1.456	1.234	1.878
radiation (Å)	0.71073	1.54178	1.54178	0.71073
T (K)	173.15	173.15	173.15	296.15
G.O.F	0.986	1.092	1.678	1.046
***R*$_1$ (I ≥ 2σI))**	0.0348	0.0350	0.1380	0.0524
***wR*$_2$ (all data)**	0.0930	0.0924	0.4067	0.1421

Table 8.5.2: Crystallographic information for compounds in Chapter 5 continued.

	[(BIMEt$_2$Pyr)$_2$Sn][OTf]$_4$	**[(MePyrO)$_5$PCl][OTf]$_4$**
formula	$C_{50}H_{42}F_{12}N_{10}SnO_{12}S_4$	$C_{34}H_{35}ClF_{12}N_5O_{17}PS_4$
mw (g mol^{-1})	1449.88	1208.33
space group	C2/c	$P2_1/c$
***a* (Å)**	11.8380(3)	13.5833(7)
***b* (Å)**	23.0964(5)	14.0497(8)
***c* (Å)**	22.5379(5)	25.0329(13)
α (°)	90	90
β (°)	96.5056(17)	92.0810(10)
γ (°)	90	90
***V* (Å^3)**	6122.5(2)	4774.2(4)
Z	4	4
ρ (g cm^{-3})	1.662	1.681
radiation (Å)	0.71073	0.71073
T (K)	173.15	296.15
G.O.F	1.021	1.032
***R*$_1$ (I ≥ 2σI))**	0.0455	0.0369
***wR*$_2$ (all data)**	0.1179	0.0848

Bibliography

1 J. J. Berzelius, *Annls. Chim. Phys*, 1836, **61**, 146.

2 A. J. B. Robertson, *Platin. Met. Rev.*, 1975, **19**, 64–69.

3 R. W. Bunsen, *Ann.*, 1837, **24**, 271.

4 D. Seyferth, *Organometallics*, 2001, **20**, 1488–1498.

5 C. Jones and G. A. Koutsantonis, *Aust. J. Chem.*, 2013, **66**, 1115–1117.

6 R. West, M. J. Fink and J. Michl, *Science*, 1981, **214**, 1343–1344.

7 K. S. Pitzer, *J. Am. Chem. Soc.*, 1948, **70**, 2140–2145.

8 R. S. Mulliken, *J. Am. Chem. Soc.*, 1950, **72**, 4493–4503.

9 M. Yoshifuji, I. Shima, N. Inamoto, K. Hirotsu and T. Higuchi, *J. Am. Chem. Soc.*, 1981, **103**, 4587–4589.

10 G. Becker, G. Gresser and W. Uhl, *Z. Naturforsch. B*, 1981, **86**, 16–19.

11 L. I. Smith and F. H. MacDougall, *J. Am. Chem. Soc.*, 1929, **51**, 3001–3008.

12 A. Newton, *J. Am. Chem. Soc.*, 1943, **65**, 2441–2443.

13 E. E. Betts and L. R. C. Barclay, *Can. J. Chem.*, 1955, **33**, 1768–1774.

14 C. J. F. Du, H. Hart and K. K. D. Ng, *J. Org. Chem.*, 1986, **51**, 3162–3165.

15 B. Schiemenz and P. P. Power, *Organometallics*, 1996, **15**, 958–964.

16 J. J. Ellison and P. P. Power, *J. Organomet. Chem.*, 1996, **526**, 263–267.

17 S. Hino, M. M. Olmstead, J. C. Fettinger and P. P. Power, *J. Organomet. Chem.*,

2005, **690**, 1638–1644.

18 N. Tokitoh, T. Matsumoto, H. Suzuki and R. Okazaki, *Tetrahedron Lett.*, 1991, **32**, 2049–2052.

19 R. J. Wright, J. Steiner, S. Beaini and P. P. Power, *Inorg. Chim. Acta*, 2006, **359**, 1939–1946.

20 T. J. Hadlington, J. Li and C. Jones, *Can. J. Chem.*, 2014, **92**, 427–433.

21 D. L. Kays, *Chem. Soc. Rev.*, 2016, **45**, 1004–1018.

22 N. Burford, J. A. C. Clyburne and M. S. W. Chan, *Inorg. Chem.*, 1997, **36**, 3204–3206.

23 L. Pu, B. Twamley and P. P. Power, *J. Am. Chem. Soc.*, 2000, **122**, 3524–3525.

24 M. Stender, A. D. Phillips, R. J. Wright and P. P. Power, *Angew. Chem. Int. Ed.*, 2002, **41**, 1785–1787.

25 A. D. Phillips, R. J. Wright, M. M. Olmstead and P. P. Power, *J. Am. Chem. Soc.*, 2002, **124**, 5930–5931.

26 A. Sekiguchi, R. Kingo and M. Ichinohe, *Science*, 2004, **305**, 1755–1757.

27 J. C. Fettinger, P. A. Gray, C. E. Melton and P. P. Power, *Organometallics*, 2014, **33**, 6232–6240.

28 J. W. Bundens, J. Yudenfreund and M. M. Francl, *Organometallics*, 1999, **18**, 3913–3920.

29 J. J. Eisch and K. C. Fichter, *J. Organomet. Chem.*, 1983, **250**, 63–81.

30 T. Mizoroki, K. Mori and A. Ozaki, *Bull. Chem. Soc. Jpn.*, 1971, **44**, 581–581.

31 M. Scholl, S. Ding, C. W. Lee and R. H. Grubbs, *Org. Lett.*, 1999, **1**, 953–956.

32 C. W. Bielawski and R. H. Grubbs, *Angew. Chem. Int. Ed.*, 2000, **39**, 2903–2906.

33 J. P. Nolley and R. F. Heck, *J. Org. Chem.*, 1972, **37**, 2320–2322.

34 B. M. Wile, R. J. Burford, R. Mcdonald, M. J. Ferguson, M. Stradiotto and C. Tg, *Organometallics*, 2006, **25**, 1028–1035.

35 R. L. Chowdhury and J.-E. Bäckvall, *J. Chem. Soc., Chem. Commun.*, 1991, **V**, 1063–1064.

36 W. Levason, M. L. Matthews, G. Reid and M. Webster, *Dalton Trans.*, 2004, 554.

37 W. Levason and G. Reid, *Coord. Chem. Rev.*, 2006, **250**, 2565–2594.

38 S. L. Benjamin, W. Levason, G. Reid and M. C. Rogers, *Dalton Trans.*, 2011, **40**, 6565–6574.

39 C. Tschersich, C. Limberg, S. Roggan, C. Herwig, N. Ernsting, S. Kovalenko and S. Mebs, *Angew. Chem. Int. Ed.*, 2012, **51**, 4989–4992.

40 D. Martin, M. Soleilhavoup and G. Bertrand, *Chem. Sci.*, 2011, **2**, 389–399.

41 A. J. Arduengo, R. L. Harlow and M. Kline, *J. Am. Chem. Soc.*, 1991, **113**, 361–363.

42 D. Bourissou, O. Guerret, F. P. Gabbaie and G. Bertrand, *Chem. Rev.*, 2000, **100**, 39–91.

43 J. Vignolle, X. Cattoën and D. Bourissou, *Chem. Rev.*, 2009, **109**, 3333–3384.

44 H. V. Huynh, *Chem. Rev.*, 2018, *ASAP*, 10.1021/acs.chemrev.8b00067.

45 W. A. Herrmann and C. Köcher, *Angew. Chem. Int. Ed.*, 1997, **36**, 2162–2187.

46 W. A. Herrmann, *Angew. Chem. Int. Ed.*, 2002, **41**, 1290–1309.

47 S. Díez-González, N. Marion, S. P. Nolan and S. Diez-Gonzalez, *Chem. Rev.*, 2009, **109**, 3612–3676.

48 G. C. Vougioukalakis and R. H. Grubbs, *Chem. Rev.*, 2010, **110**, 1746–1787.

49 Y. Wang, B. Quillian, P. Wei, C. S. Wannere, Y. Xie, R. B. King, H. F. Schaefer, III, P. von Rague Schleyer and G. H. Robinson, *J. Am. Chem. Soc.*, 2007, **129**, 12412–12413.

50 Y. Wang, Y. Xie, P. Wei, R. B. King, H. F. Schaefer, P. von R. Schleyer and G. H. Robinson, *Science*, 2008, **321**, 1069–1071.

51 Y. Wang and G. H. Robinson, *Chem. Commun.*, 2009, **7345**, 5201.

52 M. Y. Abraham, Y. Wang, Y. Xie, P. Wei, H. F. Schaefer, P. R. Von Schleyer and G. H. Robinson, *Chem. Eur. J.*, 2010, **16**, 432–435.

53 Y. Wang and G. H. Robinson, *Dalton Trans.*, 2012, **41**, 337–345.

54 S. M. I. Al-Rafia, A. C. Malcolm, R. McDonald, M. J. Ferguson and E. Rivard, *Chem. Commun.*, 2012, **48**, 1308–1310.

55 K. C. Thimer, S. M. I. Al-Rafia, M. J. Ferguson, R. McDonald and E. Rivard, *Chem. Commun.*, 2009, **112**, 7119.

56 S. M. I. Al-Rafia, A. C. Malcolm, S. K. Liew, M. J. Ferguson and E. Rivard, *J. Am.*

Chem. Soc., 2011, **133**, 777–779.

57 E. Rivard, *Dalton Trans.*, 2014, **43**, 8577–8586.

58 G. H. Spikes, J. C. Fettinger and P. P. Power, *J. Am. Chem. Soc.*, 2005, **127**, 12232–12233.

59 P. P. Power, *Nature*, 2010, **463**, 171–177.

60 C. Cui, M. M. Olmstead, J. C. Fettinger, G. H. Spikes and P. P. Power, *Science*, 2005, **6**, 17530–17541.

61 C. Cui, M. M. Olmstead and P. P. Power, *J. Am. Chem. Soc.*, 2004, **126**, 5062–5063.

62 Y. Peng, B. D. Ellis, X. Wang, J. C. Fettinger and P. P. Power, *Science*, 2009, **325**, 1668–1670.

63 E. Rivard, R. C. Fischer, R. Wolf, Y. Peng, W. A. Merrill, N. D. Schley, Z. Zhu, L. Pu, J. C. Fettinger, S. J. Teat, I. Nowik, R. H. Herber, N. Takagi, S. Nagase and P. P. Power, *J. Am. Chem. Soc.*, 2007, **129**, 16197–16208.

64 R. Kinjo, M. Ichinohe, A. Sekiguchi, N. Takagi, M. Sumimoto and S. Nagase, *J. Am. Chem. Soc.*, 2007, **129**, 7766–7767.

65 N. J. Hardman, R. J. Wright, A. D. Phillips and P. P. Power, *Angew. Chem. Int. Ed.*, 2002, **41**, 2842–2844.

66 R. J. Wright, A. D. Phillips, N. J. Hardman and P. P. Power, *J. Am. Chem. Soc.*, 2002, **124**, 8538–8539.

67 R. J. Wright, A. D. Phillips, S. Hino and P. P. Power, *J. Am. Chem. Soc.*, 2005, **127**, 4794–4799.

68 P. Bag, A. Porzelt, P. J. Altmann and S. Inoue, *J. Am. Chem. Soc.*, 2017, **139**, 14384–14387.

69 R. J. Wright, A. D. Phillips and P. P. Power, *J. Am. Chem. Soc.*, 2003, **125**, 10784–10785.

70 R. J. Wright, M. Brynda, J. C. Fettinger, A. R. Betzer and P. P. Power, *J. Am. Chem. Soc.*, 2006, **128**, 12498–12509.

71 C. A. Caputo, Z. Zhu, Z. D. Brown, J. C. Fettinger and P. P. Power, *Chem. Commun.*, 2011, **47**, 7506–8.

72 Z. Zhu, R. C. Fischer, B. D. Ellis, E. Rivard, W. A. Merrill, M. M. Olmstead, P. P. Power, J. D. Guo, S. Nagase and L. Pu, *Chem. Eur. J.*, 2009, **15**, 5263–5272.

73 J. Moilanen, P. P. Power and H. M. Tuononen, *Inorg. Chem.*, 2010, **49**, 10992–11000.

74 C. A. Caputo and P. P. Power, *Organometallics*, 2013, **32**, 2278–2286.

75 M. Y. Abraham, Y. Wang, Y. Xie, P. Wei, H. F. Schaefer, P. V. R. Schleyer and G. H. Robinson, *J. Am. Chem. Soc.*, 2011, **133**, 8874–8876.

76 H. P. Hickox, Y. Wang, Y. Xie, M. Chen, P. Wei, H. F. Schaefer and G. H. Robinson, *Angew. Chem. Int. Ed.*, 2015, **54**, 10267–10270.

77 S. Wang, M. L. McCrea-Hendrick, C. M. Weinstein, C. A. Caputo, E. Hoppe, J. C. Fettinger, M. M. Olmstead and P. P. Power, *J. Am. Chem. Soc.*, 2017, **139**, 6586–

6595.

78 G. N. Lewis, *J. Am. Chem. Soc.*, 1916, **38**, 762–785.

79 T. M. Lowry, *J. Soc. Chem. Ind.*, 1924, **43**, 17.

80 J. K. Groves, *Chem. Soc. Rev.*, 1972, **1**, 73–97.

81 C. A. Tolman, *Chem. Rev.*, 1977, **77**, 313–348.

82 H. C. Brown, H. I. Schlesinger and S. Z. Cardon, *J. Am. Chem. Soc.*, 1942, **64**, 325–329.

83 D. W. Stephan, *Acc. Chem. Res.*, 2015, **48**, 306–316.

84 D. W. Stephan, *Science*, 2016, **354**.

85 P. Spies, G. Erker, G. Kehr, K. Bergander, R. Frohlich, S. Grimme and D. W. Stephan, *Chem. Commun.*, 2007, 5072–5074.

86 D. W. Stephan and G. Erker, *Angew. Chem. Int. Ed.*, 2010, **49**, 46–76.

87 G. C. Welch, R. R. S. Juan, J. D. Masuda and D. W. Stephan, *Science*, 2006, **314**, 1124–1126.

88 P. A. Chase, G. C. Welch, T. Jurca and D. W. Stephan, *Angew. Chem. Int. Ed.*, 2007, **46**, 8050–8053.

89 M. A. Dureen, C. C. Brown and D. W. Stephan, *Organometallics*, 2010, **29**, 6422–6432.

90 H. Wang, R. Fröhlich, G. Kehr and G. Erker, *Chem. Commun.*, 2008, 5966.

91 T. Voss, C. Chen, G. Kehr, E. Nauha, G. Erker and D. W. Stephan, *Chem. Eur. J.*, 2010, **16**, 3005–3008.

92 M. H. Holthausen, R. R. Hiranandani and D. W. Stephan, *Chem. Sci.*, 2015, **6**, 2016–2021.

93 T. Vom Stein, M. Peréz, R. Dobrovetsky, D. Winkelhaus, C. B. Caputo and D. W. Stephan, *Angew. Chem. Int. Ed.*, 2015, **54**, 10178–10182.

94 A. Schäfer, M. Reißmann, A. Schäfer, W. Saak, D. Haase and T. Müller, *Angew. Chem. Int. Ed.*, 2011, **50**, 12636–12638.

95 M. Reißmann, A. Schäfer, S. Jung and T. Müller, *Organometallics*, 2013, **32**, 6736–6744.

96 D. Himmel, I. Krossing and A. Schnepf, *Angew. Chem. Int. Ed.*, 2014, **53**, 370–374.

97 G. Frenking, *Angew. Chem. Int. Ed.*, 2014, **53**, 6040–6046.

98 D. Himmel, I. Krossing and A. Schnepf, *Angew. Chem. Int. Ed.*, 2014, **53**, 6047–6048.

99 N. L. Kilah, S. Petrie, R. Stranger, J. W. Wielandt, A. C. Willis and S. B. Wild, *Organometallics*, 2007, **26**, 6106–6113.

100 M. Donath, E. Conrad, P. Jerabek, G. Frenking, R. Fröhlich, N. Burford and J. J. Weigand, *Angew. Chem. Int. Ed.*, 2012, **51**, 2964–2967.

101 S. S. Chitnis, N. Burford and M. J. Ferguson, *Angew. Chem., Int. Ed.*, 2013, **52**, 2042–2045.

102 S. S. Chitnis, Y.-Y. Carpenter, N. Burford, R. McDonald and M. J. Ferguson, *Angew. Chem., Int. Ed.*, 2013, **52**, 4863–4866.

103 R. Pietschnig, *J. Organomet. Chem.*, 2007, **692**, 3363–3369.

104 A. Haaland, *Angew. Chem., Int. Ed.*, 1989, **28**, 992–1007.

105 N. Menschutkin, *Z. Phys. Chem.*, 1890, **5**, 589.

106 S. S. Chitnis, E. MacDonald, N. Burford, U. Werner-Zwanziger and R. McDonald, *Chem. Commun.*, 2012, **48**, 7359–7361.

107 C. A. Dyker and N. Burford, *Chem. Asian J.*, 2008, **3**, 28–36.

108 N. Burford and P. J. Ragogna, *J. Chem. Soc., Dalton Trans.*, 2002, 4307–4315.

109 Y. Carpenter, C. A. Dyker, N. Burford, M. D. Lumsden and A. Decken, *J. Am. Chem. Soc.*, 2008, **130**, 15732–15741.

110 E. Conrad, N. Burford, R. McDonald and M. J. Ferguson, *J. Am. Chem. Soc.*, 2009, **131**, 17000–17008.

111 E. Conrad, N. Burford, R. McDonald and M. J. Ferguson, *Chem. Commun.*, 2010, **46**, 4598–4600.

112 A. Mitra, L. J. DePue, S. Parkin and D. A. Atwood, *J. Am. Chem. Soc.*, 2006, **128**, 1147–1153.

113 A. Earnshaw and N. Greenwood, in *Chemistry of the Elements*, Elsevier, 1997, pp. 216–267.

114 R. S. Tobias, M. J. Sprague and G. E. Glass, *Inorg. Chem.*, 1968, **7**, 1714–1721.

115 S. Bott, *J. Am. Chem. Soc.*, 1985, **107**, 1796–1797.

116 D. A. Atwood, *Coord. Chem. Rev.*, 1998, **176**, 407–430.

117 S. Dagorne and D. A. Atwood, *Chem. Rev.*, 2008, **108**, 4037–4071.

118 J. Burt, W. Levason, M. E. Light and G. Reid, *Dalton Trans.*, 2014, **43**, 14600–14611.

119 V. V. Ovchinnikov, L. R. Khazieva, L. I. Lapteva and A. I. Konovalov, *Russ. Chem. Bull.*, 1990, **49**, 33–38.

120 M. W. Chase Jr., *J. Phys. Chem. Ref. Data, Monogr. 9*, 1998, 1–1951.

121 L. Glasser and H. D. B. Jenkins, *J. Chem. Eng. Data*, 2011, **56**, 874–880.

122 *For representative examples, see:* (a) F. Chen, G. Ma, G. Bernard, R. Wasylishen, R. Cavell, R. McDonald, M. J. Ferguson, *Chem. Eur. J.*, **2013**, *19*, 2826-2838. *(b)* F. Cheng, H. L. Codgbrook, A. L. Hector, W. Levason, G. Reid, M. Webster, W. Zhang, *Polyhedron*, **2007**, *26*, 4147-4155. *(c)* C. Y. Tang, A. J. Downs, T. M. Greene, S. Marchant, S. Parsons, *Inorg. Chem.*, **2005**, *44*, 7143-7150 .

123 F. Cheng, A. L. Hector, W. Levason, G. Reid, M. Webster and W. Zhang, *Inorg. Chem.*, 2007, **46**, 7215–7223.

124 S. S. Chitnis, N. Burford, R. McDonald and M. J. Ferguson, *Inorg. Chem.*, 2014, **53**, 5359–5372.

125 T. P. Chusova, L. N. Zelenina, Y. G. Stenin, Z. I. Semenova and V. A. Titov, *Russ. Chem. Bull.*, 2007, **56**, 1313–1317.

126 B. Brunetti, V. Piacente and P. Scardala, *J. Chem. Eng. Data*, 2009, **54**, 2273–2276.

127 F. Cheng, S. I. Friend, A. L. Hector, W. Levason, G. Reid, M. Webster and W. Zhang, *Inorg. Chem.*, 2008, **47**, 9691–9700.

128 C. Trinh, M. Bodensteiner, A. V. Virovets, E. V. Peresypkina, M. Scheer, S. M. Matveev and A. Y. Timoshkin, *Polyhedron*, 2010, **29**, 414–424.

129 M. Mantina, A. C. Chamberlin, R. Valero, C. J. Cramer and D. G. Truhlar, *J. Phys. Chem. A*, 2009, **113**, 5806–5812.

130 A. Earnshaw and N. Greenwood, in *Chemistry of the Elements*, Elsevier, 1997, pp. 268–327.

131 A. Earnshaw and N. Greenwood, in *Chemistry of the Elements*, Elsevier, 1997, pp. 367–405.

132 A. Earnshaw and N. Greenwood, in *Chemistry of the Elements*, Elsevier, 1997, pp. 328–366.

133 P. W. Atkins and D. F. Shriver, *Inorganic Chemistry*, Oxford University Press, 5th edn., 2010.

134 J. D. Corbett, *Angew. Chem. Int. Ed.*, 2000, **39**, 670–690.

135 S. Scharfe, F. Kraus, S. Stegmaier, A. Schier and T. F. Fässler, *Angew. Chem. Int. Ed.*, 2011, **50**, 3630–3670.

136 C. Hoch, M. Wendorff and C. Röhr, *Acta Crystallogr. Sect. C Cryst. Struct. Commun.*, 2002, **58**, i45–i46.

137 E. Zintl, J. Goubeau and W. Dullenkopf, *Z. Phys. Chem.*, 1931, 1–46.

138 W. Levason, G. Reid and W. Zhang, *Coord. Chem. Rev.*, 2011, **255**, 1319–1341.

139 J. Burt, W. Levason and G. Reid, *Coord. Chem. Rev.*, 2014, **260**, 65–115.

140 P. A. Rupar, R. Bandyopadhyay, B. F. T. Cooper, M. R. Stinchcombe, P. J. Ragogna, C. L. B. Macdonald and K. M. Baines, *Angew. Chem. Int. Ed.*, 2009, **48**, 5155–5158.

141 F. Cheng, A. L. Hector, W. Levason, G. Reid, M. Webster and W. Zhang, *Angew. Chem. Int. Ed.*, 2009, **48**, 5152–5154.

142 P. A. Rupar, V. N. Staroverov and K. M. Baines, *Science*, 2008, **322**, 1360–1363.

143 P. A. Rupar, V. N. Staroverov, P. J. Ragogna and K. M. Baines, *J. Am. Chem. Soc.*, 2007, **129**, 15138–15139.

144 S. S. Chitnis, A. P. M. Robertson, N. Burford, B. O. Patrick, R. McDonald and M. J. Ferguson, *Chem. Sci.*, 2015, 6545–6555.

145 S. S. Chitnis, A. P. M. Robertson, N. Burford, J. J. Weigand and R. Fischer, *Chem. Sci.*, 2015, **6**, 2559–2574.

146 S. S. Chitnis, K. A. Vos, N. Burford, R. McDonald and M. J. Ferguson, *Chem. Commun.*, 2016, **52**, 685–688.

147 A. P. M. Robertson, S. S. Chitnis, H. a. Jenkins, R. McDonald, M. J. Ferguson and N. Burford, *Chem. Eur. J.*, 2015, **21**, 7902–7913.

148 *For representative examples see:* A. G. Sykes, *et. al., J. Coord. Chem.,* **2010**, *63*,

2261–2267*;* G. Reid*, et. al., Polyhedron,* **2015**, *85*, 530–536*;* N. T. Kuznetsov*, et. al., Zh. Neorg. Khim, 2002, 1168*, .

149 F. Cheng, J. M. Dyke, F. Ferrante, A. L. Hector, W. Levason, G. Reid, M. Webster and W. Zhang, *Dalton Trans*, 2010, **39**, 847–856.

150 S. J. Archer, K. R. Koch and S. Schmidt, *Inorg. Chim. Acta*, 1987, **126**, 209–218.

151 P. Pyykkö and M. Atsumi, *Chem. Eur. J.*, 2009, **15**, 186–197.

152 M. Mantina, A. C. Chamberlin, R. Valero, C. J. Cramer and D. G. Truhlar, *J. Phys. Chem. A*, 2009, **113**, 5806–5812.

153 V. S. V. S. N. Swamy, S. Pal, S. Khan and S. S. Sen, *Dalton Trans.*, 2015, **44**, 12903–12923.

154 F. Cheng, A. L. Hector, W. Levason, G. Reid, M. Webster and W. Zhang, *Inorg. Chem.*, 2010, **49**, 752–760.

155 M. F. Davis, W. Levason, G. Reid and M. Webster, *Dalton Trans*, 2008, **4**, 2261–9.

156 C. Gurnani, A. L. Hector, E. Jager, W. Levason, D. Pugh and G. Reid, *Dalton Trans.*, 2013, **42**, 8364–8374.

157 N. Miyaura and A. Suzuki, *J. Chem. Soc. Chem. Commun.*, 1979, 866–867.

158 Y. Mizuhata, T. Sasamori and N. Tokitoh, *Chem. Rev.*, 2009, **109**, 3479–3511.

159 G. D. Frey, V. Lavallo, B. Donnadieu, W. W. Schoeller and G. Bertrand, *Science*, 2007, **316**, 439–441.

160 Y. Peng, B. D. Ellis, X. Wang and P. P. Power, *J. Am. Chem. Soc.*, 2008, **130**,

12268–12269.

161 Y. Peng, J.-D. Guo, B. D. Ellis, Z. Zhu, J. C. Fettinger, S. Nagase and P. P. Power, *J. Am. Chem. Soc.*, 2009, **131**, 16272–16282.

162 M. Usher, A. V. Protchenko, A. Rit, J. Campos, E. L. Kolychev, R. Tirfoin and S. Aldridge, *Chem. Eur. J.*, 2016, **22**, 11685–11698.

163 A. V. Protchenko, J. I. Bates, L. M. A. Saleh, M. P. Blake, A. D. Schwarz, E. L. Kolychev, A. L. Thompson, C. Jones, P. Mountford and S. Aldridge, *J. Am. Chem. Soc.*, 2016, **138**, 4555–4564.

164 G. D. Frey, V. Lavallo, B. Donnadieu, W. W. Schoeller and G. Bertrand, *Science*, 2007, **316**, 439–441.

165 D. Bourissou, O. Guerret, F. P. Gabbai and G. Bertrand, *Chem. Rev.*, 2000, **100**, 39–91.

166 R. Bandyopadhyay, J. H. Nguyen, A. Swidan and C. L. B. Macdonald, *Angew. Chem. Int. Ed.*, 2013, **52**, 3469–3472.

167 R. K. Raut and M. Majumdar, *Chem. Commun.*, 2017, **53**, 1467–1469.

168 J. J. Weigand, S. D. Riegel, N. Burford and A. Decken, *J. Am. Chem. Soc.*, 2007, **129**, 7969–7976.

169 J. J. Weigand, N. Burford, A. Decken and A. Schulz, *Eur. J. Inorg. Chem.*, 2007, **2007**, 4868–4872.

170 D. M. U. K. Somisara, M. Bühl, T. Lebl, N. V Richardson, A. M. Z. Slawin, J. D. Woollins and P. Kilian, *Chem. Eur. J.*, 2011, **17**, 2666–2677.

171 S. S. Chitnis, H. A. Sparkes, V. T. Annibale, N. E. Pridmore, A. M. Oliver and I. Manners, *Angew. Chem. Int. Ed.*, 2017, **56**, 9536–9540.

172 C. C. Hsu and R. A. Geanangel, *Inorg. Chem.*, 1980, **19**, 110–119.

173 A. Bondi, *J. Phys. Chem.*, 1964, **68**, 441–451.

174 T. W. Hambley, *Inorg. Chem.*, 1998, **37**, 3767–3774.

175 A. P. M. Robertson, S. S. Chitnis, S. Chhina, H. J. C. S., B. O. Patrick, H. A. Jenkins and N. Burford, *Can. J. Chem.*, 2016, **94**, 424.

176 H. Sinclair, R. Suter, N. Burford, R. McDonald and M. J. Ferguson, *Can. J. Chem.*, 2018, **5**, 1–5.

177 B. D. Ellis and C. L. B. Macdonald, *Inorg. Chim. Acta*, 2007, **360**, 329–344.

178 K. Vos, BSc. Thesis 2015.

179 H. C. Sinclair, MSc Thesis, 2017.

180 J. F. Binder, S. C. Kosnik and C. L. B. Macdonald, *Chem. Eur. J.*, 2018, **24**, 3556–3565.

181 S. C. Kosnik, M. C. Nascimento, J. F. Binder and C. L. B. Macdonald, *Dalton Trans.*, 2017, 17080–17092.

182 S. C. Kosnik and C. L. B. Macdonald, *Dalton Trans.*, 2016, **45**, 6251–6258.

183 J. W. Dube, V. A. Béland, P. D. Boyle and P. J. Ragogna, *Can. J. Chem.*, 2015, **93**, 253–264.

184 L. W. Pineda, V. Jancik, H. W. Roesky, D. Neculai and A. M. Neculai, *Angew.*

Chem. Int. Ed., 2004, **43**, 1419–1421.

185 R. Suter, A. Swidan, C. L. B. Macdonald and N. Burford, *Chem. Commun.*, 2018, 8–11.

186 E. MacDonald, L. Doyle, S. S. Chitnis, U. Werner-Zwanziger, N. Burford and A. Decken, *Chem. Commun.*, 2012, **48**, 7922–7924.

187 D. W. Stephan, *J. Am. Chem. Soc.*, 2015, **137**, 10018–10032.

188 G. C. Welch and D. W. Stephan, *J. Am. Chem. Soc.*, 2007, **129**, 1880–1881.

189 P. A. Gray, K. D. Krause, N. Burford and B. O. Patrick, *Dalton Trans.*, 2017, **46,** 8363-8366.

190 A. P. M. Robertson, N. Burford, R. McDonald and M. J. Ferguson, *Angew. Chem. Int. Ed.*, 2014, **53**, 3480–3483.

191 S. Decarlo, D. H. Mayo, W. Tomlinson, J. Hu, J. Hooper, P. Zavalij, K. Bowen, H. Schnöckel and B. Eichhorn, *Inorg. Chem.*, 2016, **55**, 4344–4353.

192 J. England and K. Wieghardt, *Inorg. Chem.*, 2013, **52**, 10067–10079.

193 E. MacDonald, L. Doyle, N. Burford, U. Werner-Zwanziger and A. Decken, *Angew. Chem. Int. Ed.*, 2011, **50**, 11474–11477.

194 G. Linti and A. Seifert, *Z. Anorg. Allg. Chem.*, 2008, **634**, 1312–1320.

195 R. J. Baker, C. Jones, M. Kloth and D. P. Mills, *New J. Chem.*, 2004, **28**, 207.

196 C. E. Strasser, W. F. Gabrielli, O. Schuster, S. D. Nogai, S. Cronje and H. G. Raubenheimer, *J. Chem. Crystallogr.*, 2009, **39**, 478–483.

197 R. Suter, P. A. Gray, N. Burford and R. McDonald, *Chem. Eur. J.*, 2018, **24**, 4718–4723.

198 V. Gutmann, *Coord. Chem. Rev.*, 1976, **18**, 225–255.

199 M. H. Holthausen, M. Mehta and D. W. Stephan, *Angew. Chem. Int. Ed.*, 2014, **53**, 6538–6541.

200 R. R. Maar, A. Rabiee Kenaree, R. Zhang, Y. Tao, B. D. Katzman, V. N. Staroverov, Z. Ding and J. B. Gilroy, *Inorg. Chem.*, 2017, **56**, 12436–12447.

201 A. M. Poitras, J. A. Bogart, B. E. Cole, P. J. Carroll, E. J. Schelter and C. R. Graves, *Inorg. Chem.*, 2015, **54**, 10901–10908.

202 C. B. Caputo, L. J. Hounjet, R. Dobrovetsky and D. W. Stephan, *Science*, 2013, **341**, 1374–1377.

203 C. Lepetit, V. Maraval, Y. Canac and R. Chauvin, *Coord. Chem. Rev.*, 2016, **308**, 59–75.

204 O. Ekkert, G. Kehr, R. Fröhlich and G. Erker, *J. Am. Chem. Soc.*, 2011, **133**, 4610–4616.

205 Y. Nakayama, Y. Baba, H. Yasuda, K. Kawakita and N. Ueyama, *Macromolecules*, 2003, **36**, 7953–7958.

206 A. Y. Timoshkin and G. Frenking, *Organometallics*, 2008, **27**, 371–380.

207 M. a Beckett, D. S. Brassington, S. J. Coles and M. B. Hursthouse, *Inorg. Chem. Commun.*, 2000, **3**, 530–533.

208 C. B. Caputo, D. Winkelhaus, R. Dobrovetsky, L. J. Hounjet and D. W. Stephan, *Dalton Trans.*, 2015, **44**, 12256–12264.

209 A. P. M. Robertson, J. N. Friedmann, H. A. Jenkins and N. Burford, *Chem. Commun.*, 2014, **50**, 7979.

210 R. West and G. A. Gornowicz, *J. Am. Chem. Soc.*, 1971, **93**, 1714–1720.

211 M. Webster and H. E. Blayden, *J. Chem. Soc. A*, 1969, 2443–2451.

212 C. U. Davanzo and Y. Gushikem, *Inorg. Chim. Acta*, 1982, **60**, 219–222.

213 A. W. Addison and P. J. Burke, *J. Heterocycl. Chem.*, 1981, **18**, 803–805.

214 C. Frazee, N. Burford, R. McDonald, M. J. Ferguson, A. Decken and B. O. Patrick, *Chem. Eur. J.*, 2018, **24**, 4011–4013.

215 A. Prieto, M. R. Fructos, M. Mar Díaz-Requejo, P. J. Pérez, P. Pérez-Galán, N. Delpont and A. M. Echavarren, *Tetrahedron*, 2009, **65**, 1790–1793.

216 Z. Zhang, S. Du Lee, A. S. Fisher and R. A. Widenhoefer, *Tetrahedron*, 2009, **65**, 1794–1798.

217 M. Liu, H. Wang, H. Zeng and C. J. Li, *Sci. Adv.*, 2015, **1**, 1–10.

218 G. Fang and X. Bi, *Chem. Soc. Rev.*, 2015, **44**, 8124–8173.

219 V. K.-Y. Lo, A. O.-Y. Chan and C.-M. Che, *Org. Biomol. Chem.*, 2015, **13**, 6667–6680.

220 H. Braunschweig and M. Colling, *Coord. Chem. Rev.*, 2001, **223**, 1–51.

221 A. Amgoune and D. Bourissou, *Chem. Commun.*, 2011, **47**, 859–871.

222 J. Wagler, A. F. Hill and T. Heine, *Eur. J. Inorg. Chem.*, 2008, 4225–4229.

223 J. Wagler and E. Brendler, *Angew. Chem. Int. Ed.*, 2010, **49**, 624–627.

224 H. Yang and F. P. Gabbal, *J. Am. Chem. Soc.*, 2015, **137**, 13425–13432.

225 D. You, H. Yang, S. Sen and F. P. Gabbaï, *J. Am. Chem. Soc.*, 2018.

226 Gaussian 09, Revision E.01, M. J. Frisch, G. W. Trucks, H. B. Schlegel, G. E. Scuseria, M. A. Robb, J. R. Cheeseman, G. Scalmani, V. Barone, G. A. Petersson, H. Nakatsuji, X. Li, M. Caricato, A. Marenich, J. Bloino, B. G. Janesko, R. Gomperts, B. Mennucci, H. P. Hratchian, J. V. Ortiz, A. F. Izmaylov, J. L. Sonnenberg, D. Williams-Young, F. Ding, F. Lipparini, F. Egidi, J. Goings, B. Peng, A. Petrone, T. Henderson, D. Ranasinghe, V. G. Zakrzewski, J. Gao, N. Rega, G. Zheng, W. Liang, M. Hada, M. Ehara, K. Toyota, R. Fukuda, J. Hasegawa, M. Ishida, T. Nakajima, Y. Honda, O. Kitao, H. Nakai, T. Vreven, K. Throssell, J. A. Montgomery, Jr., J. E. Peralta, F. Ogliaro, M. Bearpark, J. J. Heyd, E. Brothers, K. N. Kudin, V. N. Staroverov, T. Keith, R. Kobayashi, J. Normand, K. Raghavachari, A. Rendell, J. C. Burant, S. S. Iyengar, J. Tomasi, M. Cossi, J. M. Millam, M. Klene, C. Adamo, R. Cammi, J. W. Ochterski, R. L. Martin, K. Morokuma, O. Farkas, J. B. Foresman, and D. J. Fox, Gaussian, Inc., Wallingford CT, 2016.

227 Gaussian 16, Revision B.01, M. J. Frisch, G. W. Trucks, H. B. Schlegel, G. E. Scuseria, M. A. Robb, J. R. Cheeseman, G. Scalmani, V. Barone, G. A. Petersson, H. Nakatsuji, X. Li, M. Caricato, A. V. Marenich, J. Bloino, B. G. Janesko, R. Gomperts, B. Mennucci, H. P. Hratchian, J. V. Ortiz, A. F. Izmaylov, J. L. Sonnenberg, D. Williams-Young, F. Ding, F. Lipparini, F. Egidi, J. Goings, B.

Peng, A. Petrone, T. Henderson, D. Ranasinghe, V. G. Zakrzewski, J. Gao, N. Rega, G. Zheng, W. Liang, M. Hada, M. Ehara, K. Toyota, R. Fukuda, J. Hasegawa, M. Ishida, T. Nakajima, Y. Honda, O. Kitao, H. Nakai, T. Vreven, K. Throssell, J. A. Montgomery, Jr., J. E. Peralta, F. Ogliaro, M. J. Bearpark, J. J. Heyd, E. N. Brothers, K. N. Kudin, V. N. Staroverov, T. A. Keith, R. Kobayashi, J. Normand, K. Raghavachari, A. P. Rendell, J. C. Burant, S. S. Iyengar, J. Tomasi, M. Cossi, J. M. Millam, M. Klene, C. Adamo, R. Cammi, J. W. Ochterski, R. L. Martin, K. Morokuma, O. Farkas, J. B. Foresman, and D. J. Fox, Gaussian, Inc., Wallingford CT, 2016.

228 NBO 6.0, E. D. Glendening, J, K. Badenhoop, A. E. Reed, J. E. Carpenter, J. A. Bohmann, C. M. Morales, C. R. Landis, and F. Weinhold, Theoretical Chemistry Institute, University of Wisconsin, Madison, WI, 2013.